LA-5651-M
Manual

UC-15
Reporting Date: June 1974
Issued: September 1974

c. 1

Fundamentals of Passive Nondestructive Assay of Fissionable Material

by

R. H. Augustson and T. D. Reilly

Nuclear Analysis Research Group, A-1

LOS ALAMOS NATIONAL LABORATORY
3 9338 00377 3040

los alamos
scientific laboratory
of the University of California
LOS ALAMOS, NEW MEXICO 87544

DO NOT CIRCULATE

PERMANENT RETENTION

REQUIRED BY CONTRACT

UNITED STATES
ATOMIC ENERGY COMMISSION
CONTRACT W-7405-ENG. 36

Printed in the United States of America. Available from
National Technical Information Service
U.S. Department of Commerce
5285 Port Royal Road
Springfield, Virginia 22151
Price: Printed Copy $5.45 Microfiche $1.45

This report was prepared as an account of work sponsored by the United States Government. Neither the United States nor the United States Atomic Energy Commission, nor any of their employees, nor any of their contractors, subcontractors, or their employees, makes any warranty, express or implied, or assumes any legal liability or responsibility for the accuracy, completeness or usefulness of any information, apparatus, product or process disclosed, or represents that its use would not infringe privately owned rights.

LOS ALAMOS NATL. LAB. LIBS.
3 9338 00377 3040

FOREWORD

The U.S. Atomic Energy Commission's Nondestructive Assay Training Program in Perspective

Since 1966 the Atomic Energy Commission and the Los Alamos Scientific Laboratory have pioneered the development of new technology for inspection, accountability, and surveillance of special nuclear materials (SNM) to meet foreseen requirements for stringent control of these materials on a time scale consistent with the projected growth of the nuclear industry.

Today's urgent need for tight SNM controls, long foreseen by safeguards people, has recently been underscored by widespread publicity on the problems of nuclear materials theft, diversion, terrorism, etc. The key to an effective balanced national system of stringent safeguards lies in the new nondestructive assay (NDA) techniques and instrumentation being developed and now beginning to be applied throughout the nuclear industry. This new instrumentation, coupled with advances in low-cost computers will provide automated on-line accountability and control of nuclear materials on an essentially real time basis. This automated in-plant control of SNM promises not only stringent, economic safeguards, but also other important economic benefits through upgraded process and quality control, criticality safety, and the reduction or elimination of costly shutdown and cleanout procedures at inventory time.

Experience to date in the development, evaluation, and inplant deployment of NDA equipment has shown that an array of specialized NDA instrumentation is required to measure the many different forms, compositions, and containments in which SNM appears in the nuclear fuel cycle. The task of successfully implementing and transferring this new technology to the nuclear industry is indeed prodigious.

Clearly the most important single factor in the successful transfer of NDA technology is the training of personnel in practical use of instruments. To that end, the U.S. Atomic Energy Commission established the Nondestructive Assay Training Program at Los Alamos in the fall of 1973. Although enrollment was initially limited to AEC inspectors, future course offerings (on a semiannual basis) will be available to the growing number of users of NDA equipment in both government and private sectors of the nuclear community. Courses are designed to cover both the underlying principles and the use of NDA instruments with emphasis on practical assay and verification measurements of specific interest to attendees. A formal training manual is prepared and used extensively with each course. This first manual provides a general reference on the use of portable NDA instrumentation together with a summary of measurement principles basic to the understanding of other more advanced NDA techniques, both passive and active.

The U.S. Atomic Energy Commission Nondestructive Assay Training Program provides an excellent opportunity for direct exchange of ideas, discussion of special problems, etc., between the developers and users of NDA instrumentation. Such direct person-to-person interaction has proved by far the most effective method of NDA technology transfer and provides one of the major practical benefits of the AEC's ongoing NDA training program.

G. Robert Keepin, Group Leader
Nuclear Analysis Research Group, A-1

CONTENTS

INTRODUCTION

This manual is written as a general reference to the basic principles of nondestructive assay of fissionable material. It is the foundation for a course on the use of portable instrumentation conducted at the Los Alamos Scientific Laboratory. The manual is written at an introductory level and requires minimal background in nondestructive assay. The philosophy is to explain the basic principles and then use specific examples to illustrate the application of these principles to practical assay problems. It is impossible to discuss all of the measurements required in the nuclear industry; however, by emphasizing the basic concepts the assayist is better prepared to handle a wide range of measurement problems. The first six chapters deal with gamma-ray assay including gamma-ray production and interaction, detection principles, quantitative assay, and enrichment measurements. The last three chapters discuss passive neutron measurements including basic signatures and interactions, neutron detectors, and verification measurements. Although the manual emphasizes portable instrumentation, it includes material on more advanced, nonportable equipment. Lithium-drifted germanium detectors are discussed in detail in Chap. 3. Spontaneous fission neutron detectors are described briefly in Chap. 9. Although this is not directly applicable to portable instrument assay, it provides valuable background material on advanced assay procedures.

Many people have helped to generate this manual and set up the initial course session. Larry East was largely responsible for writing Chaps. 3 and 4. Albert Evans, Jack Parker, and Darryl Smith also contributed to the writing. The course instructors, Thomas Atwell, John Foley, Jack Parker, and Roddy Walton, helped decide the content of the manual and were responsible for setting up the laboratory sessions, which were the bulk of the course. The help and support of all these people and of Joan Rosul is gratefully acknowledged.

FUNDAMENTALS OF PASSIVE NONDESTRUCTIVE ASSAY OF FISSIONABLE MATERIAL

by

R. H. Augustson and T. D. Reilly

ABSTRACT

This manual is an introduction to the fundamental principles of passive gamma-ray and neutron assay for fissionable material accountability.

---

1. GAMMA-RAY PRODUCTION AND INTERACTION WITH MATTER

1.1.a. Gamma-Ray Production

This section discusses the processes that enable fissionable material to be measured using its naturally occurring gamma-ray activity. Gamma rays are a form of high-energy electromagnetic radiation. The broad electromagnetic spectrum shown in Fig. 1.1 ranges from radiowaves to visible light to x rays and gamma rays. Radiowaves and light usually are described in terms of frequency or wavelength, but x rays and gamma rays are characterized by their energy in keV or MeV. Energy (E) and frequency (ν) are directly related by $E = h\nu$ (Planck's constant, h, equals 4.14×10^{-15} eV-s). The relation between energy and wavelength (λ) is $E = hc/\lambda$, where c is the speed of light ($hc = 1.24 \times 10^{-6}$ eV-m). Gamma rays have very high frequencies and very short wavelengths. Gamma rays arise from excitations within the nucleus, whereas x rays come from excitations of the atomic electrons.

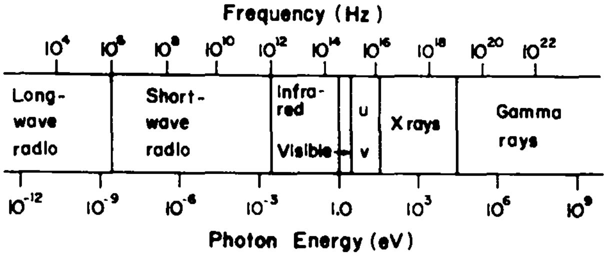

Fig. 1.1.
The electromagnetic spectrum.

Many radioactive isotopes emit gamma rays during decay. The energy and intensity of these gamma rays are uniquely characteristic of the isotope. Figure 1.2 shows a portion of the characteristic gamma-ray spectrum of ^{235}U. There is little probability that gamma rays from different isotopes will exactly overlap in energy, therefore, gamma rays can be used to identify uniquely the presence of particular isotopes. All fissionable material is unstable, emitting some form of radiation by alpha, beta, or spontaneous fission decay. In this decay process, some fissionable isotopes emit gamma radiation that can be quantitatively and uniquely related to the original isotope. Such a gamma ray can be called a signature of that isotope. For example, ^{235}U alpha decays to ^{231}Th, leaving the ^{231}Th in excited states which, in turn, decay and emit gamma rays. The alpha particle is accompanied by a 186-keV gamma ray 54% of the time. This production rate (186-keV gamma rays/s-g^{235}U) is a constant of nature. In an unknown sample, the production rate of 186-keV gamma rays is directly proportional to the number of atoms (or grams) of ^{235}U in that sample. The existence of these unique signatures provides the basis for gamma-ray assay of nuclear material. The measurement of real samples is complicated by many factors; for example, (1) not all of the gamma rays escape from the

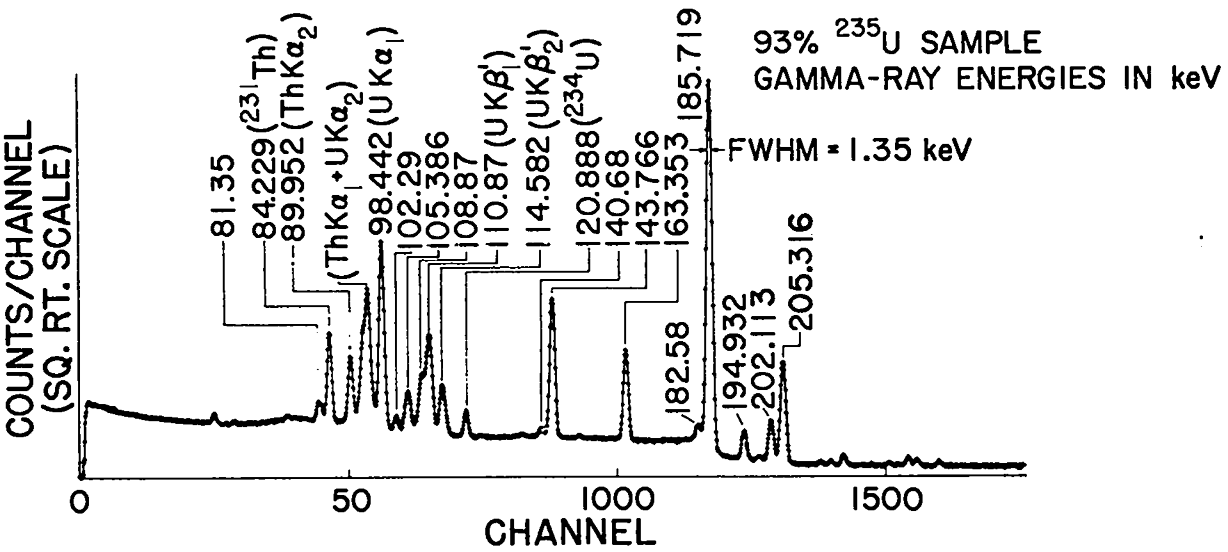

Fig. 1.2.
Characteristic gamma rays of ^{235}U. This spectrum was measured with a high-resolution Ge(Li) detector.

sample, (2) only a fraction of those that do are detected, and (3) other gamma rays may interfere with the detection of the signature of interest. This is the subject for the first six chapters of this manual.

1.1.b. Half-Life and Decay Rate

The rate at which an isotope decays is commonly given in terms of its half-life. Half-life is defined as the time it takes for one-half of the atoms in a sample to decay. The expression for the number of atoms left in a sample after time t is

$$N(t) = N(0)e^{-\lambda t} , \qquad (1.1)$$

where

N(0) = number of atoms at initial time 0. This time is arbitrary: for example, it might be the beginning of sample observation.

N(t) = number of atoms remaining at time t,

where λ is given the name "disintegration constant." Half-life and disintegration constant can be used interchangeably, and the relation between them can be derived as follows.

$$N(t_{\frac{1}{2}}) = \tfrac{1}{2}N(0) = N(0)e^{-\lambda t_{\frac{1}{2}}} ,$$

$$e^{\lambda t_{\frac{1}{2}}} = 2, \text{ and}$$

$$t_{\frac{1}{2}} = \ln 2/\lambda = 0.693/\lambda . \qquad (1.2)$$

The decay rate, R, in disintegrations per second, is given by

$$R = \frac{dN(t)}{dt} = -\lambda N(t)$$

$$= -\lambda[N(0)e^{-\lambda t}] , \qquad (1.3)$$

where the minus sign indicates that the number of atoms is decreasing with time. The decay rate is equal to the product of the disintegration constant and the number of atoms in the sample. The number of atoms in 1 g of a sample with atomic weight A is equal to Avogadro's number (6.023 x 10^{23}) divided by the atomic weight. This relation and Eq. (1.2) combine to give a useful expression for R.

$$N = 6.023 \times 10^{23}/A \ ,$$

$$\lambda = 0.693/t_{\frac{1}{2}} \ ,$$

$$1 \text{ yr} = 3.156 \times 10^{7} \text{ s, and}$$

$$R = \lambda N = \frac{(0.693)(6.023 \times 10^{23})}{A\, t_{\frac{1}{2}}\, (3.156 \times 10^{7})} \ .$$

$$\boxed{R = \frac{1.32 \times 10^{16}}{A\, t_{\frac{1}{2}}}} \ , \qquad (1.4)$$

Where A = atomic weight.

$t_{1/2}$ = half-life in years, and

R = decay rate in disintegrations per gram per second.

For example, ^{235}U with a half-life of 7.13×10^{8} yr has a decay rate of

$$R = \frac{(1.32 \times 10^{16})}{(235)(7.13 \times 10^{8})} = 7.88 \times 10^{4}/\text{g-s} \ .$$

Approximately 54% of the ^{235}U decays lead to a 186-keV gamma ray, therefore the specific activity of this signature is $(0.54 \times 7.88 \times 10^{4}) = 4.3 \times 10^{4}/\text{g-s}$. The count rate in a detector would be equal to the product of the specific activity and the overall counting efficiency. If the sample had no self-absorption and were positioned 10 cm from a 5-cm-diam by 1.3-cm-thick NaI detector, the observed count rate would be approximately 500 counts/g-s. Detector efficiency will be discussed in later sections.

1.1.c. Specific Gamma-Ray Signatures

The major gamma-ray signatures for the fissionable isotopes are listed in Table 1.1. References 1.1 - 1.4 at the end of this chapter contain more complete tabulations of gamma-ray data. As indicated in Table 1.1, some signatures involve gamma rays from a daughter product of the fissionable isotope of interest. Such signatures are usually useful only when the daughter product and parent isotope are in equilibrium. If the material has recently undergone a physical or chemical process that can separate the isotopes, quantitative measurements are usually reliable only after equilibrium has been reestablished. The time to equilibrium is determined by the longest half-life in the decay chain between the parent and the daughter (this includes the half-life of the daughter). If four half-lives have elapsed since the separation time, the concentration of the daughter product will be within 6.25% of the equilibrium concentration. Consider the following example.

$$^{241}\text{Pu} \xrightarrow{\alpha} {}^{237}\text{U} \xrightarrow[6.75 \text{ days}]{\beta^- + 208 \text{ keV } \gamma} {}^{237}\text{Np} \ .$$

Following a chemical separation of uranium and plutonium, the rate of the 208-keV gamma rays will increase with time as equilibrium is reestablished between ^{241}Pu and ^{237}U. Within 4 to 5 wk, the 208-keV activity will stabilize and will be proportional to ^{241}Pu. Consider another example.

$$^{238}\text{U} \xrightarrow{\alpha} {}^{234}\text{Th} \xrightarrow[24.1 \text{ d}]{\beta^-}$$

$$^{234m}\text{Pa} \xrightarrow[1.18 \text{ min}]{\beta^- + 1001 \text{ keV } \gamma} {}^{234}\text{U} \ .$$

The thorium and protactinium can be separated from uranium by a variety of chemical and physical processes: (1) diffusion of UF_6 through a porous barrier, (2) melting or vaporization of solid UF_6, and (3) various oxide conversion processes. After such a separation, 3 to 4 months are required before the 1001-keV gamma ray is a reliable signature for ^{238}U.

1.2.a. Interaction of Gamma Rays with Matter

The interaction of gamma rays with matter influences assay measurements in two ways. First, as the gamma rays travel out of the sample they interact with the material in that sample, including the fissionable material emitting the gamma rays. These interactions reduce the number of gammas that leave the sample with their original energy. This is called sample attenuation. Second, all nuclear detectors require a moving charged particle to initiate the detection process. To be detected, a gamma ray, which is electrically neutral, must transfer some of its

TABLE 1.1

MAJOR GAMMA-RAY SIGNATURES FOR THE FISSIONABLE ISOTOPES

Isotope	Energy (keV)	Intensity $(g\text{-}s)^{-1}$	Comments
^{235}U	185.72	4.3×10^4	Only intense gamma ray. Resolved with NaI as well as Ge(Li). Useful for enrichment and quantitative measurements. Several much weaker peaks are seldom useful.
^{238}U	1001.10 766.40	1.0×10^2 3.9×10^1	These actually arise from the ^{234m}Pa daughter of ^{238}U. After chemical separation about 100 days are required for the activity to come into equilibrium at the levels stated. Plutonium-238 gives rise to the same 766.40-keV gamma and would produce interference in U-Pu mixtures. Useful for work with Ge(Li) or NaI.
^{238}Pu	766.40 152.77	1.5×10^5 6.5×10^6	Most useful for quantitative assay. Ge(Li) or NaI. Useful for isotopic determinations with Ge(Li).
^{239}Pu	413.69	3.4×10^4	The 413.69 usually provides the basis for Ge(Li) assays. The 413.69 plus the 375.02 and its weak neighbors form a complex upon which NaI assays are based.
^{239}Pu	129.28	1.4×10^5	Useful for isotopic determinations with Ge(Li). Plutonium-239 has over 100 gamma rays, some of which are useful for careful work with Ge(Li).
^{240}Pu	—	—	Several weak gamma rays but all suffer bad interference from gammas of other isotopes. Requires very careful work with high-resolution detector to make use of any of them.
^{241}Pu	207.98	2.0×10^7	Actually from ^{237}U daughter and requires about 25 days after chemical separation to come into equilibrium at stated value. May also have a few percent interference from ^{241}Am which emits same gamma. Nevertheless a good clean strong gamma useful with both NaI and Ge(Li).
	164.59	1.8×10^6	Useful with Ge(Li). Also from ^{237}U.
	148.60	7.5×10^6	Useful with Ge(Li). Direct from ^{241}Pu.
^{241}Am	59.54	4.6×10^{10}	Very strong gamma but attenuation problems. Useful with Ge(Li) or NaI. Has several other *much* less intense gammas sometimes useful for Ge(Li) work.
^{242}Pu	—	—	No useful gamma rays at all. Nature failed us at this point.

energy to electrons in the detector. Understanding the interaction processes is therefore of fundamental importance to the assayist. For more complete information the book by Evans[1.5] is recommended.

1.2.b. Exponential Attenuation

The intensity of a beam of x rays or gamma rays is reduced on passage through matter. This attenuation is proportional to the incident intensity and the thickness of the material. Figure 1.3 illustrates the absorption experienced by a beam of gamma rays of initial intensity I_o. Equation (1.5) is the fundamental law of gamma-ray attenuation.

$$I = I_o e^{-\mu_\ell L} \qquad (1.5)$$

The proportionality constant μ_ℓ is called the linear absorption coefficient. Its magnitude depends on the absorbing material and the gamma-ray energy. Figure 1.4 illustrates the attenuation of gamma rays as they pass through various thicknesses of lead. Note that 400-keV gamma rays are significantly more penetrating than those at 200 keV. Due to the exponential nature of their absorption, gamma rays do not have a definite range as do alpha or beta particles. The quantity $1/\mu_\ell$ is often called a mean free path; it is the thickness of the absorber which reduces the gamma-ray intensity to 1/e (0.37) of its initial value.

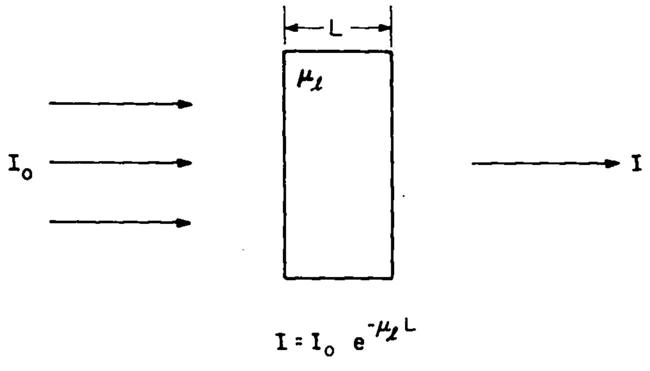

Fig. 1.3.
Fundamental law of gamma-ray attenuation.

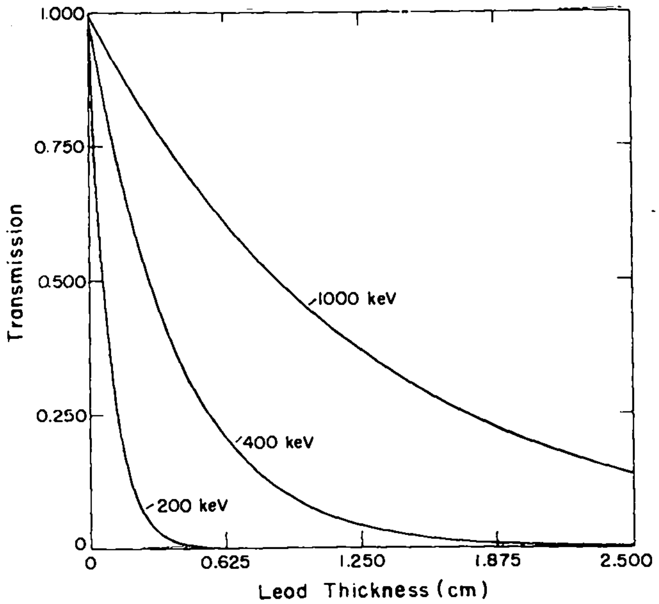

Fig. 1.4.
Exponential attenuation curves for lead.

1.2.c. Mass Absorption Coefficient

In addition to the linear absorption coefficient μ_ℓ, it is convenient to define a mass absorption coefficient μ_m where

$$\mu_m = \frac{\mu_\ell}{\rho} \qquad (1.6)$$

and ρ is the density of the material. The mass absorption coefficient is more fundamental than the linear absorption coefficient because it is independent of the density and physical state (gas, liquid, or solid) of the absorber. This is important in the nuclear fuel cycle where material can be found in various chemical forms (UF_6, UO_2, etc.), and in combination with other matrix material such as carbon powder or rubber gloves. Tables of absorption coefficients[1.6] will usually list mass absorption coefficients. Equation (1.5) can now be written as

$$I = I_o e^{-\mu_m x} , \qquad (1.7)$$

where $x = \rho L (g/cm^2)$. For a sample with more than one element, you can calculate $\mu_{m\ total}$ by

$$\left(\mu_m\right)_{\text{total}} = \left(\mu_m\right)_1 w_1 + \left(\mu_m\right)_2 w_2 + \ldots , \qquad (1.8)$$

where w's are the weight fractions of each element in the sample and the x in Eq. (1.7) is equal to the product of sample thickness and bulk density. For example, μ_m for a sample of solid UF$_6$, $\rho = 5.1$ g/cm^3 (318 lbs/ft^3) at 200 keV, is

$$\mu_m = \left(\mu_m\right)_1 \frac{238}{238 + 6(19)} + \left(\mu_m\right)_2 \frac{6 \times 19}{238 + 6(19)} ,$$

$$\mu_m = (1.23)(0.68) + (0.123)(0.32) = 0.88 \text{ cm}^2/\text{g}, \text{ and}$$

$$\mu_\ell = (0.88 \text{ cm}^2/\text{g})(5.1 \text{ g/cm}^3) = 4.5 \text{ cm}^{-1} , \text{ where}$$

$\left(\mu_m\right)_1$ = mass absorption coefficient for uranium at 200 keV = 1.23 cm^2/g, and

$\left(\mu_m\right)_2$ ≡ mass absorption coefficient for fluorine at 200 keV = 0.123 cm^2/g .

As an additional example, consider a 5-liter scrap container weighing 5 kg. The material in the container consists of the oxides of low-Z elements and 250 g of uranium spread uniformly throughout the container. Only a small error is made if the matrix material is assumed to attenuate like oxygen. Making this assumption, μ_m can be calculated as follows.

$$\mu_m(200 \text{ keV}) = (1.23)\left(\frac{250 \text{ g}}{5000 \text{ g}}\right) + (0.123)\left(\frac{4750 \text{ g}}{5000 \text{ g}}\right) ,$$

$$\mu_m(200 \text{ keV}) = \underbrace{0.061}_{\text{U contribution}} + \underbrace{0.117}_{\text{O contribution}}$$

$$= 0.178 \text{ cm}^2/\text{g} ,$$

$$\rho_{\text{bulk}} = \frac{5000 \text{ g}}{5000 \text{ cm}^3} = 1 \text{ g/cm}^3 , \text{ and}$$

$$\mu_\ell = 0.178 \text{ cm}^2/\text{g} \times 1 \text{ g/cm}^3$$

$$= 0.178 \text{ cm}^{-1} .$$

1.2.d. Energy Loss Processes

There are numerous processes by which gamma rays interact with matter and lose energy. These processes contribute in differing degrees for different energy gammas. The gamma rays emitted in nuclear decay usually have energies ranging from 100 keV to a few MeV. In this range the three main processes by which gammas interact with matter are: *photoelectric effect*, *Compton scattering*, and *pair production*. These are schematically represented in Fig. 1.5.

1.2.e. Photoelectric Effect

For a photoelectric interaction the incident gamma ray is totally absorbed by one of the atomic electrons, causing that electron to move through the material with an energy

$$E_e = E_\gamma - B ,$$

where E_γ is the energy of the incident γ, and B is the binding energy of the electron. The energy represented by B appears as characteristic x rays of the atom whose electron absorbed the incident γ. These x rays are in turn absorbed by the material, ejecting further lower energy electrons. The photoelectric process is important for the detection of gammas in that it converts all the gamma-ray energy into the motion of charged particles. This electron motion is transformed into an electrical pulse at the output of the detector. For NaI and semiconductor detectors, the size of a pulse produced by a photoelectric event is proportional to the energy of the gamma that caused the event.

Table 1.2 illustrates the dependence of the photoelectric effect on atomic number Z and gamma energy. As the Z of the material increases, μ_m (photoelectric) increases rapidly. Not only does μ_m (photoelectric) increase, but also

$$\frac{\mu_m(\text{photoelectric})}{\mu_m(\text{total})}$$

gets larger. At Z = 92 and E_γ = 200 keV, the dominant interaction process is, by far, the photoelectric effect. For higher energies the effect drops off rapidly as seen when comparing the μ_m's at 200 keV and 400 keV. The Z and E_γ dependences go roughly as $Z^3/E_\gamma{}^3$.

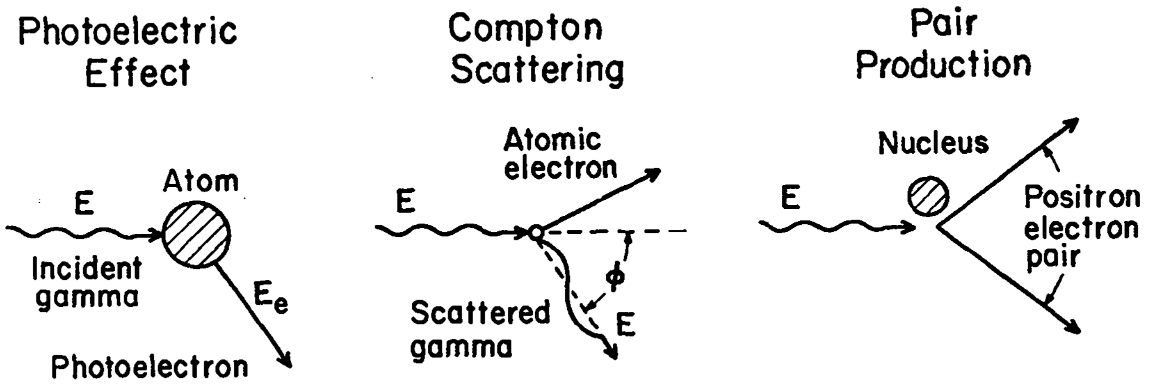

Fig. 1.5.
Representation of major gamma-ray interaction processes.

TABLE 1.2

Z DEPENDENCE OF PHOTOELECTRIC MASS ABSORPTION COEFFICIENTS FOR $E_\gamma = 200$ and 400 keV

Element	Z	Photoelectric μ_m (cm^2/g) 200 keV	Photoelectric μ_m (cm^2/g) 400 keV	$100 \times \frac{\mu_m(\text{photoelectric})}{\mu_m(\text{total})}$ 200 keV (%)	$100 \times \frac{\mu_m(\text{photoelectric})}{\mu_m(\text{total})}$ 400 keV (%)
Al	13	0.0018	0.00022	1	0.2
Fe	26	0.024	0.0025	17	3
Sn	50	0.199	0.0284	66	26
W	74	0.609	0.0976	87	56
Pb	82	0.800	0.133	89	64
U	92	1.08	0.185	92	71

An interesting feature of μ_m(photoelectric) is the presence of absorption edges. Figure 1.6 shows μ_m (PE) vs E_γ for lead. At approximately 90 keV there is a large step increase in μ_m(PE) labeled the "K absorption edge." At the K edge a gamma ray has just enough energy to start removing the most tightly bound K electrons from the atom. Because there are more possibilities for interaction, μ_m increases rapidly. For larger values of Z, the K edge occurs at higher energies. For example, the K edge of uranium is 116 keV. The small steps around 15 keV are called the "L absorption edges." In this region, a gamma ray has just enough energy to remove the next most tightly bound L electrons from the atom.

1.2.f. Compton Scattering

Compton scattering is a process by which the incident gamma ray interacts with a free electron and is scattered with a lower energy, the rest of the energy being taken up by the recoiling electron. Because the outer electrons in an atom are loosely bound and the energies of the incident gamma rays are comparatively high, we can treat these as free electrons. When an incident photon of energy E_γ strikes a free electron with a rest mass m_o, the interaction results in a scattered gamma ray of energy $E_\gamma'(<E_\gamma)$ and a recoiling electron with energy E_e, where

$$E_e = E_\gamma - E_\gamma' \ .$$

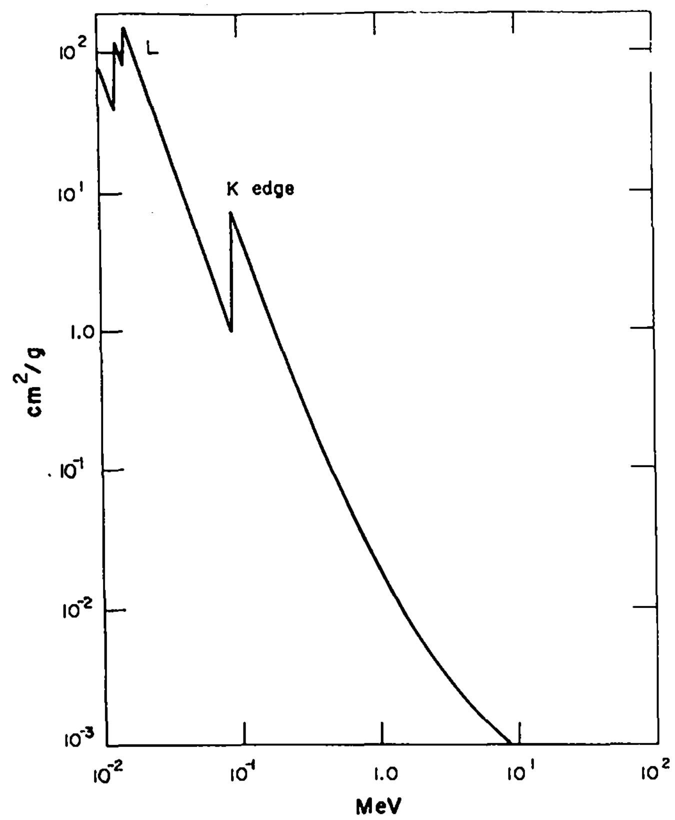

Fig. 1.6.
Photoelectric mass absorption coefficient for lead.

The energy of the scattered gamma ray is given by Eq. (1.9).

$$E'_\gamma = \frac{m_o c^2}{1 - \cos\varphi + m_o c^2 / E_\gamma} \,, \qquad (1.9)$$

where

$m_o c^2$ = rest mass of electron = 511 keV, and

φ = angle between incident gamma ray and scattered gamma ray .

E_γ' decreases as the scattering angle increases.

For $\varphi = 0°$ ($\cos\varphi = 1$) ,

$$E'_\gamma = E_\gamma \,.$$

Small-angle scatters result in very little energy loss.

For $\varphi = 180°$ ($\cos\varphi = -1$) ,

$$E'_\gamma = \frac{m_o c^2}{2 + m_o c^2 / E_\gamma}$$

.

if $E_\gamma \gg m_o c^2$,

$$E'_\gamma \sim m_o c^2/2 \sim 256 \text{ keV} \,.$$

The maximum energy transfer occurs when the scattered gamma ray goes in the back direction and the recoil electron goes in the forward direction. These equations show there is a maximum energy that can be given to the electron in a Compton collision. This maximum energy is given by

$$E_{max} = E_\gamma (1 + m_o c^2 / 2E_\gamma)^{-1} \,. \qquad (1.10)$$

For example, if $E_\gamma = 200$ keV, then $E_{max} = 88$ keV, which is the maximum energy that can be deposited in a detector in a single Compton interaction. Figure 1.7 is a graph of Eq. (1.10). The scattered gamma ray can escape from the detector or can be absorbed in further interactions. Figure 1.8 shows a Ge(Li) detector spectrum of ^{137}Cs, a monoenergetic gamma-ray source. The shoulder below the full energy photopeak is caused by single Compton interactions in the detector. The feature labeled Compton edge represents the maximum energy that can be deposited in the detector in a single Compton scattering.

Table 1.3 illustrates an interesting feature which makes it easier to calculate Compton scattering contributions. Note that the Compton effect has only small dependence on Z. Therefore at a given E_γ, for low-Z material where the photoelectric effect is small, the μ_m(Compton) dominates and is approximately constant. So the assumptions made in the example in Sec. 1.2.c were justified. The energy dependence of

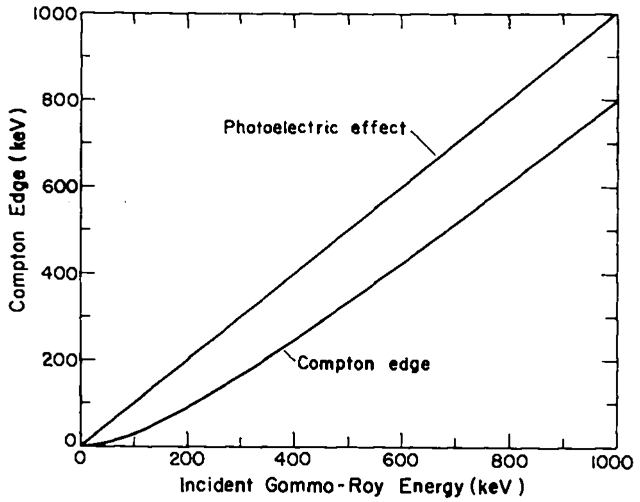

Fig. 1.7.
Compton edge (E_{max}) vs incident gamma-ray energy.

Compton scattering is much smaller than that of the photoelectric effect. Between 100 and 1000 keV, the μ_m(PE) will decrease by factors of 100 and greater, whereas μ_m (Compton) will decrease by 2 to 3.

There are assay situations in which the attenuation effect due to Compton scattering can be overpredicted. Consider the case in which the dominant interaction process in the sample to be measured is Compton scattering, as would be the case for low-Z matrix material (combustible waste) or for higher energy gamma rays such as the ~1-MeV lines used as ^{238}U signatures. If the detector is large (a 12.7-cm-diam NaI), and is relatively close to the sample, then some fraction of those gammas scattered through small angles can be counted in the energy window of the data collection electronics. Remember that the gamma-ray's energy loss depends on the angle through which it is scattered. Small-angle scattering corresponds to small energy loss. Therefore even though a gamma was scattered, it can be counted in the full-energy peak as an unattenuated event. This effect causes the observed attenuation to be lower than predicted by μ_ℓ and Eq. (1.5). It is particularly pronounced for low-resolution detectors, such as NaI, which require wide count windows. For high-resolution detectors, such as Ge(Li), even a small energy loss removes the scattered gamma ray from the full-energy peak. This points up a major advantage of Ge(Li); it is easier to interpret the spectral information and estimate sample attenuation.

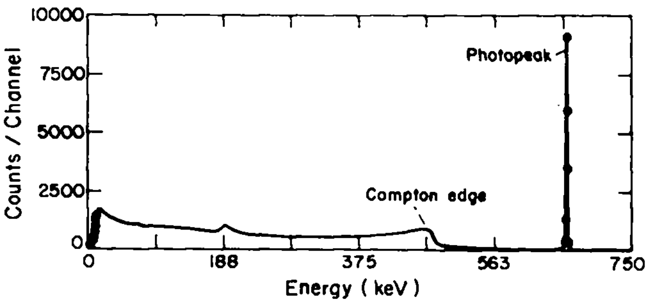

Fig. 1.8.
Ge(Li) detector spectrum of ^{137}Cs showing full energy photopeak and Compton edge from 662-keV gamma ray.

TABLE 1.3

μ_m FOR COMPTON SCATTERING

Element	Z	μ_m(Compton) 200 keV	μ_m(Compton) 400 keV
O	8	0.122	0.095
Al	13	0.118	0.092
Fe	26	0.114	0.089
Sn	50	0.103	0.080
W	74	0.099	0.077
Pb	82	0.097	0.076
U	92	0.095	0.074

1.2.g. Pair Production

The third process by which photons lose their energy is electron-positron pair production. The threshold energy for this process is 1.02 MeV. Because most fissionable material signatures are below this threshold, only a brief description of this process will be given. If a gamma of energy greater than 1.02 MeV strikes a foil of high-Z material, the gamma can disappear, and an electron-positron pair is formed in its place. The probability of this process increases with increasing gamma energy. The conservation of energy requires

$$E_\gamma = 2m_oc^2 + E_+ + E_- ,$$

where E_γ is the energy of the incident photon, $2m_oc^2$

is the energy equivalent to the rest mass of the electron and the positron, and E_+, E_- are the resulting energies of the positron and electron, respectively.

1.2.h. Summary of Contributions to μ_m(total)

Figure 1.9 shows the relative contribution of the three interaction processes to the linear absorption coefficient $\mu_m \rho$ for NaI. The photoelectric effect is the largest contributor at lower energies, falling very rapidly with E_γ. Note the K absorption edge of iodine at 33 keV. At about 260 keV the Compton and photoelectric effects cross, with the Compton scattering becoming dominant at higher energies. Pair production is not significant until gamma energies reach several MeV. Figure 1.10 illustrates the Z dependence of μ_m(total) on the material shown. The differences in μ_m(total) from element to element become greater at lower gamma energies. This is a consequence of the $Z^3/E_\gamma{}^3$ dependence for the photoelectric effect.

Even though two elements have the same mass absorption coefficients, they may have very different attenuations. For example, at E_γ = 400 keV what is the attenuation through 2.54 cm of iron metal compared to aluminum metal?

$$\mu_m = 0.092\ \text{cm}^2/\text{g for both aluminum and iron},$$

$$\rho_{Al} L = 2.70\ \text{g/cm}^3 \times 2.54\ \text{cm} = 6.86\ \text{g/cm}^2,$$

$$\rho_{Fe} L = 7.86\ \text{g/cm}^3 \times 2.54\ \text{cm} = 19.96\ \text{g/cm}^2, \text{ and}$$

$$e^{-\mu \rho L} = 0.53 \text{ for Al}$$

$$= 0.16 \text{ for Fe}.$$

Therefore, the attenuation through 2.54 cm of iron is much greater than that for a similar thickness of aluminum. The mass absorption coefficient is independent of density, but the attenuation (or conversely the transmission) is not.

REFERENCES

1.1. C. M. Lederer, J. M. Hollander, I. Perlman, "Table of Isotopes," 6th Ed., (John Wiley and Sons, Inc., NY, 1967). This is a tabulation of gamma rays from all radioactive isotopes. It includes nuclear energy level diagrams, x-ray information, and much more. It is a very useful reference for gamma-ray measurements.

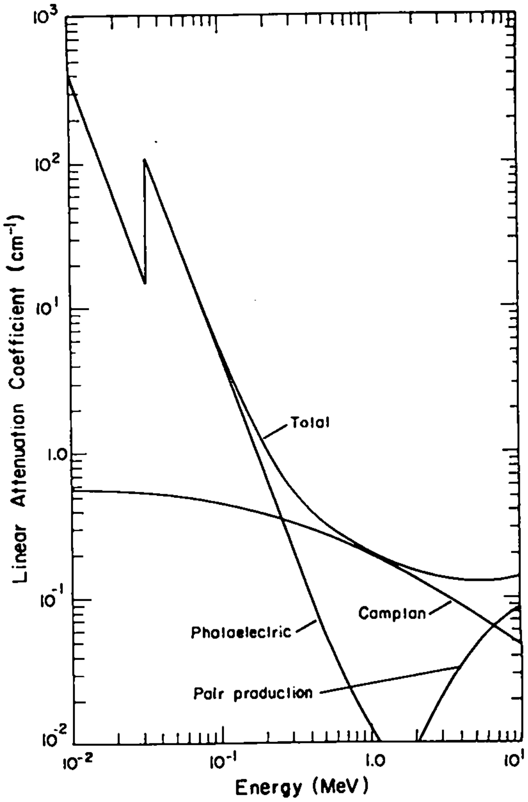

Fig. 1.9.
Linear absorption coefficient for NaI showing contributions from photoelectric effect, Compton scattering, and pair production. Note the use of log-log scales. (Data from NBS Circular 583 after "Harshaw Scintillation Phosphors," Harshaw Chemical Company.)

1.2. J. E. Cline, "Gamma Rays Emitted by the Fissionable Nuclides and Associated Isotopes," Idaho Nuclear Corporation report IN-1448 (January 1971) and supplement. "Gamma Rays Emitted by the Fissionable Nuclides and Associated Isotopes," Aerojet Nuclear Company report ANCR-1069 (July 1972). These list all gamma rays from the fissionable isotopes and related isotopes. They include typical Ge(Li) spectra of the materials of interest. There are some significant discrepancies between this reference and Ref. 1.3 regarding line intensities.

1.3. R. Gunnink and R. J. Morrow, "Gamma-Ray Energies and Absolute Branching Intensities for $^{238, 239, 240, 241}$Pu and ^{241}Am," Lawrence Livermore Laboratory report UCRL-51087 (July 1971). This lists gamma rays from the plutonium isotopes and shows typical Ge(Li) spectra. It probably contains the best available data on plutonium gamma-ray intensities.

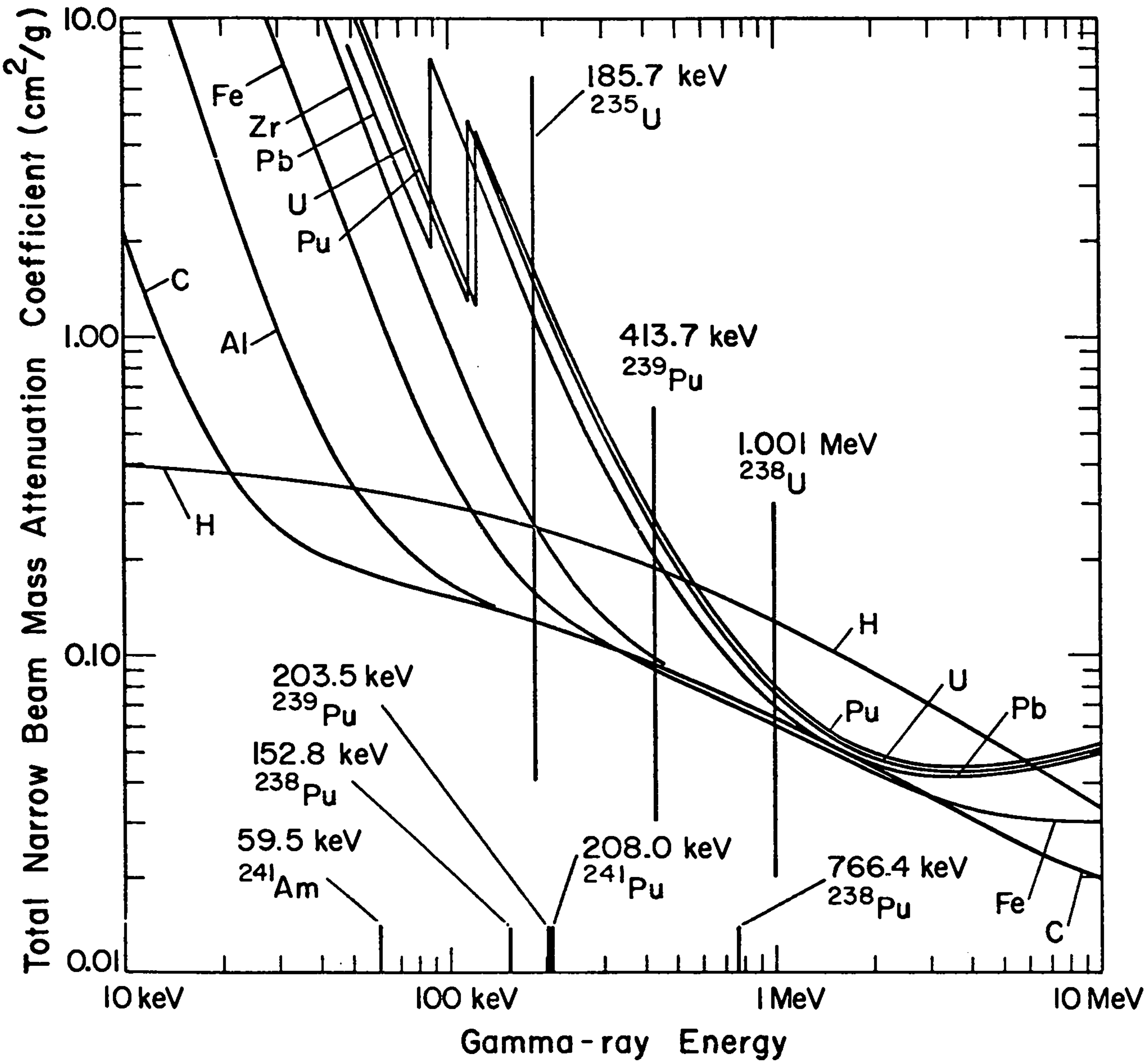

Fig. 1.10.
Mass absorption coefficients for selected elements.

1.4. R. Gunnink and J. F. Tinney, "Analysis of Fuel Rods by Gamma-Ray Spectroscopy," Lawrence Livermore Laboratory report UCRL 51086 (August 1971). Appendix C contains a listing of gamma rays from the fissionable isotopes (similar to Ref. 1.2), which is included in this manual as Appendix A.

1.5. R. D. Evans, *The Atomic Nucleus*, (McGraw-Hill Book Company, Inc., 1955). Though old, this is one of the best texts on nuclear physics. Recommended chapters include: 15—Radioactive Decay, 23-25—Interaction of Electromagnetic Radiation with Matter, and 26—Statistical Fluctuations in Nuclear Processes.

1.6. J. H. Hubbell, "Photon Cross Sections, Attenuation Coefficients and Energy Absorption Coefficients from 10 keV to 100 GeV," NSRDS-NBS-29, Superintendent of Documents, U. S. Government Printing Office, August 1969. This is one of the most recent and most complete listings of gamma-ray attenuation coefficients.

2. GAMMA-RAY DETECTORS I

2.1 General

Nuclear radiation detection is accomplished through the interaction of the radiation with matter. All detection methods generally are based on the process of excitation or ionization of atoms in the detector by energetic charged particles. For gamma radiation, the energetic charged particles are electrons produced by one or more of the three processes discussed in Secs. 1.2.e, 1.2.f, and 1.2.g, namely photoelectric effect, Compton scattering, and pair production. In gamma-ray spectrometry, only those interactions that result in the total absorption of the gamma-ray photon in the detector are important. Therefore, interactions by the Compton effect alone and the broad energy range of the recoil electrons they produce are a drawback in gamma-ray spectrometry. Consequently, detectors made of high-Z material are preferred, all other factors being equal, to enhance photoelectric (and to a lesser extent pair production) over Compton interactions. Increased detector volume not only increases the detection efficiency due to the higher probability of an interaction occurring within the detector, but also enhances its usefulness in spectrometry because the total absorption of gamma rays becomes more probable due to multiple interactions. After one or more Compton interactions, the scattered gamma ray will have a lower energy thereby increasing the probability of a photoelectric interaction. Through the principle of energy conservation, the same amount of energy will be deposited in the detector regardless of whether total absorption occurred by a single interaction or multiple interactions.*

The major features of the detector spectrum are illustrated in Fig. 2.1. The photopeak is formed by those interactions where the entire gamma-ray energy is absorbed in the detector. As explained above this can be either a single photoelectric interaction or a multiple interaction involving both the Compton and photoelectric processes. The importance of multiple interactions can be emphasized by noting that, at 662 keV, Compton scattering is the dominant interaction process for both NaI and Ge (Fig. 1.9). The number of counts under the photopeak is the parameter of interest for nuclear material assay because it is proportional to the mass of the isotope emitting the gamma signature. This parameter is shown as the shaded area of the NaI photopeak in Fig. 2.1. The major difference between the two spectra is in the width of the photopeaks. The intrinsic energy widths of the gamma-ray transitions of interest are very small (0.01-1.0 eV). However, the detection process is a statistical one, and the deposition of a fixed amount of energy in a detector results in a distribution of electrical pulse heights at the detector output. The peak of this distribution corresponds to the gamma-ray energy, and the width of the distribution is a property of the particular detector and its associated electronics. This width is usually characterized by a parameter called "resolution" and is a function of gamma-ray energy.

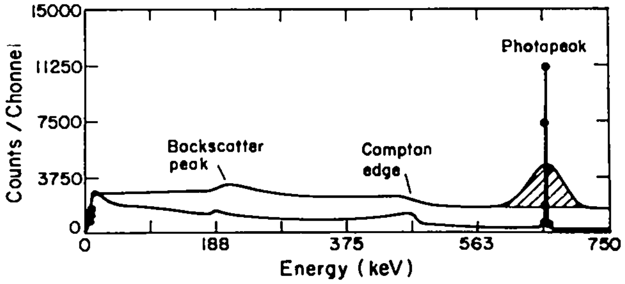

Fig. 2.1.
NaI and Ge(Li) spectra of ^{137}Cs (662 keV). The shaded area represents the net counts in the photopeak and is the parameter of interest for nuclear material assay. The NaI spectrum represents a longer count time; there are approximately 10 times more counts in the NaI peak than in the Ge(Li).

---

*Loss of energy due to electrons escaping from the detector volume is ignored. This effect will also be reduced by going to a larger detector volume.

The shoulder below the photopeak (beginning at about 475 keV) is caused by single Compton interactions in the detector. The Compton edge (here at 475 keV) corresponds to the maximum energy that can be deposited in a single Compton scattering (Fig. 1.7). The theoretical Compton edge is a sharp cutoff, which is broadened in the measured spectrum because of the finite detector resolution. The region between the photopeak and the Compton edge is filled by events from three major sources: (1) multiple Compton scatters in the detector which deposit less than the initial gamma-ray energy, (2) small-angle Compton scatters in the sample which produce a scattered gamma ray whose energy is less than the initial gamma-ray energy, and (3) Compton interactions of higher energy gamma rays (>662 keV) in the detector. The last effect can be due to higher energy gamma rays in the source or in the general background radiation. Common background gamma rays are ^{40}K(1461 keV), ^{208}Tl(2615 keV, a thorium daughter), and those from the plutonium and uranium stored around nuclear facilities. These higher energy gamma rays also cause the background continuum above the photopeak. The number of counts in the photopeak is represented by the shaded area in Fig. 2.1. A correction must usually be made to subtract the Compton background continuum from under the photopeak of interest. This is particularly important for the gamma-ray spectra of uranium and plutonium where some of the peaks of interest are always superimposed on very large Compton backgrounds caused by higher energy gamma rays from the sample.

The small backscatter peak is caused by a Compton interaction with an electron at the surface of the detector where the recoil electron goes out of the crystal, depositing little or no energy, and the scattered gamma ray is absorbed in the detector through other interactions. This is the inverse of the event which leads to the Compton edge, that is, the gamma ray transfers the maximum energy to the electron, but the electron escapes and the backscattered gamma ray is absorbed. The equation for the energy of the backscatter peak is

$$E_{bs} = \frac{m_o c^2}{2 + m_o c^2/E_\gamma} \quad . \qquad (2.\ 1)$$

This has a maximum value of $m_o c^2/2 = 256$ keV. Because this is basically a surface effect, it is more prominent in small detectors.

2.2. Energy Calibration

As described above the pulse-height spectrum from a NaI or Ge(Li) detector is usually a series of photopeaks superimposed on a more or less smoothly varying background. The peak locations indicate gamma-ray energy. To determine the energy, the detector system must first be calibrated. For NaI and Ge(Li) detectors, the relation between gamma energy and output pulse height is nearly linear. Therefore, two known peaks of sufficiently different energy will serve to establish the energy calibration. Let E_1 and E_2 be the known energies of the peaks, and let X_1 and X_2 be the peak locations as measured in the pulse-height spectrum. The pulse height (X) can be a channel number from a multichannel analyzer spectrum, or it can be a threshold setting for a single-channel analyzer spectrum. The energy (E) associated with a pulse height (X) is then given by

$$\left.\begin{aligned} E &= mX + b \\ m &= (E_2 - E_1)/(X_2 - X_1) \\ b &= E_1 - mX_1 \end{aligned}\right\} \quad . \qquad (2.\ 2)$$

Figure 2.2 shows a NaI spectrum containing the 662-keV peak from ^{137}Cs and the 122-keV peak from ^{57}Co. This spectrum can be used to illustrate a sample energy calibration. This procedure can be used for NaI or Ge(Li), multichannel or single-channel electronics. Table 2.1 gives a short list of useful calibration sources and their energies.

2.3. Resolution

As mentioned above, the detector resolution characterizes the width of gamma-ray peaks in a measured spectrum. It is usually specified as the full width at half maximum (FWHM) for a particular gamma-ray peak. By convention, Ge(Li) detectors are usually characterized by the FWHM in keV at the 1332-keV line of ^{60}Co. Sodium iodide detectors are characterized by the relative width, in percent, of the 662-keV line of ^{137}Cs (i.e., resolution = 100 • (FWHM in keV)/662). Figure 2.3 shows an expanded view of the ^{137}Cs peak from Fig. 2.2 and illustrates a sample computation of NaI resolution. The indicated resolution at 662 keV is approximately 12%; the corresponding resolution at 122 keV is approximately 16%.

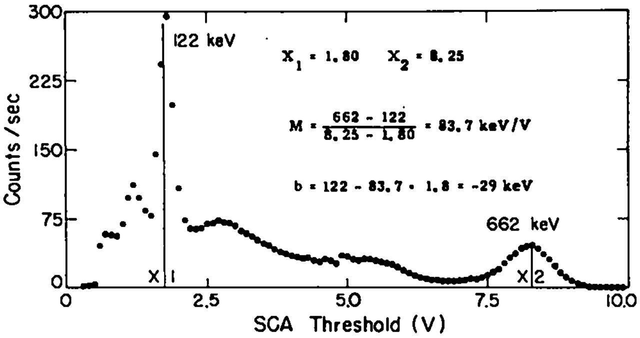

Fig. 2.2.
Energy calibration of a NaI detector system using ^{57}Co(122 keV) and ^{137}Cs (662 keV). The system is a 5.1-cm-diam by 1.3-cm-thick NaI and an Eberline SAM-II. The spectrum was acquired with the single-channel analyzer in the SAM-II by setting a narrow window and taking short counts at different threshold settings.

This crystal (5-cm-diam by 1.3-cm-thick) is chosen to optimize performance at 186 keV(^{235}U), and its resolution at 662 keV is only fair. A thicker crystal (5-7 cm) should be used for higher energy gamma rays (5-cm-diam by 5-cm-thick is about right for portable plutonium analysis). A good quality 7.6-cm-diam by 7.6-cm-thick detector will have a resolution of about 7% at 662 keV. Figure 2.4 shows the variation of resolution with energy for three different NaI detectors.

TABLE 2.1

GAMMA-RAY ENERGY CALIBRATION SOURCES

Source	Energy (keV)
^{241}Am	59.5
^{57}Co	122.0
^{235}U	185.7
^{203}Hg	279.2
^{22}Na	511.0
	1274.5
^{137}Cs	661.6
^{54}Mn	834.9
^{88}Y	898.0
	1836.1
^{60}Co	1173.2
	1332.5

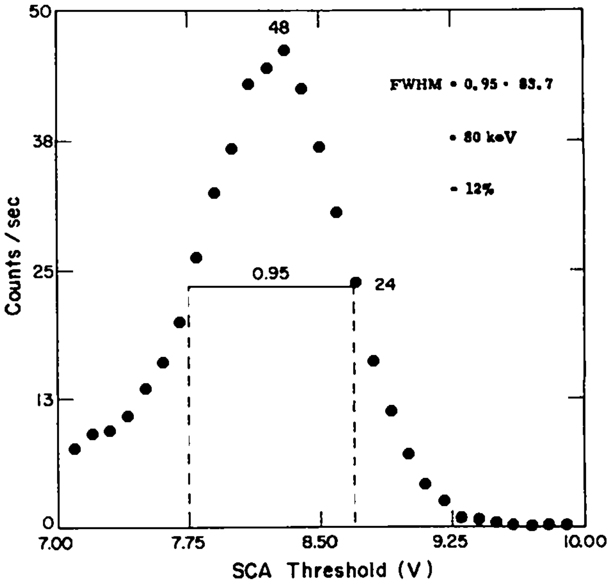

Fig. 2.3.
Expanded view of ^{137}Cs peak from Fig. 2.2 showing calculation of resolution for a 5.1-cm by 1.3-cm-thick NaI detector.

Resolution is a measure of a detector's ability to separate two gamma rays of similar energy. Two gamma rays separated by less than two resolution widths (FWHM) are usually not resolved. Under similar counting situations, a high-resolution detector will also have a better signal-to-background ratio.

The resolution of Ge(Li) detectors will be discussed in detail in Secs. 2.5 and 3.6. The following is a brief

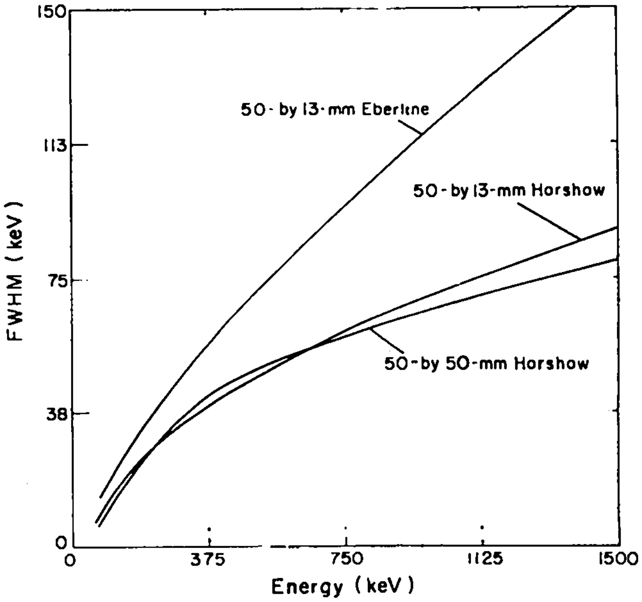

Fig. 2.4.
Resolution vs energy for three NaI detectors. Same electronics (SAM-II) used with each detector.

description of a convenient procedure for measuring the resolution of a Ge(Li) spectrometer system at 1332 keV. Once the system is operating properly, collect a spectrum from ^{60}Co. Adjust the multichannel analyzer conversion gain and digital offset so that about 800 channels separate the 1173- and 1332-keV lines from ^{60}Co. Now measure the positions of the two peaks (X_1,X_2) and the number of channels, FWHM = N_r, in the 1332-keV peak. The resolution (in keV) of the detector system is then $N_r \cdot 159/(X_2 - X_1)$. This procedure is illustrated in Fig. 2.5.

2.4. Efficiency

The efficiency of a counting system depends on a number of factors such as detector size and type and sample-to-detector distance. Several types of efficiency are commonly defined and care must be exercised to determine which type is being used in any specific instance. Three types of efficiency will be discussed here; the reader should concentrate on the definitions and not on the names because the names may vary from one writer to another.

2.4.a. Intrinsic Photopeak Efficiency

The intrinsic photopeak efficiency is the probability that a gamma ray which strikes the detector will produce a count in the corresponding photopeak, that is, the probability that it will deposit its total energy in the detector. Photopeak efficiency depends on the size, shape, and material of the detector in a complicated way. In general, it increases with detector size and decreases with gamma-ray energy. Figure 2.6 shows the variation of photopeak efficiency with energy for three different NaI detectors. A very rough estimate of photopeak efficiency can be obtained by using the following expression.

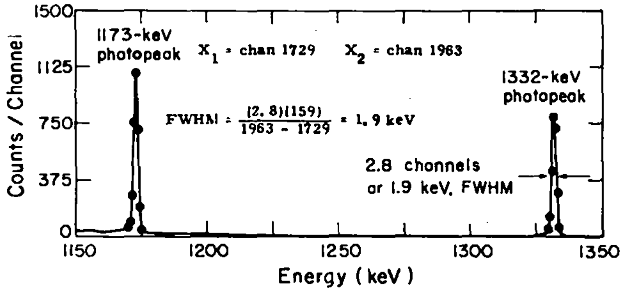

Fig. 2.5.
Measurement of Ge(Li) detector system resolution using ^{60}Co.

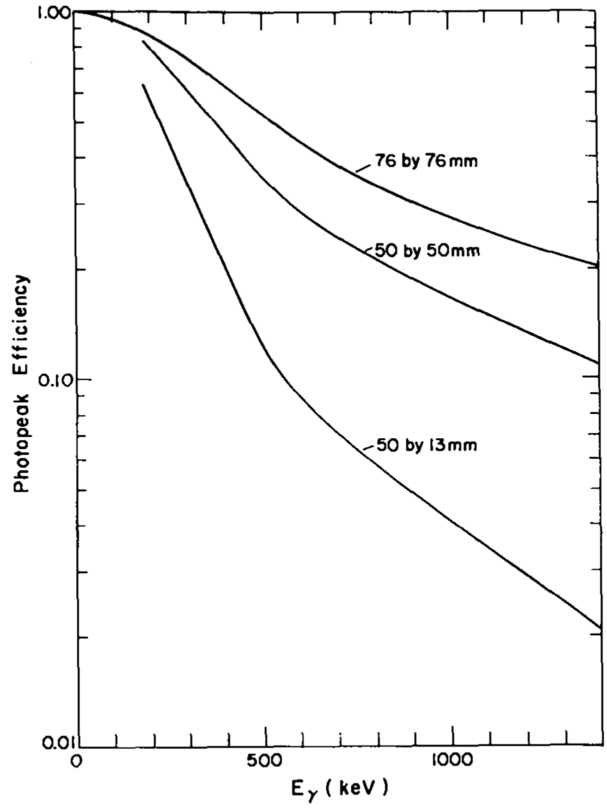

Fig. 2.6.
Photopeak efficiency vs energy for three different size NaI detectors.

$$\epsilon_p = 1 - e^{-\mu_\ell t} . \qquad (2.3)$$

ϵ_p = photopeak efficiency ,

μ_ℓ = linear attenuation coefficient of detector at energy of interest, and

t = thickness of detector .

This expression gives the fraction of incident gamma rays that interact in the detector. It will always give a number larger than the actual photopeak efficiency because all interactions do not result in full-energy deposition. When the photoelectric effect is a large part of μ_ℓ (e.g., NaI at 186 keV), Eq. (2.3) is reasonably accurate. It demonstrates the dependence of ϵ_p on gamma-ray energy and detector size. The photopeak efficiency of Ge(Li) detectors is also discussed in Sec. 3.5.

2.4.b. Absolute Efficiency

The absolute (or total) efficiency ϵ_T of a counting system is the probability that a gamma ray emitted from a point source at a particular source-to-detector distance will produce a count in the corresponding photopeak [Eq. (2.4)].

$$\epsilon_T = \frac{\text{photopeak count rate}}{\gamma\text{-ray emission rate}} \quad . \tag{2.4}$$

The absolute efficiency is the product of the probability that a gamma ray will strike the detector, and the probability that it will interact and produce an event in the photopeak. In general, it depends on the source-to-detector distance, the area of the detector visible to the source, and the intrinsic photopeak efficiency of the detector. Equation (2.4) can be restated as

$$\epsilon_T = \epsilon_g \cdot \epsilon_p \tag{2.5}$$

ϵ_g = probability of gamma ray striking detector, sometimes called the geometric efficiency.

The following is a discussion of ϵ_g.

Consider a point gamma-ray source of intensity I (γ/s) at the center of a sphere of radius r(cm). The number of gamma rays per second that pass through a unit area of the sphere is called the flux, F. Flux has units of gamma rays per unit area per unit time (γ/cm^2-s). Because the surface area of the sphere is $4\pi r^2$, F can be expressed as

$$F = I/4\pi r^2 \quad , \tag{2.6}$$

which says that the flux is proportional to $1/r^2$. The flux at a distance 2r from the source is one-fourth the flux at r; at 3r it is one-ninth the flux at r. This is called the inverse square law and it applies to all electromagnetic radiation, including gamma radiation.

Consider a detector area A positioned a distance r from a point gamma-ray source. The artifice of a point source (and sometimes a point detector) is conveniently used so that the source-to-detector distance can be specified as a single number. Real sources and detectors have finite extent, and in an exact treatment require an integration of these simple expressions over the extent of the source and detector. If the largest dimensions of the source and the detector are much smaller than the average source-to-detector distance, the expressions given here are very good approximations. If r is several times the detector diameter, the fraction of gamma rays striking the detector (ϵ_g) is given by

$$\epsilon_g = \frac{A}{4\pi r^2} \quad , \text{ where} \tag{2.7}$$

A = area of detector visible at the point source. This will be different from the frontal area of the detector if the detector is collimated or if the point source is located off the axis of the detector.

From Eq. (2.5), the absolute counting efficiency can now be expressed as

$$\epsilon_T = \frac{A \cdot \epsilon_p}{4\pi r^2} \quad , \text{ where} \tag{2.8}$$

ϵ_T = absolute (or total) efficiency ,

ϵ_p = photopeak efficiency ,

A = visible area of detector , and

r = source-to-detector distance .

The absolute efficiency is a function of counting geometry and intrinsic detector efficiency. The absolute efficiency determines the actual measured count rate for a given situation. The measured count rate (CR) is given by

$$CR = R \cdot \epsilon_T = \frac{R \cdot A \cdot \epsilon_p}{4\pi r^2} \quad ; \tag{2.9}$$

R = emission rate of source .

Consider the example given in Sec. 1.1.b (^{235}U positioned 10 cm from a 5-cm-diam by 1.3-cm-thick NaI crystal).

$$R = 4.3 \times 10^4\ \gamma/\text{g-s}$$

$$A = \pi(2.5)^2 = 19.6\ \text{cm}^2\ ,$$

$$r = 10\ \text{cm}\ .$$

The photopeak efficiency ϵ_p can be taken from Fig. 2.6 ($\epsilon_p \approx 0.7$), or it can be computed from Eq. (2.3).

$$\mu_\ell\,(186\ \text{keV}) = 1.3\ \text{cm}^{-1}\ ,$$

$$t = 1.3\ \text{cm}\ ,$$

$$\epsilon_p = 1 - e^{-1.3 \times 1.3} = 0.82\ .$$

Substituting these values into Eq. (2.9).

$$CR \approx \frac{(4.3 \times 10^4)(19.6)(0.82)}{4\pi\,(10)^2}\ \text{and}$$

$$CR \approx 550\ \text{counts/g-s}\ .$$

The ($\approx$) is used because of the many approximations in this discussion. (1) Equation (2.3) for ϵ_p is only a rough approximation. (2) A real sample will not be a point source and the detector diameter here is a significant fraction of the source-to-detector distance (r) so that Eq. (2.8) is only an approximation (reasonably good here). (3) No account has been taken of sample self-attenuation or gamma-ray attenuation in the can surrounding the detector. These considerations would lead to a count rate slightly lower than computed above. However, if applied with some understanding, these arguments and the associated expressions can yield useful estimates of expected count rate, often within 20% of the measured rate. For the more complex sample geometries usually encountered in nuclear material assay, Eq. (2.8) can, in principle, be integrated over the actual sample and detector to yield the absolute efficiency. This procedure is complicated and is subject to considerable error. For accurate work, it should not be used as a substitute for calibration with known standards. For measurements of odd geometries where a standard is not available (or even feasible), such as many process equipment holdup measurements, this type of computation may be the only calibration available.

2.4.c. Relative Efficiency

Relative efficiency is a term used mainly by the manufacturers of Ge(Li) detectors to specify their products. In principle it is the ratio (in percent) of the absolute efficiency (ϵ_T) of the Ge(Li) detector for counting the 1332-keV gamma ray from ^{60}Co at $r = 25$ cm to the absolute efficiency of a 7.6-cm-diam by 7.6-cm-thick NaI at the same source-to-detector distance. In actuality the comparison is usually to the calculated absolute efficiency of a standard NaI rather than a comparison with a real detector. This is discussed more fully in Sec. 3.5.

2.5. Types of Gamma-Ray Detectors

The two types of gamma-ray detectors presently in greatest use in fissionable material assay are sodium iodide or cesium iodide scintillation detectors and solid-state germanium detectors. The low detection efficiency of gas proportional detectors makes their use impractical except in high-flux environments. Similarly, the low detection efficiency of silicon solid-state detectors limits their usefulness primarily to x-ray detection. Although the relatively new CdTe semiconductor detectors may prove useful in nuclear safeguards applications in the near future, they are not in general use at this time. Chapter 3 contains more detailed information on the properties of semiconductor and scintillation detectors. For more information, the book *Applied Gamma-Ray Spectrometry*[2.1] is highly recommended. Several detector manufacturers have also published booklets on detector theory and operation.[2.2]

2.5.a Scintillation Detectors

A scintillation detector consists of a luminescent material, called a phosphor, optically coupled to a photomultiplier tube. The electrons produced by the interactions of gamma rays in the phosphor excite the atoms and molecules of the phosphor; the subsequent deexcitation results in the emission of fluorescent ultraviolet and visible light radiation.

The directions of the emitted light photons are random, therefore the phosphor is usually surrounded by a reflector to maximize the number of photons collected by the photosensitive cathode of the photomultiplier tube. The electrons emitted by the photosensitive cathode produce additional electrons by secondary emission within the photomultiplier and are eventually collected on the photomultiplier anode to produce an electrical pulse. This pulse generally undergoes amplification and shaping by some type of external electronic amplifier. If the final pulse height is proportional to the incident gamma-ray energy, the system can be used as a scintillation spectrometer.

Figure 2.7 shows a drawing of a typical scintillation detector. The most common scintillation detector in use for nuclear material assay is NaI. A complete scintillation spectrometer generally consists of a scintillation crystal-photomultiplier tube assembly (the detector), some type of electronic amplifier to amplify the photomultiplier pulses, a high-voltage source for the photomultiplier (usually 1000 to 2000 V is required), and some type of pulse-height analyzing circuitry. The complexity of the pulse-height analyzing part of the system ranges all the way from a simple scaler, that counts all of the pulses from the detector above some threshold level, up to a computer-controlled multichannel pulse-height analyzer. Portable systems useful for safeguards applications are now available commercially. The simplest of these systems has a detector and a small box containing a high-voltage power supply, amplifier, single-channel pulse-height analyzer, scaler, and timer. The unit may be powered from normal 110-V ac or a rechargeable battery pack. A slightly larger unit is also available that contains a second single-channel analyzer for background measurement, and stabilization circuitry to minimize the effects of temperature changes. (The light output of scintillators and the gain of photomultiplier tubes are both temperature sensitive.) The use of these instruments in practical assay applications will be discussed in a later section.

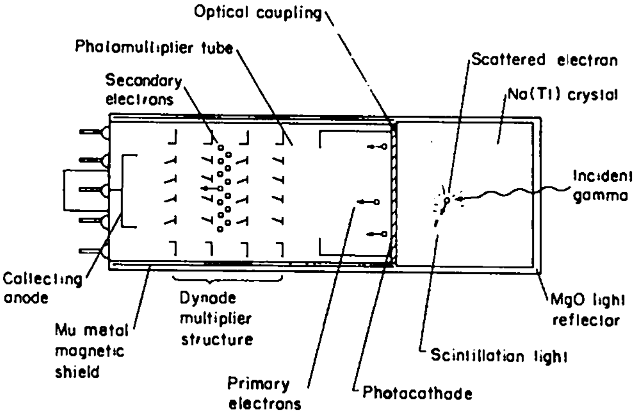

Fig. 2.7.
The scintillation detector.

2.5.b Semiconductor Detectors

The operating principle of semiconductor radiation detectors is completely different from that of scintillation detectors, although the end result is the same; namely, the production of an electrical pulse in response to interactions of nuclear radiation within the detector volume. A semiconductor detector can be thought of as the solid-state equivalent of a gas ionization detector. Interactions of nuclear radiation with the detector material give rise to free-charge carriers that are swept through the material by an applied electric field producing an electrical pulse.

The attractiveness of semiconductor detectors results from their improved energy resolution compared to scintillation detectors and from the increased stopping power for radiation of a solid compared to a gas. Basically, the reason for the improved energy resolution lies in the fact that less energy is required to produce a given number of free-charge carriers.

For simplicity, we assume that the energy resolution of a detector is determined solely by the statistical fluctuations in the number of charge carriers produced for a given energy deposition. In a semiconductor detector made from silicon or germanium, about 3 eV is required to produce one free-charge carrier (called an electron-hole pair); for a gas ionization detector, 30 eV is required to produce one electron-positive ion pair. Scintillation detectors suffer from the inefficient multistep scintillation process, and about 300 eV is required to emit one electron from the photocathode.

The total amount of charge liberated, Q, by the deposition of a given amount of energy, E, in a detector is given by

$$Q = (E/\epsilon)q \ , \qquad (2.10)$$

where ϵ is the energy required to produce a single-charge carrier (electron-hole pair, electron-positive ion pair, or photoelectron), and q is the charge of an electron. If the creation of charge carriers is purely random, then the standard deviation in the number of carriers produced, σ, is given by

$$\sigma = \sqrt{E/\epsilon} \ . \qquad (2.11)$$

A measure of the energy resolution obtainable is given by

$$\sigma/Q = \sqrt{\varepsilon/E} \cdot (1/q) \quad . \tag{2.12}$$

According to this simple theory, the resolution of a semiconductor detector should be about 10 times better than that obtainable from a scintillation detector. In fact, the improvement in resolution obtainable from semiconductor over scintillation detectors can be greater than suggested by the above argument because the fluctuation in the number of electron-hole pairs is less than given by Eq. (2.11). An additional degradation in the energy resolution of a scintillation detector is produced by small statistical fluctuations within the photomultiplier tube. Other factors affecting the energy resolution of germanium gamma-ray detectors are discussed in Chap. 3.

The semiconductor detector most commonly used today is the lithium-drifted germanium or Ge(Li) detector. These are available with resolutions of 1 keV or less for 186-keV gamma rays compared with 22 keV for the best NaI detector. The major disadvantage is that they must be maintained and operated at cryogenic temperatures and they require vacuum containment and liquid nitrogen cooling.

A complete germanium spectrometer consists of the same basic components as a scintillation spectrometer: detector, high-voltage power supply, pulse amplifier, and pulse-height analyzer. However, the pulse amplifying and pulse analysis equipment tend to be more complex to take advantage of the resolution capabilities of the detector. In particular, more effort goes into designing components of the system for high stability and low noise than is required for a scintillation spectrometer. A multichannel pulse-height analyzer is normally required for spectra analysis, rather than a simple single-channel analyzer, although in some safeguards applications such complexity is not required. Although the components of a germanium spectrometer are more complex, the interpretation of the data obtained by such a system is often simpler than from a scintillation spectrometer because its greater resolution considerably reduces problems caused by background radiation.

2.5.c. Ultrahigh Purity Germanium Detectors (UHP Ge)

If germanium crystals could be grown with sufficiently low impurity levels, the lithium-drift process would not be required to produce good detectors. Such material has become available within the last few years, and small planar detectors fabricated without using the lithium ion drift process are now available from at least three commercial sources. These detectors are available with sensitive volumes up to about 1 cm^3, and are used primarily for x-ray and low-energy gamma-ray detection. The ultrahigh purity germanium required for such detectors is still very expensive, which is the main reason that larger detectors are not presently being produced commercially. However, reports show that UHP Ge detectors have been fabricated in various laboratories with volumes in the 10 to 30-cm^3 range.

UHP Ge detectors need not be stored at low temperatures as do Ge(Li) detectors, which is a distinct advantage in many situations. However, UHP Ge spectrometers must be operated at low temperatures (usually LN$_2$) to sufficiently reduce leakage currents. They are therefore packaged in the same manner as Ge(Li) detectors, and their operation from the user's point of view is the same except for one important point—forgetting to fill the LN$_2$ dewar will not result in damage to a detector worth several thousand dollars! A note of caution, however—avoid applying bias voltage to a UHP Ge detector at room temperature because it may damage the preamplifier.

REFERENCES

2.1. F. Adams and R. Dams, *Applied Gamma-Ray Spectrometry*, (Pergamon Press, Inc., NY, 1970). This book contains a wealth of information on gamma spectrometry. The first three chapters cover gamma-ray emission and interaction, and the properties and characteristics of scintillation and semiconductor detectors. Chapter 5 deals with associated detector instrumentation. The appendixes include many useful tables, graphs, and spectra [e.g., x-ray absorption edges and emission energies (table); NaI gamma-ray spectra (over 250 actual pulse-height spectra); Ge(Li) spectra (over 200); intrinsic efficiencies of NaI detectors (tables); and tables of gamma-ray energies]. This is a useful reference for the gamma assayist.

2.2. "Harshaw Scintillation Phosphors," (Harshaw Chemical Company, Solon, Ohio, 1962); and "Ge(Li) Handbook," (Princeton Gamma-Tech, Inc., Princeton, NJ, 1970), 3rd Ed. These are semipromotional monographs published by two commercial detector manufacturers. However, they contain very readable, simple descriptions of detector properties, sample spectra, resolution, efficiency, and operation.

3. GAMMA-RAY DETECTORS II

Chapter 2 discussed general characteristics of gamma-ray detectors. This chapter discusses in detail the specific properties of the alkali-halide scintillation detectors and germanium semiconductor detectors. The subjects discussed include detector materials, construction, and operation. This is information for the nuclear assayist who desires more background material about the detectors in use. Most of this material will not be covered in the formal course, but can be used as a source of reference.

3.1. Scintillator Materials

The phosphor used in a scintillation detector may be organic or inorganic. Organic phosphors may be crystals, such as anthracene, plastics, or liquids. Inorganic phosphors are usually alkali-halide crystals, such as NaI and CsI, in which luminescent centers have been activated by impurities, such as Tl, introduced into the crystal lattice. Other inorganic materials, such as ZnS and certain types of glass, are also useful scintillator phosphors.

Details of the actual fluorescent processes occurring in the phosphor will not be given here. However, one property of the fluorescent process worth noting is that the intensity of light emission decays exponentially as a function of time. The intensity of the light from a single scintillation event therefore decays from an initial value I_0 according to $I = I_0 \exp(-t/\tau)$. The time constant τ is a specific property of each scintillator, with typical values ranging from 10^{-9} to 10^{-6} s. The wavelength spectrum of the emitted light also varies between phosphors. To obtain efficient collection of the emitted light, it is important that the phosphor be transparent to its emitted light. Zinc sulphide does not satisfy this condition; for this reason, ZnS scintillators are usually very thin, or consist of ZnS powder dispersed in a transparent medium, such as plastic. The emitted spectrum should also correspond to the sensitive wavelength range of the photomultiplier photocathode, which is normally in the near ultraviolet-to-blue range of the spectrum.

Table 3.1 lists the properties of some of the more common scintillator phosphors. Organic scintillators are not commonly used for gamma-ray detection because of their small photoelectric absorption coefficients. Sodium and cesium iodide activated with thallium are particularly well suited for gamma-ray detection. The photoelectric absorption coefficients are reasonably large, and their scintillation efficiencies are at least as good as the best organic scintillator, anthracene. A disadvantage of these scintillators is their long time constants, which are highly temperature-dependent.

Thallium-activated sodium iodide is the most widely used scintillator for gamma-ray spectrometry. Sodium iodide is a clear cubic crystal that can be grown to large sizes. Because the material is quite

TABLE 3.1

PROPERTIES OF SOME COMMON SCINTILLATOR PHOSPHORS

Scintillator	Emission Spectrum Maximum (Å)	Time Constant (μs)	Density (g/cm^3)	Scintillation Efficiency Relative to Anthracene
NaI(Tl)	4200	0.25	3.67	2.1
CsI(Tl)	5650	1.1	4.51	1.0
CsI(Na)	5650	1.0	4.51	1.7-1.8
CaF_2(Eu)	4350	0.9	3.18	0.7-1.1
Anthracene	4400	0.032	1.25	1.0
Plastics	3500-4500	0.002-0.005	1.06	0.2-0.5
Liquids	3500-4500	0.001-0.01	0.86	0.2-0.5

hygroscopic, all machining and polishing must be done in a dry atmosphere, and must be sealed in airtight containers. Sodium iodide (thallium) crystals may be obtained from several manufacturers in sealed cans with glass windows for coupling to photomultiplier tubes, or the crystal face may be coupled directly to the photomultiplier tube. Such crystals may be obtained in virtually any configuration desired. Although single crystals with linear dimensions larger than about 25 cm are very expensive, cylindrical crystals 60 cm in diameter and larger have been produced.

Next to NaI(Tl), CsI(Tl) is probably the most used inorganic scintillator for gamma-ray detection. Owing to its higher Z and slightly higher density, the gamma-ray attenuation of this material is about 1.5 times greater than an equivalent size NaI(Tl) scintillator. Cesium iodide is not hygroscopic, and can therefore be more easily machined and packaged than NaI. It is also softer and more plastic than NaI, and can withstand severe mechanical shocks and large temperature gradients. Cesium iodide (thallium) is considerably more expensive than NaI(Tl), so that its general use is not justified economically. However, in instances where higher detection efficiency for a fixed size or resistance to thermal or mechanical shock is an important consideration, this material may be preferable to NaI(Tl) in spite of its increased cost.

A promising scintillator made commercially available within the last few years is sodium-activated cesium iodide. It has good light output, is much less hygroscopic, and is usable at higher temperatures than NaI(Tl). However, it is also more expensive.

Europium-activated calcium fluoride scintillators are also used to some extent. These crystals have many properties that provide advantages over other commonly used scintillators for x-ray and charged-particle detection, but the material's lower Z is a distinct disadvantage for gamma-ray detection. Other scintillator materials, such as zinc sulphide, lithium iodide, glass, and boron compounds, are utilized for the detection of alpha particles and neutrons but are not generally useful for gamma-ray detection.

3.2. Scintillation Light Collection

The light collection on the photomultiplier tube photocathode should be as efficient as possible. For this reason, the scintillator is usually surrounded by a reflector, and one side is optically coupled to the glass of the photomultiplier. In some cases a light guide between the scintillator and photomultiplier, usually consisting of polished plastic rods or strips, may be required. The photocathode must be sensitive in the wavelength region emitted by the scintillator, and should be uniformly sensitive over its area. Within the photomultiplier tube, the electrons emitted from the photocathode must be collected onto the multiplying elements, called dynodes. The photomultiplier tube should be encased in a magnetic shield to reduce the effects of stray magnetic fields upon the electrons emitted from the photocathode.

The most commonly used reflecting materials are aluminum metal, magnesium oxide, and alumina. The particular material used depends upon the particular scintillator configuration, and is usually a compromise between light collection efficiency and convenience.

The design of the can surrounding the scintillator depends upon the particular application and to some extent upon the scintillator material. Sodium iodide (thallium), for example, requires a moisture-proof can whereas CsI(Tl) does not. For gamma-ray spectrometry, it is generally desirable to minimize the mass of the can to reduce distortions in the pulse-height spectrum caused by gamma-ray interactions in the can material. Aluminum is usually used for the cans around NaI(Tl) and Cs(Tl), although stainless steel is sometimes used in applications requiring more rugged construction. Cans with thin beryllium entrance windows are frequently used in applications involving the detection of beta particles or low-energy x rays. Another major consideration in the choice of can material is the problem of radioactive contamination, particularly in very low-level counting applications. In applications requiring very low backgrounds, aluminum should be avoided because it invariably contains trace amounts of radium and uranium. However, backgrounds induced by the can material are generally not a problem in safeguards applications.

The purpose of the optical coupling between the scintillator and photocathode is to reduce the light loss that would normally occur by reflection from the scintillator-glass interface. To be effective in this respect, the material used to join the scintillator to the phototube should have a lower refractive index than the window of the phototube. Transparent fluids such as mineral or silicone oils are frequently used as the coupling medium. A clear silicone grease, such as Dow Corning C-2-0057, is preferred because it does not flow out of the interface. In some applications, a clear epoxy is used to join the scintillator to the phototube; however, the resulting rigid interface leads to possible thermal expansion problems.

The photomultiplier tube is the component of scintillation detectors that has undergone the greatest improvement in the last decade or so. Present-day photomultiplier tubes have highly sensitive and uniform photocathodes and relatively low thermionic noise.

3.3 Semiconductor Detector Materials

For a material to be useful as a solid-state ionization detector, it must be possible to collect the charge produced by the interacting radiation. Furthermore, there must be no large leakage currents in the material as a result of applying the electrical field required to collect the charge. The collection of the charge carriers requires that they not interact with atoms in the crystal during the time required for them to be swept to the collecting electrodes. Consequently, the collection time must be small compared to the lifetime of the charge carriers. This condition is met only in nearly perfect nonmetalic crystals.

The above requirement places severe limitations on the materials that can be used to fabricate solid-state ionization detectors. Table 3.2 lists the properties of some successfully used materials. Silicon and germanium single crystals are the only available materials with the required high purity for routine fabrication of high-quality detectors. Because of its higher atomic number, germanium is preferred over silicon for gamma-ray detection. Research for using higher Z materials for gamma-ray detectors is being pursued actively. Cadmium telluride is presently the most promising material, although only relatively small detectors can be successfully fabricated now because of charge carrier trapping problems. However, such detectors have found applications in nuclear medicine because of the high gamma-ray sensitivity obtainable in a small volume. The possible use of CdTe in some safeguards applications is also being investigated.

The following discussion will be limited to germanium gamma-ray spectrometers constructed from lithium-drifted germanium, Ge(Li), or ultrahigh purity (intrinsic) germanium.

TABLE 3.2

PROPERTIES OF SOME SEMICONDUCTOR DETECTOR MATERIALS

Property	Si	Ge	GaAs	CdTe
Atomic number	14	32	32[a]	50[a]
Density	2.33	5.33	5.32	5.86
Dielectric constant	12	16	---	---
Energy per hole-electron pair (eV)	3.6	2.9	4.5	4.6

---

[a] Effective Z.

3.4. Lithium-Drifted Germanium Detectors—Ge(Li)

To understand why the lithium ion drift process is used, it is necessary to explore briefly the effects of impurities present in the germanium crystal. For the present discussion, impurities may be classified as being either "donors" or "acceptors," depending upon whether they have more or fewer valence electrons than germanium.When a valence electron of germanium is excited into the conduction band of the crystal, it leaves behind a "hole" in the valence band. Both the electron and the hole propagate through the crystal until they are neutralized in some manner. In a solid-state detector, such neutralization occurs by collecting electrons on a positively charged electrode and injecting electrons into the holes from a negatively charged electrode. The effect of donor impurities is the trapping of holes, and the effect of acceptors is the trapping of electrons. A major requirement for a material to be useful as a solid-state detector is its ability to collect the charge carriers, therefore the concentration of "uncompensated" donor or acceptor impurities must be extremely low.

Germanium (and silicon) crystals can be grown that are very pure except for a low concentration of uniformly distributed acceptor impurities. The trapping centers that result from these acceptor impurities may be compensated for by using a mobile donor impurity that migrates to these trapping centers, thereby neutralizing them by donating their own free electrons. Lithium, a very fast diffuser in silicon and germanium, is used for this purpose. An almost exact compensation of the semiconductor material is achieved by using the lithium ion drift process.

The lithium-drift process will not be discussed here because it is an involved process, and in many respects is still more of an art than a science.

One disadvantage of Ge(Li) detectors is that they must be stored at low temperatures (-20°C or below) to prevent the lithium ions from thermally diffusing thereby producing uncompensated regions in the crystal. Germanium (lithium) detectors left at room temperature for any appreciable time will no longer function. In most instances, if a detector is warmed up for a short time, repairs can be made by lithium redrifting. Redrifting can be done by the detector manufacturer for about 25%, or less, of the price of a new detector. The usual procedure is to store and operate Ge(Li) detectors at the boiling temperature of liquid nitrogen (—196°C at sea level, and approximately —206°C at Los Alamos), which has the advantage of drastically reducing leakage currents in the detector.

Lithium-drifted germanium detectors are normally housed in a vacuum-insulated stainless steel cryostat that resides in a liquid nitrogen (LN_2) storage dewar. Occasionally, the detector cryostat is an integral part of the dewar. An aluminum cap usually covers the germanium crystal. The crystal is affixed to a copper "cold finger" that extends from the end of the cryostat into the liquid nitrogen. Several different crystal geometries are available for different applications.

Detectors are commercially available with volumes ranging from 100 mm^3 or less up to about 100 cm^3. Good quality detectors with volumes greater than about 50 cm^3 are still difficult to produce and are therefore expensive. The factors that presently limit detector size are the availability of large germanium crystals sufficiently pure and defect-free, and problems associated with drifting lithium ions to depths greater than 1 to 1.5 cm (drift depths of ~2 cm are achievable, however).

Detectors are described as being planar, true coaxial, or wrap-around coaxial, depending upon how the lithium-drift process is carried out. In planar-type detectors, lithium is diffused into one face of a germanium slab, usually cut from a cylindrical crystal, and drifted into the material from that face. The face into which lithium was diffused is used as one electrode (positive) and the other face as the other (negative) electrode. In coaxial geometries, lithium is diffused into the sides of the crystal, usually a right circular cylinder. Wrap-around, or closed end, coaxial detectors are made by also diffusing lithium into one crystal face. After the lithium-drift process, a small core of uncompensated germanium protrudes through one or both faces of the crystal, and is used as the negative electrode of the detector. Only the compensated part of the crystal is useful for detecting radiation (referred to as the sensitive volume), therefore it is desirable to minimize the size of the uncompensated core present in coaxial crystals, and the amount of uncompensated material left at the rear face of a planar detector. At present, detectors with volumes greater than 1 to 5 cm^3 are coaxial, with the larger ones usually being the wrap-around type. In safeguards applications, wrap-around coaxial detectors with volumes of the order of 25 to 50 cm^3 are generally appropriate. Using larger detectors in such applications is not justified economically.

3.5. Detection Efficiency

Although early Ge(Li) detectors suffered from low detection efficiency (as do presently available UHP Ge detectors) because of their small size, the larger detectors presently available compare favorably with the smaller sodium iodide detectors. For example, a 5- by 5-cm Ge(Li) detector with an active volume of 90 cm^3 has about two-thirds the intrinsic full-energy peak detection efficiency of a 5- by 5-cm NaI(Tl) detector at 1.33 MeV. Manufacturers normally specify detection efficiency in terms of the absolute efficiency of a 7.6- by 7.6-cm NaI(Tl) detector for the 1.33-MeV gamma ray from a point ^{60}Co source located 25 cm from the detector face. In actual practice, no such comparison is made, but rather the absolute efficiency of the Ge(Li) detector in question is measured for a ^{60}Co source of known strength located 25 cm from the face of the germanium crystal, and the result is multiplied by 8.33×10^4 to obtain the percent efficiency relative to a 7.6- by 7.6-cm NaI(Tl). Such a relative efficiency value for the 90-cm^3 Ge(Li) described above would be about 20%; for a 30-cm^3 detector, it would be around 5%.

For high-efficiency germanium spectrometry, it is not only necessary that the sensitive volume be large, but an optimum shape is also required. A thick detector with a small frontal area will be less efficient than a thinner detector of the same volume having a greater area. In safeguards applications, one usually is interested in detecting the 186-keV gamma rays from ^{235}U or the 414-keV gamma rays from ^{239}Pu, which does not require a detector thickness greater than 2 to 3 cm. The loss in total absolute detection efficiency that would result from using a 30-cm^3 Ge(Li) detector (2-cm-thick) rather than a 50-cm^3 detector (4-cm-thick) is about 17% for 186-keV gamma rays and about 37% for 414-keV gamma rays, but the saving in cost is almost a factor of two. The use of a thinner detector also reduces the background from high-energy gamma rays, as, for example, from the 1-MeV gamma ray occurring in ^{238}U; the total detection efficiency of a 2-cm-thick Ge(Li) detector is about one-half of that of a 4-cm-thick detector at 1 MeV.

Figure 3.1 shows the absolute efficiency of a typical large-area 30-cm^3 Ge(Li) detector as a function of energy. The sharp drop-off in efficiency

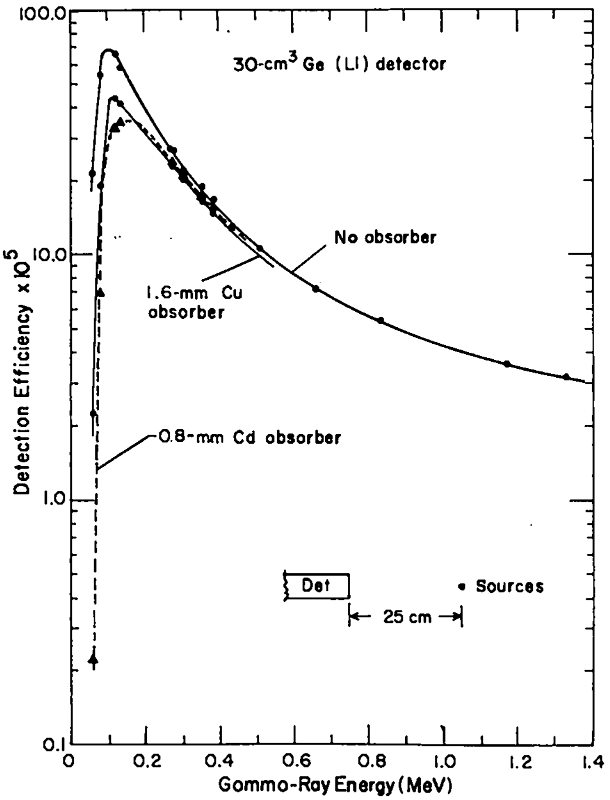

Fig. 3.1.
Absolute efficiency vs energy for 30-cm^3 Ge(Li) detector.

below 100 keV results from absorption in a thin (0.3- to 0.5-mm) "dead layer" on the detector surface that results from the lithium-drift process. In small planar detectors designed for use at energies below 100 keV, this dead layer is removed. In plutonium measurement, a thin cadmium absorber is usually placed in front of the detector to attenuate the 59-keV gamma rays from ^{241}Am. The effect of such an absorber is also shown in Fig. 3.1; a 0.8-mm cadmium absorber reduces the 59-keV detection efficiency by a factor of 100, but only reduces the detection efficiency at 414 keV by about 3%.

3.6. Energy Resolution

The energy resolution obtainable with semiconductor detectors depends not only on the statistical variation in the number of electron-hole pairs collected, but also on the noise generated in the detector and by subsequent pulse amplifiers. Obviously these noise sources must be reduced to a minimum. For the detector, noise reduction is mainly a matter of reducing the surface leakage current by proper surface treatment during the manufacturing process. Amplifier noise is produced primarily by leakage currents and capacitance at the input of the first amplifier stage (the preamplifier), which may be reduced by proper design of the system. All presently available preamplifiers designed for use with solid-state detectors use field-effect transistors (FET's) as the first amplifying element; these devices introduce less noise into the system than standard transistors or vacuum tubes. In very high-resolution systems, the FET used in the preamplifier is mounted inside the detector cryostat and cooled to near LN$_2$ temperature. This not only reduces leakage currents within the FET, but also reduces stray capacitance. Another, often overlooked factor affecting energy resolution is gain instabilities in the pulse amplifying or processing equipment. The resolution obtainable from a detector-amplifier system should be considered as a whole, because a noisy preamplifier will severely degrade the performance of a good detector, and vice versa.

The energy resolution attainable when all noise sources are eliminated is important because it provides the theoretical limit of the resolving power of germanium detectors. For this limit to be approached, it is also necessary that there be negligible loss of charge carriers in the detector due to trapping and recombination. The "theoretical limit" of detector resolution has become less, over the last few years, as better quality germanium crystals have become available—detector systems are now available commercially that have resolutions better than the theoretical limit of 5 or 6 yr ago!

The effects that various noise sources have on system resolution are determined largely by pulse shaping within the amplifier. For scintillation detectors, the main need for pulse shaping in the amplifier is to reduce pile-up effects. For solid-state detectors, an additional consideration is the effect of pulse shaping on the overall system resolution. The pulse shaping networks act as frequency filters, and because different noise sources have different frequency spectra, a network can be chosen, in principle, that will give optimum resolution for a particular system. In practice, the type of pulse shaping network used is a compromise between such factors as noise reduction, pile-up effects, ease of implementation, overload recovery, and in some cases time resolution. The type of shaping network now used in most good quality linear amplifiers designed for solid-state detectors is referred to as Gaussian or modified Gaussian. This type of network produces a fairly symmetrical pulse, has good overload recovery characteristics, and is close to an ideal filter for the types of noise spectra associated with most solid-state detector-preamplifier combinations. The shaping time constants used range from 1 to 10 μs, with the shorter time constants generally used with the larger coaxial detectors and the longer time constants used with small planar detectors at low count rates. As the counting rate increases, it is usually advantageous to decrease the pulse-shaping time constant to reduce pile-up effects. With most linear amplifiers, from three to five different time constants can be selected by a front panel switch.

Most present-day linear amplifiers incorporate what are called "pole-zero" cancellation networks and base line restoration networks. These networks are adjustable, to some extent, either by front panel or internal controls, and their adjustment procedures are described in the manual supplied with the amplifier. The proper adjustment of these networks can greatly improve system resolution at high count rates.

Energy resolution of a detector system is normally expressed in terms of the full width at half height (or half maximum) of a full energy peak, and is abbreviated FWHM. The unit of measure may be either electron volts (eV) or kiloelectron volts (keV). The FWHM of a full energy peak from an ideal (noiseless) detector is directly related to the standard deviation in the number of charge carriers produced. Equation (2.11) shows that this quantity is proportional to the square root of the incident gamma-ray energy. One would therefore expect, for an ideal detector, that a fourfold increase in energy would result in a twofold increase in the full-energy peak FWHM. In practice, the FWHM will increase more slowly at low energies due to the presence of noise that sets a lower limit on the attainable FWHM, and may increase more rapidly at energies above ~500 keV due to charge carrier trapping.

Trapping of charge carriers is readily apparent from the detector's pulse-height spectrum. If trapping is present, the full-energy peaks become asymmetric on the low-energy side. This peak asymmetry, or "tailing," tends to decrease and the peak positions shift upward in the spectrum as the detector bias is increased. Complete charge collection stabilizes the peak shape and position. As the detector bias is increased beyond the point required for complete charge collection, the peaks will eventually begin to broaden due to increased leakage currents. A prerequisite for a good detector is that leakage currents be negligible at the bias level required for complete charge collection. Good detectors generally exhibit constant resolution over an operating voltage range of several hundred volts. Germanium detectors are normally operated at bias voltages that produce fields in the detector of 150 to 200 V/mm, at which point the charge carrier velocities saturate at about 2×10^7 cm/s.

Figure 3.2 shows the FWHM of two good-quality Ge(Li) detectors, one an 80-cm^3 coaxial and the other a 1-cm^3 planar, plotted against the square root of the energy of the full-energy peak. The FET used in the preamplifiers associated with both detectors was cooled to near LN$_2$ temperature. The higher capacitance and surface leakage currents associated with the large detector limit its minimum attainable FWHM to about 800 eV, compared to about 300 eV for the small detector.

Detector manufacturers normally specify the FWHM attainable with particular detector-preamplifier combinations at one or two energies. For small planar detectors, the FWHM is usually specified for the 122-keV ^{57}Co gamma ray, and for the 5.9-keV ^{55}Fe x ray if the detector is intended for use at low energies. The FWHM of coaxial detectors is specified for the 1.33-MeV ^{60}Co gamma ray, and usually for the 122-keV ^{57}Co gamma ray. The FWHM measured at 122 keV normally ranges from about 500 eV for high-quality planar detectors up to 1.5 keV or more for large coaxial detectors with room-temperature preamplifiers. The FWHM at 1.33 MeV may range from about 1.6 keV for very good detectors up to 3 keV or more for poor detectors. For most nuclear safeguards applications, a FWHM at 122 keV of 1.2 keV or less and a FWHM at 1.33 MeV of 2.3 keV or less is usually sufficient. Note that coaxial detectors with resolutions less than 2.0 keV at 1.33 MeV generally cost about 15-20% more than similar detectors with resolutions in the vicinity of 2.2 to 2.5 keV.

Many detector manufacturers also specify the full width at one-tenth maximum (FW0.1M) resolution

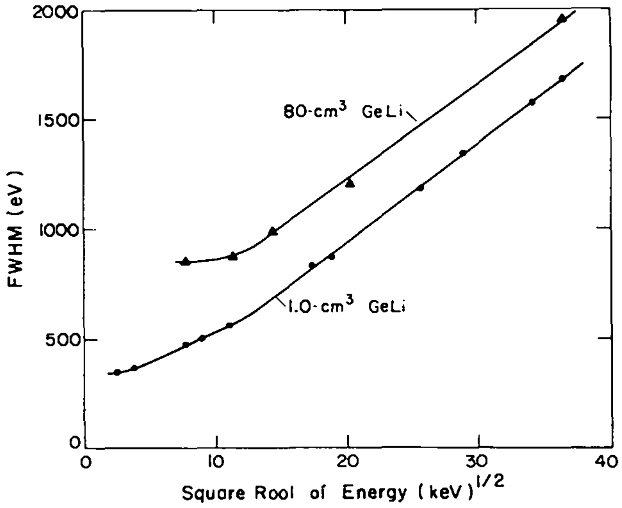

Fig. 3.2.
Resolution vs energy for two Ge(Li) detectors.

obtained at 1.33 MeV as a measure of any peak tailing present caused by incomplete charge collection. The value of the FW0.1M/FWHM ratio for a detector with minimal charge collection problems will be 1.85 to 1.90; ratios greater than 2.0 indicate noticeable tailing of full-energy peaks, which should generally be avoided. Some detector experts advocate using the FW0.05M or even FW0.01M resolution as a more sensitive indicator of peak tailing, but these quantities are more difficult to measure. For an ideal detector, the value of FW0.05M/FWHM is 2.079; values in the range 2.1 to 2.3 are obtainable with good detectors.

4. ANALYSIS OF GAMMA-RAY PULSE-HEIGHT SPECTRA

As previously discussed, the electrical pulses produced by scintillation and solid-state spectrometers are proportional to the energy deposited in the detector by ionizing radiation. A multichannel pulse-height analyzer is generally used to digitize the pulses from such spectrometers. The pulse-height analyzer (PHA) typically contains between 100 and 4100 channels, each channel corresponding to a small range of pulse heights. For example, in a 2000-channel PHA having an input pulse-height range of 0 to 10 V, each channel would correspond to a 10/2000-V or 5-mV range of input pulses. The number of pulses that occur with heights falling within the range of each channel is stored in an electronic memory within the PHA. A plot of the number of events, or counts, stored in each channel vs the channel number produces what is termed a pulse-height spectrum.

A PHA is typically an expensive, nonportable instrument. An alternative method for measuring gamma-ray pulse-height spectra involves the use of a single-channel analyzer (SCA). This is less expensive and is available in portable instruments; however, it is a tedious and time-consuming procedure and can be used only with scintillation detectors (NaI). An SCA accepts the amplified detector pulse and determines if it is within a preset pulse-height range. This range (or window) corresponds to a single channel of a PHA or multichannel analyzer. When a detector pulse is within the selected energy window, the SCA issues an output pulse which is usually fed to a scaler. A pulse-height spectrum can be measured in the following way: set the energy window for a small ΔE (e.g., if amplifier range is 0 to 1 V, set $\Delta E = 0.01$ V), set the threshold (E) at 0 and take a short count, record the resulting scaler value, increase the threshold setting and take another count, continue until the upper limit of the threshold control is reached, and, finally, plot the scaler counts vs threshold setting. The resulting plot will be identical to that which would be obtained with a 100-channel analyzer; however, it will have taken at least 100 times as long to collect.

The pulse-height spectra obtained from gamma-ray spectrometers generally contain a series of peaks superimposed on a smoothly varying background. The peaks represent gamma rays that have deposited all of their energy in the detector; their positions are a measure of the gamma-ray energies, and the areas under the peaks (above background) are a measure of the gamma-ray intensities. The peak widths are a measure of the system energy resolution, as described previously.

Pulse-height spectra obtained from a 30-cm^3 Ge(Li) detector and a 7.6- by 7.6-cm NaI(Tl) detector exposed to plutonium gamma rays are shown in Fig. 4.1. The superior energy resolution obtainable with a Ge(Li) spectrometer is clearly evident in Fig. 4.1; the Ge(Li) pulse-height spectrum is a much better representation of the incident gamma-ray energy spectrum than the NaI(Tl) spectrum. A Ge(Li) pulse-height spectrum from an enriched uranium sample is shown in Fig. 4.2. For comparison, Fig. 4.3 is a NaI-SCA spectrum of enriched uranium.

In general, the analysis of such pulse-height spectra consists of determining the peak positions for energy measurement and the peak areas for intensity measurement. The gamma-ray intensities, and therefore the peak areas, are directly proportional to the amount of material producing the gamma rays (ignoring, for the moment, absorption within the sample). Only the areas of selected strong peaks are usually of interest in assay measurements. For ^{235}U assay the area under the 185.7-keV peak is normally used. The 413.7-keV peak (and sometimes the 375-keV peak) is used for ^{239}Pu determination. The 186-keV peak from ^{235}U is reasonably well resolved in a NaI(Tl) pulse-height spectrum. Plutonium gamma rays are clearly not well resolved by a NaI(Tl) spectrometer, as shown in Fig. 4.1. Although NaI(Tl) detectors can be (and indeed are) used for plutonium assay, background determination is more difficult than with Ge(Li), particularly if varying amounts of ^{241}Pu are present.

A simple, yet fairly general, method of determining photopeak areas will now be described. The method is applicable to PHA data, or to data obtained from scalers connected to single-channel analyzers. Figure 4.4 shows a portion of a pulse-height spectrum containing a single photopeak. The area under the peak, P, may be obtained by summing the contents of the channels as shown in the figure. The background under the peak can be approximated by a straight line, shown dashed in the figure. Groups of channels lying on each side of the peak may be averaged to estimate the background. If n_1 channels are used on the low side of the peak, n_2 channels are used on the high side, and n

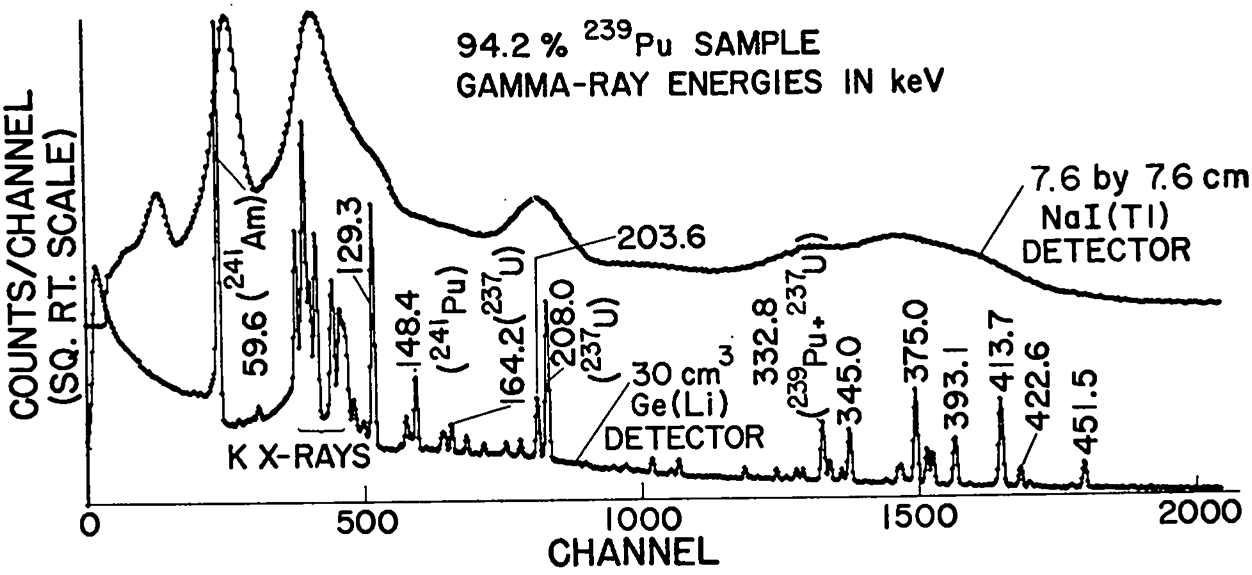

Fig. 4.1.
Comparison of plutonium gamma-ray spectra from 30-cm^3 Ge(Li) detector and 7.6- by 7.6-cm NaI detector. Note the square root scale.

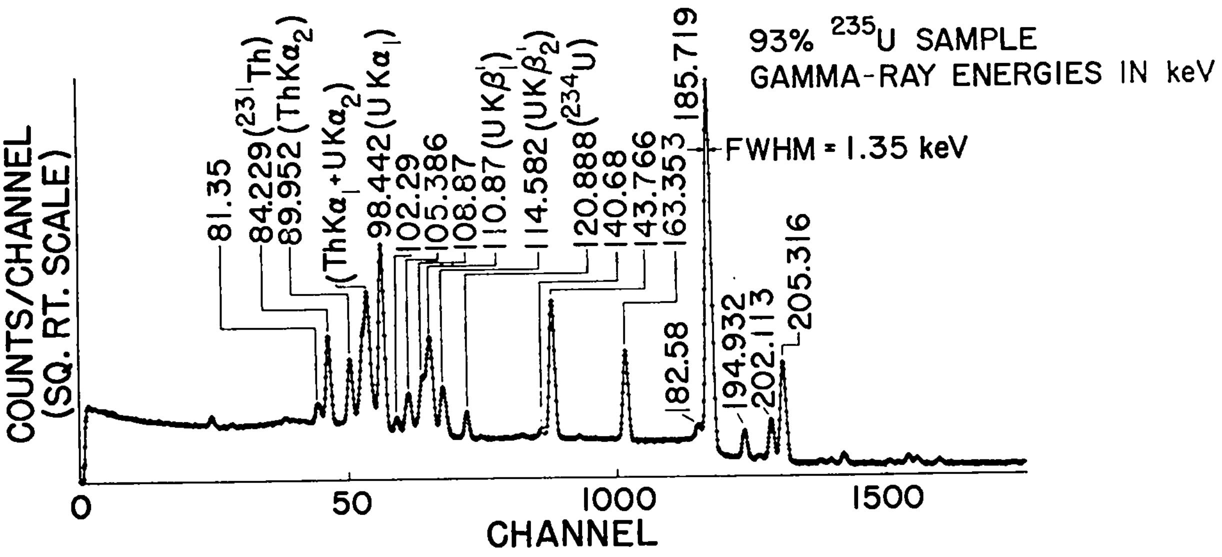

Fig. 4.2.
Enriched uranium gamma-ray spectrum as measured with a high-resolution Ge(Li) detector.

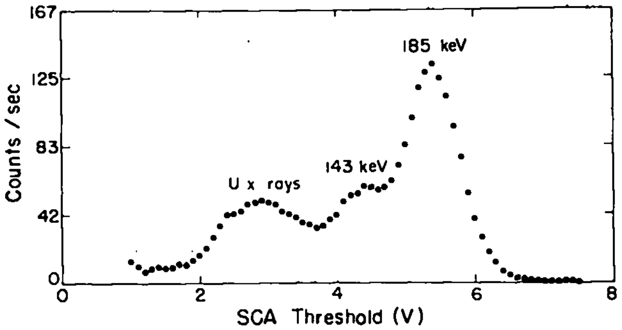

Fig. 4.3.
Enriched uranium gamma-ray spectrum as measured with a NaI detector. Data were taken with SCA in SAM-II.

channels are used in the peak, then the background is given by

$$B = (n/2) \cdot (B_1/n_1 + B_2/n_2) \ . \qquad (4.1)$$

The peak area corrected for background is then given by

$$\boxed{\begin{array}{ll} A = P - (n/2) \cdot (B_1/n_1 + B_2/n_2) & (4.2) \\ A = P - (n/2n_1) \cdot (B_1 + B_2), \text{ if } n_1 = n_2 & (4.2a) \\ A = P - (B_1 + B_2) \text{ if } n_1 = n_2 = n/2 \ . & (4.2b) \end{array}}$$

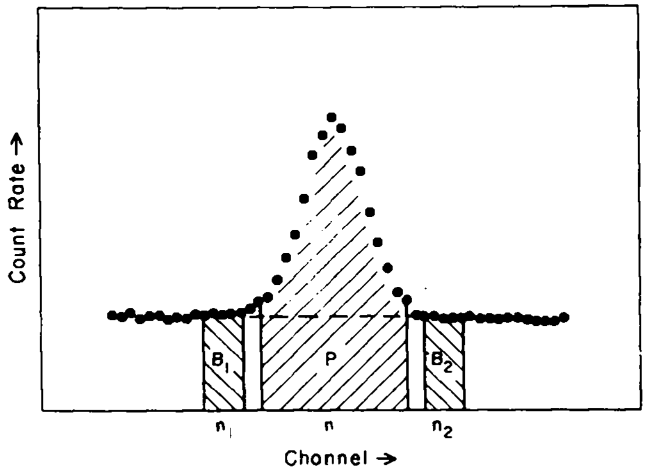

Fig. 4.4.
Pulse-height spectrum of single photopeak illustrating general procedure for determining photopeak area. The area of interest is above the dashed line which is determined from B₁ and B₂.

If the slope of the straight line background is essentially constant for a particular set of measurements, then channels on one side of the peak only can be used for the background determination. The peak area would then be given by

$$A = P - (n/n_1) \cdot (k \cdot B) \ , \qquad (4.3)$$

where k is a factor that corrects for the background slope (k = 1 for a "level" background) determined from an appropriate calibration. This situation is illustrated in Fig. 4.5.

This "two-window" procedure is commonly used with NaI-SCA instrumentation. For this, one SCA window is set over the peak and the other is set slightly higher in energy. Scalers attached to the SCA's measure P and B, respectively. If only one SCA-scaler combination is available, two separate counts can be made at different threshold settings. The net peak area then becomes

$$\boxed{A = P - (k \cdot B)} \ , \qquad (4.3a)$$

where k is determined during the system calibration.

When the photopeak area has been determined, the statistical uncertainty of the measured area is also of interest because this gives an estimate of the measurement precision. The standard deviation in the number of counts N registered by a nuclear radiation detector is given by $\sqrt{N}$. Therefore the standard deviation in P, the peak area uncorrected

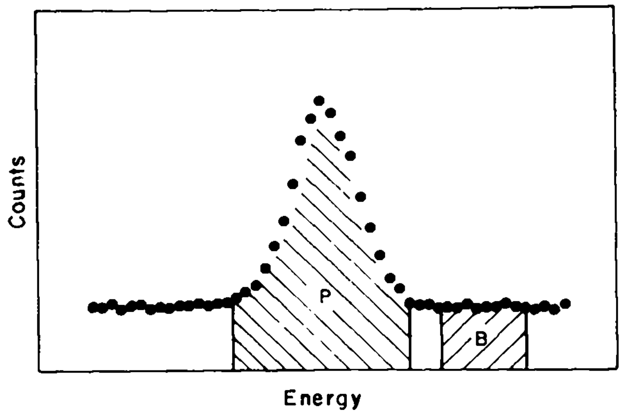

Fig. 4.5.
Pulse-height spectrum of single photopeak illustrating two-window method for determining photopeak area. This is the most common procedure for NaI-SCA measurements.

for background, is given by $\sqrt{P}$. Without proof, the standard deviation of the measured background is given by

$$\sigma(B) = (n/2) \cdot \sqrt{B_1/(n_1)^2 + B_2/(n_2)^2} \ , \qquad (4.4)$$

and the standard deviation in A [calculated from Eq. (4.2)] is given by

$$\sigma(A) = \sqrt{\sigma^2(P) + \sigma^2(B)}$$

$$\boxed{\begin{aligned} \sigma(A) &= \sqrt{P + (n/2)^2 \cdot \left[B_1/(n_1)^2 + B_2/(n_2)^2\right]} && (4.5) \\ &= \sqrt{P + (n/2n_1)^2 \ (B_1 + B_2)} \quad \text{if } n_1 = n_2 && (4.5a) \\ &= \sqrt{P + B_1 + B_2} \quad \text{if } n_1 = n_2 = n/2 && (4.5b) \end{aligned}}$$

The standard deviation associated with the two-channel method for SCA's [Eq. (4.3a)] is

$$\sigma(A) = \sqrt{P + k^2 B} \ . \qquad (4.6)$$

Two things should be noted from Eq. (4.5).

1. The precision of a measurement can be improved by using more PHA channels or larger SCA windows to determine the background,

2. The precision in the measurement of a small peak situated on a large background will be poor, because $\sigma(A)/A$ will be large. In 1, the number of channels used for background measurement should be limited to the immediate vicinity of the photopeak of interest so that other peaks are not included. As an example of 2, assume that the following values have been measured.

$P = 15\ 000$,

$B_1 = 7500$,

$B_2 = 6000$, with

$n = 10$,

$n_1 = n_2 = 5$.

Then from Eq. (4.2b) the peak area is

$$A = 15\ 000 - (7500 + 6000) = 1500 \ .$$

The standard deviation of A is given by

$$\sigma(A) = \sqrt{P + B_1 + B_2} = 168.8 \ .$$

The estimate of the measurement precision of A is $\sigma(A)/A$, or about 11%. However, the quantity P, the peak area uncorrected for background, was measured with an estimated precision of about 1%! [$\sigma(P)/P = \sqrt{15\ 000}/15\ 000 = 0.008$.] The precision of the measurement in this case could have been improved only slightly by using twice as many channels to determine the background. For example, if

$B_1 = 15\ 000$,

$B_2 = 12\ 000$, and

$n_1 = n_2 = 10$,

then

$$\sigma(A)/A = \sqrt{P + (1/2)^2 \cdot (B_1 + B_2)}/A$$

$$= 147.5/1500 = 0.098 \ ,$$

or about 10%. A further discussion of counting statistics is given in Appendix B.

The foregoing method of photopeak analysis assumes that the photopeak of interest is well resolved from neighboring peaks. However, for poorly resolved multiple peaks due to gamma rays arising from the decay of the same isotope, this technique could be used to determine the total area of the peaks for an assay measurement. For unresolved peaks arising from different isotopes, an assay could be performed on the combined isotopes using this method, but not on the individual isotopes unless additional information was available from another measurement.

More general methods of analysis have been developed to analyze poorly resolved spectra. Such methods are usually not required in safeguards assay of plutonium and uranium, and will not be discussed here. When more extensive analysis is required, it is usually performed by an on-line computer system.

5. QUANTITATIVE GAMMA-RAY ASSAY

5.1. Introduction

The general procedure for gamma-ray assay is outlined in Eq. (5.1).

$$\boxed{M = \frac{CR \cdot CF}{K}} \quad , \tag{5.1}$$

where

M = mass of isotope of interest ,

CR = measured count rate from signature of isotope ,

CR = correction factor for sample attenuation , and

K = calibration factor (corrected counts per gram) .

The calibration factor (K) is determined by measuring a known standard. This can be represented by inverting Eq. (5.1).

$$\boxed{K = \frac{CR_s \cdot CF_s}{M_s}} \quad , \tag{5.2}$$

where

M_s = known mass of emitting isotope in standard ,

CR_s = measured count rate from standard , and

CF_s = correction factor for attenuation in standard .

The standard essentially provides a measurement of the detector efficiency, the specific activity of the signature of interest, and the effects of sample geometry (size, shape, and sample-to-detector distance). These equations assume that the standard is the same shape and is measured in the same position as the unknowns. If not, corrections must be applied for the effect of different sample-to-detector distances. The above ideas may be stated simply, but the assayist needs a good understanding of the many factors involved to apply them correctly. The following is a list of important factors to be considered when attempting gamma-ray assay of fissionable material.

1. Gamma-Ray Signatures. The assayist must know the energies and intensities of the relevant gamma rays. These place fundamental restrictions on the sensitivity, precision, and accuracy of any assay. This information is listed in Table 1.1 and Appendix A. The important formulas are

$$N(t) = N(0)\, e^{-\lambda t} \quad . \tag{1.1}$$

where

$$\lambda = 0.693/t_{\frac{1}{2}} \text{(half-life)} \quad ;$$

$$R = \frac{1.32 \times 10^{16}}{A\, t_{\frac{1}{2}}} \; (\gamma/\text{g-s}), \; t_{\frac{1}{2}} \text{ in years} \tag{1.4}$$

2. Detectors and Gamma-Ray Spectra. A qualitative understanding of detector properties and the general appearance of pulse-height spectra are necessary to interpret the output data. This is discussed in Chaps. 1 and 2. The material in Sec. 2.1 (especially Fig. 2.1) is of particular importance.

3. Spectral Peak Stripping and Background Subtraction. These are the basic procedures for extracting information from the measured spectrum. The assayist must be very familiar with the material in Chap. 4, especially the application of Eqs. (4.2)-(4.6), which include the two-window SCA procedure.

$$A = P - (k \cdot B) \quad , \tag{4.3a}$$

where

A = net counts ,

P = counts in peak SCA ,

B = counts in background SCA ;

$$\sigma(A) = \sqrt{P + k^2 B} \; . \qquad (4.6)$$

4. Detector Efficiency and the Inverse Square Law. This is covered in Sec. 2.4. Section 5.2 contains further discussion of how $1/r^2$ affects gamma-ray assays. The important formulas here are

$$\epsilon_p \approx 1 - e^{-\mu_\ell t} \quad \text{photopeak efficiency,} \; (2.3)$$

where

t = detector thickness , and

μ_ℓ = detector attenuation coefficient ,

$$\epsilon_T = \frac{A \cdot \epsilon_p}{4 \pi r^2} \quad \text{absolute efficiency ,} \; (2.8)$$

where

A = visible detector area .

5. Attenuation of Gamma Rays. The discussion in Chap. 1 is reemphasized and extended in Sec. 5.3. The assayist should be able to make simple computations of attenuation and should know the values of some important mass attenuation coefficients. The important formulas are

$$I = I_o e^{-\mu_\ell L} \; , \qquad (1.5)$$

where

$\mu_\ell(\text{cm}^{-1})$ = linear attenuation coefficient ;

$$\mu_m = \frac{\mu_\ell}{\rho} \; , \qquad (1.6)$$

where

$\mu_m(\text{cm}^2/\text{g})$ = mass attenuation coefficient .

6. Attenuation Correction Factors. The attenuation correction is probably the most important factor in Eq. (5.1), and will be discussed in detail in Sec. 5.4.

5.2. Gamma-Ray Assay and the Inverse Square Law

The inverse square law of gamma-ray flux was discussed in Sec. 2.1. The basic formula for absolute efficiency for a point source is given as

$$\epsilon_T = \frac{A \cdot \epsilon_p}{4 \pi r^2} \; , \qquad (2.8)$$

where

A = visible detector area ,

ϵ_p = detector photopeak efficiency , and

r = source-to-detector distance .

Most samples for fissionable material assay are extended sources, so that r and ϵ_T vary from one point to another on the sample. This means 1 g of uranium may yield different count rates depending on its location within the sample. Consider the cross section of a 55-gal drum (diam = 60 cm) illustrated in Fig. 5.1. One gram of material in position 2 counts 4 times as much as in position 4. If all samples were uniform, this variation of response (count rate) with position would be unimportant. Because many samples are not uniform (particularly the waste stored in 55-gal drums), this represents a potential source of error that can be minimized. This can be accomplished by increasing the sample-to-detector distance, but only at the expense of count rate. If the detector in Fig. 5.1 were 120 cm from the drum edge, the ratio of count rates between position 2 and position 1 would be $(150/120)^2 = 1.56$, but the overall count rate would

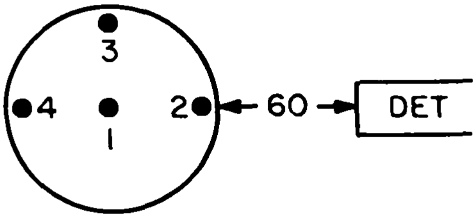

r_1 = 90 cm	$CR_1/CR_1 = (90/90)^2 = 1$
r_2 = 60	$CR_2/CR_1 = (90/60)^2 = 2.25$
r_3 = 95	$CR_3/CR_1 = (90/95)^2 = 0.90$
r_4 = 120	$CR_4/CR_1 = (90/120)^2 = 0.56$

Fig. 5.1.
Illustration of count rate variation with position in 55-gal drum.

have dropped to nearly one-third that at 60 cm. A better procedure is to rotate the sample. Consider the following diagram.

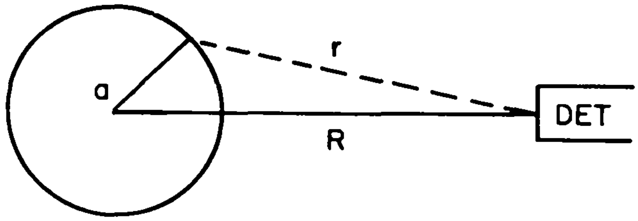

The ratio of the average response of a source rotating on the radius (a) to the response at the center is

$$\frac{CR(a)}{CR(0)} = \frac{1}{1 - (a/R)^2} \quad . \qquad (5.3)$$

Table 5.1 lists this function for several values of a/R. By rotating the sample, the maximum count rate variation in Fig. 5.1, due to position, is reduced from 2.25 to 1.125 with no loss in overall count rate. Therefore, whenever possible, the sample should be rotated to minimize the potential error caused by nonuniform distributions of material within the sample. Rotation minimizes the effect of radial variations. If the sample is taller than it is wide, the vertical variation must be considered also. This is illustrated in Fig. 5.2 where L = 1/2 height of container and n • L = distance from detector to center of container. The maximum variation is reduced to 10% with a sample-to-detector distance of 3L.

TABLE 5.1

THE EFFECT OF SAMPLE ROTATION ON COUNT RATE VARIATION

a/R	CR(a)/CR(0) Rotating	CR(R-a)/CR(R) Not Rotating
1/2	1.33	4
1/3[a]	1.125	2.25
1/4	1.067	1.78
1/5	1.042	1.56
1/6	1.029	1.44
1/7	1.021	1.36

---

[a] This is the case illustrated in Fig. 5.1.

In general, the choice of sample-to-detector distance is a compromise between minimizing the response variation and maintaining an adequate count rate. A general guideline can be given as follows. The maximum count rate variation with position is less than ±10%, if the distance between the center of the sample and the detector is equal to or greater than three times the larger of the dimensions a or L (radius or 1/2 height) and if the sample is rotated.

$\frac{\Delta CR}{CR} \leq 10\%$ if R ≥ 3a or 3L, whichever is larger, where a radius of sample and L = ½ height and the sample is rotated. This applies to $1/r^2$ variations only. (5.4)

If the sample cannot be rotated, it should at least be counted in two orientations 180° apart. Usually there will be little need to increase the sample-to-detector distance beyond this because of considerations of sample attenuation which will usually be the largest source of count rate variation. A source at the center of the sample will experience a larger attenuation than will a similar source near the edge. This effect cannot be minimized by increasing the sample-to-detector distance. In most samples it will be the domi-

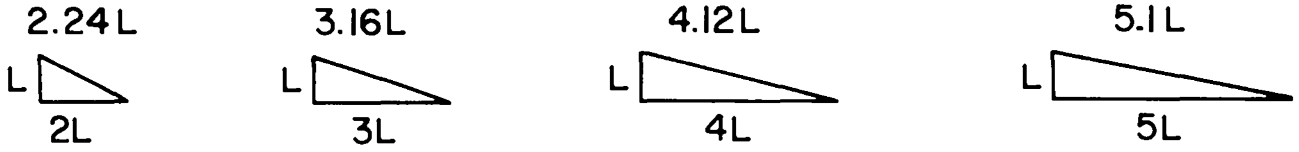

$\frac{CR(2.24)}{CR(2)}$ 0.8 $\frac{CR(3.16)}{CR(3)}$ 0.90 $\frac{CR(4.12)}{CR(4)}$ 0.94 $\frac{CR(5.1)}{CR(5)} = 0.96$

Fig. 5.2.
Maximum vertical count rate variation as function of sample-to-detector distance.

nant effect, so sample-to-detector distances larger than indicated by the above discussion and Eq. (5.4) are usually of little value.

5.3. Gamma-Ray Attenuation

Figure 5.3 is a graph of mass attenuation coefficient vs energy for a selected range of elements. It contains nearly all the qualitative attenuation information necessary for performing gamma-ray assay. Several important features should be noted. Between 1 and 3 MeV, the mass attenuation coefficients of all elements are equal within ~ ±20%; the average value is about 0.05 cm^2/g. In this region, Compton scattering is the dominant process. If nature had equipped the isotopes of interest with an intense gamma ray in this range, gamma assay would be much easier. Unfortunately only ^{238}U is so equipped. At lower energies the coefficients of the high-Z elements of interest become much larger than those of the lower Z materials, reaching values about 20 times higher near the K-absorption edge of uranium. These large differences make quantitative assay by low-energy gamma rays difficult or even impossible. The mass absorption coefficients of uranium and plutonium are nearly six times larger at 186 keV than at 414 keV. This means the gamma assay of ^{235}U is subject to a greater potential error than the assay of ^{239}Pu due to the higher self-absorption of the 186-keV gamma ray. The region between 80 and 120 keV is usually not useful for assay measurements because of the K x rays of uranium and plutonium. Below 80 keV most attenuation coefficients increase rapidly, making attenuation problems unmanageably severe for most cases. Nearly all uranium and plutonium assay is done with gamma rays between 100 and 1000 keV.

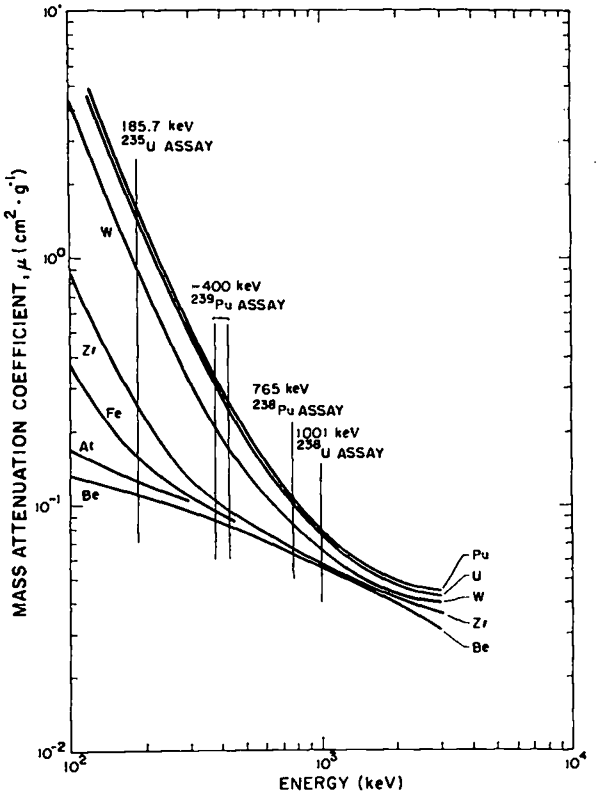

Fig. 5.3.
Mass attenuation coefficient vs energy for selected elements. The energies of several important assay lines are indicated on the graph.

5.4. Attenuation Corrections

The correction for sample attenuation is probably the most important factor in gamma-ray assay. For this text the attenuation correction factor (CF) is defined by the following expression.

$$CF = \frac{CR(\mu = 0,\ \text{no attenuation})}{CR(\text{actual observed count rate})} . \qquad (5.5)$$

This expression is symbolic. CF cannot be computed from Eq. (5.5) because $CR(\mu = 0)$ cannot be measured directly. The product CR • CF [see Eq. (5.1)] is sometimes called the "corrected count," that is, the count rate which would be measured in the absence of attenuation. As defined, the correction factor has a minimum value of one. Experience has shown that the maximum value that can be determined with reasonable accuracy (±5%) is about five. It should be emphasized that CF = 5 is a large correction implying that only 20% of the gamma rays of interest escape from the sample. Large values of CF imply high potential for error. Sample nonuniformities become more troublesome as CF increases.

The basic assumption for all gamma assay is that *the mixture of uranium or plutonium and matrix material* (everything other than uranium or plutonium in the sample) *is reasonably uniform, and the uranium or plutonium particles are small enough to ignore self-attenuation* within the emitting particles. It is difficult to define "reasonably uniform," but some rough guidelines can be discussed. If the individual particles of uranium or plutonium have significant self-attenuation, the assay results will be low unless special procedures are used to correct for this. (These procedures are beyond the scope of this text;

they are also imperfect and impractical for most portable instrumentation.) The self-attenuation of the individual particles can be estimated from the following formula.

$$CF = \frac{\mu x}{1 - e^{-\mu x}} \tag{5.6}$$

$$CF \approx 1 + \mu x/2 \quad \text{if } \mu x \le 1 \tag{5.6a}$$

$$CF \approx \mu x \quad \text{if } \mu x \ge 3 \,, \tag{5.6b}$$

where

μ = linear attenuation coefficient of emitting material,

x = mean linear dimension of particle and the approximations (a,b) are good to 5%.

The actual particles are irregular shapes and their size is not usually well known, so it is difficult to compute the self-attenuation exactly. This formula should only be used to estimate the order of magnitude of the particle self-attenuation. Figure 5.4 illustrates the variation of self-attenuation with particle size for uranium and plutonium. Small particles can have significant self-attenuation, particularly uranium. A 130-μ particle of uranium oxide will absorb 10% of the 186-keV gamma rays emitted by ^{235}U within the particle. Larger particles, such as fuel pellets, are even worse. A 1-cm pellet of UO_2 requires a correction factor of about 15 [$\mu x \approx$ (1.5 cm^2/g) (10 g/cm^3)(1 cm) = 15] for the 186-keV gamma ray. A similar plutonium recycle pellet would require a correction factor of about 2.5 for the 414-keV gamma ray. If such pellets were in a container of low-density combustible waste (rags, gloves, Kimwipes, etc.), they would not meet the requirement of reasonable uniformity. HTGR-coated particles come close to meeting the requirement, but assay results will still be 5-10% low if corrections are not made for particle size. Pure powders (PuO_2, UO_2, U_3O_8, etc.) do meet the requirement as do certain well-mixed powder scrap materials such as most incinerator ash. Small quantities of powder mixed with combustibles may meet the requirement if the powder is distributed uniformly in the matrix and is not in lumps.

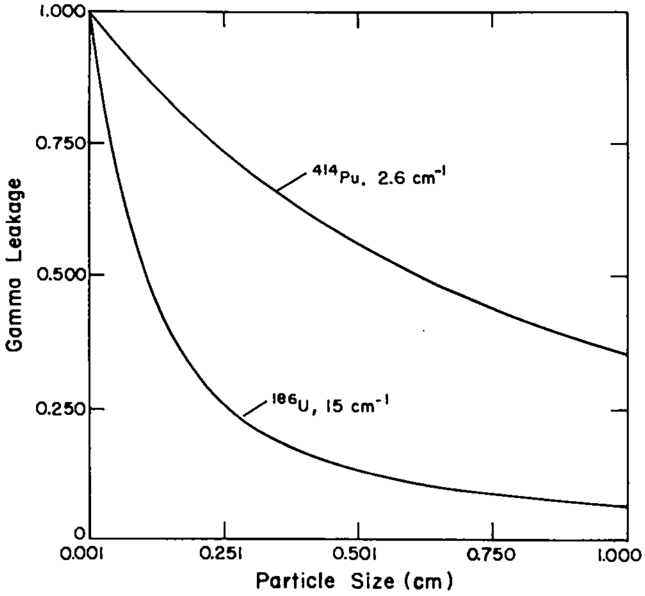

Fig. 5.4.
Self-attenuation vs particle size.

The above discussion illustrates some of the basic problems of gamma-ray assay. There are some techniques that allow less stringent uniformity conditions, but these are beyond the scope of this text and the capability of portable instrumentation. To perform gamma-ray assay with any assurance of accuracy, the assayist must know that the samples meet the basic assumption of uniformity. In favorable cases, accuracies of ±5% (one sigma) are readily obtainable; however, for samples that depart far from uniformity, measurements can be low by a factor of two or more. The remainder of this chapter will discuss common ways of computing the attenuation correction factor and will give several examples of specific assay problems.

5.4.a. Correction Factor Expressions

Equations (5.7) list several common expressions for the correction factor.

$$CF = \frac{\mu D}{1 - e^{-\mu D}} \quad \text{slab} \tag{5.7a}$$

$$CF = \frac{\pi/4 \mu D}{1 - e^{-\pi/4 \mu D}} \quad \text{cylinder} \tag{5.7b}$$

$$CF = e^{+\mu L} \quad \text{absorber} \tag{5.7c}$$

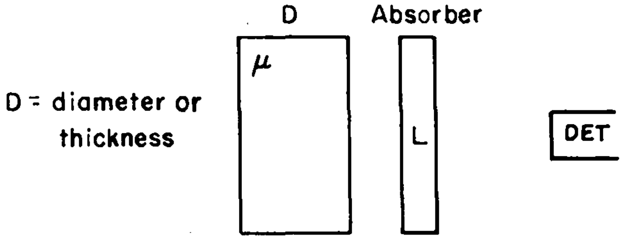

The slab formula [Eq. (5.7a)] is an exact expression for the case where the sample-to-detector distance is very large compared with the dimensions of the source and the detector (this is sometimes called the far-field approximation). It is used for rectangular samples (plates, boxes, air filters, etc.) viewed parallel to a side (usually through the thin dimension). The expression works well even for fairly small sample-to-detector distances (one or two times the sample thickness). Equation (5.7b) is a nearly exact expression for cylindrical samples. It has the same form as Eq. (5.7a) with μD replaced by $\pi/4\ \mu D$ ($\pi/4 = 0.785$). This expression works well even when the detector is only 1 diam from the edge of the sample. Both Eq. (5.7a) and Eq. (5.7b) are plotted in Fig. 5.5. Equation (5.7c) is merely the fundamental law of gamma attenuation and is used for absorbers placed between the sample and the detector. This expression would be applied to the walls of the sample container. For this case, the total correction factor would be the product of Eq. (5.7a) or Eq. (5.7b) times Eq. (5.7c).

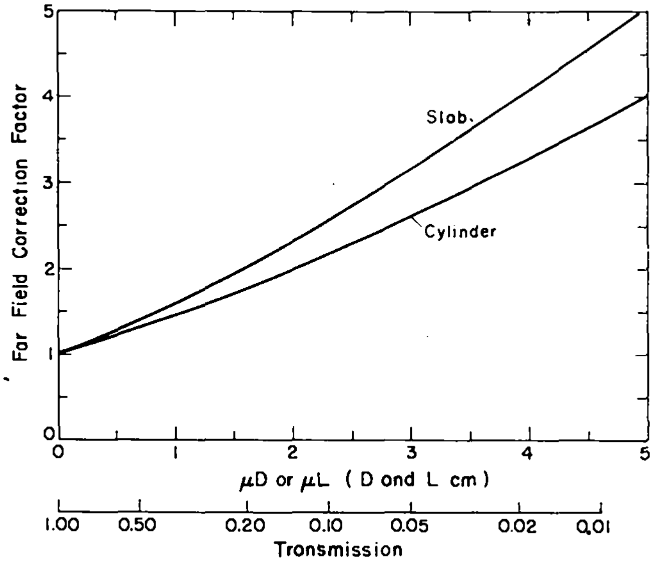

Fig. 5.5.
Attenuation correction factor vs μD, T for slab and cylinder.

In general, these expressions are approximate but accurate, particularly for use with high-resolution detectors. For NaI they usually overestimate CF due to the effects of small-angle scatters in the sample, as discussed in Chap. 1. In many cases, μD can be determined by an external source transmission measurement as described in the next section. At other times (for equipment holdup and large waste containers) μD is estimated from knowledge of the sample and CF is computed directly from the appropriate expression above.

5.4.b. Transmission-Corrected Gamma-Ray Assay

Consider the situation pictured in Fig. 5.6. The sample is placed between the detector and an external gamma-ray source. I_0 is the measured intensity of the source with no sample, and I is the intensity with the sample in place. The transmission, T, is defined as

$$T = I/I_0 \ , \tag{5.8}$$

that is, the fraction of gamma rays from the source which penetrates the sample with no change in energy. From the fundamental attenuation relationship [Eq. (1.5)],

$$T = e^{-\mu D} \ . \tag{5.8a}$$

The correction factor equations [Eqs. (5.7)] can be rewritten in terms of T.

$$\boxed{\begin{array}{ll} CF = \dfrac{-\ln T}{1 - T} & \text{slab} \\[2ex] CF = \dfrac{-\pi/4 \ln T}{1 - T^{\pi/4}} & \text{cylinder} \end{array}} \ . \qquad \begin{array}{r} (5.9a) \\[2ex] (5.9b) \end{array}$$

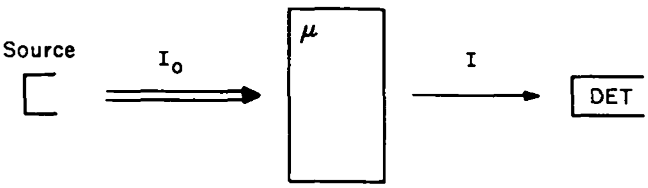

Fig. 5.6.
Diagram of a transmission measurement.

Figure 5.5 shows a plot of CF vs T. For T greater than 0.2, CF is less than 2.0 and doesn't change rapidly. This is a favorable range for assay work. For T less than 0.2, CF rises rapidly and the possibility of error increases. Measured transmissions become less accurate when T is less than 10%. For careful work with high-resolution detectors, transmissions as low as ~0.5% (CF ~5.3) can be measured with confidence. Caution is advised when measuring transmissions below 10% with NaI.

Table 5.2 lists some of the common transmission sources. Equations (5.9a) and (5.9b) assume that the transmission is measured at the same energy as the assay gamma ray. As indicated in Table 5.2, transmission and assay energies may be different, in which case a correction must be applied for the difference in attenuation between the two energies. This correction usually involves some knowledge of the composition of the sample. The relation between the transmissions at the two energies is given by

$$T_a = T_t^{\alpha} , \tag{5.10}$$

where

a refers to assay energy ,

t refers to transmission energy , and

$\alpha = \mu_a/\mu_t$.

The measured transmission is raised to the μ_a/μ_t power before substitution into Eqs. (5.9). Consider the assay of ^{239}Pu (414 keV) contaminated incinerator ash using ^{137}Cs (662 keV) as a transmission source. As in Chap. 1, this mixture can be treated as two components, one having the attenuation properties of oxygen and the other having those of plutonium. Equation (1.8) is then used to calculate the composite attenuation. Table 5.3 illustrates the change in $\alpha(\mu_a/\mu_t)$ with the plutonium weight fraction. Most incinerator ash will be less than 10% plutonium by weight, so $\alpha = 1.27$ might be picked as an average value for the measurements. If a wider range of weight fractions is encountered, it may be necessary to perform an iteration (that is, pick a trial F_{Pu}, calculate the mass of plutonium, calculate F_{Pu} from this value and the sample net weight, recompute the mass of plutonium, etc.).

The choice of a transmission source is frequently limited by the equipment and sources available. Uranium or plutonium is usually available, and neither of them requires any energy correction as above. There are, however, three bad aspects of their use: they require a double measurement (with and without source) to compensate for the activity in the sample; at low transmissions this requires the subtraction of two large and nearly equal numbers, the result of which usually has a low statistical precision; and, finally, the high self-attenuations of uranium and plutonium make it difficult to get high-intensity sources. Sources such as ^{169}Yb and ^{75}Se are usually chosen for use with high-resolution detectors. These are near enough to the assay energy to consider $\alpha = 1$. NaI requires the use of uranium or plutonium or sources such as ^{22}Na and ^{137}Cs which are of sufficiently different energy as to reduce the interference with the plutonium gamma rays.

TABLE 5.2

COMMON TRANSMISSION SOURCES

Assay Isotope	Assay Energy (keV)	Transmission Source	Assay Energy (keV)
^{235}U	186	^{169}Yb	177, 198
		^{235}U	186
^{238}U	1001	^{137}Cs	662
		^{54}Mn	834
		^{22}Na	1275
^{239}Pu	414	^{75}Se	401
		^{22}Na	511
		^{137}Cs	662
		^{239}Pu	414

TABLE 5.3

THE VARIATION IN $\mu(414)/\mu(662)$ WITH PLUTONIUM WEIGHT FRACTION

F_{Pu}	$\alpha = \mu(414)/\mu(662)$	414 keV	662 keV
0	1.21	$\mu_{Pu} = 0.26\ cm^{-2}/g$	0.13
0.1	1.33	$\mu_{o} = 0.093$	0.077
0.3	1.54		
0.5	1.71		
0.7	1.84		
0.9	1.95		

If the sample is uniform, one transmission measurement will adequately define μD. In more advanced procedures, the sample is scanned to measure T as a function of position.[5.1] This is usually not practical with portable equipment; however, measurements of transmission at more than one position may provide a crude check of sample uniformity and lend confidence to the assay.

5.4.c. Other Attenuation Corrections

Equation (5.11) gives an approximate correction factor which may be used for transmissions over ~0.2. This assumes that the average

$$CF \approx 1/\sqrt{T} \qquad \text{slab} \qquad (5.\,11a)$$

$$CF \approx 1/\sqrt{T^{\pi/4}} \qquad \text{cylinder ,} \qquad (5.\,11b)$$

path length within the sample is one-half the slab thickness or one π/8th of the cylinder diameter. Table 5.4 gives a comparison of Eqs. (5.11) with the exact expressions of Eqs. (5.9). For T greater than 0.2 the approximate slab expression is less than 12% high and the cylinder expression is less than 7% high.

Cline[5.2] has described a method for assaying plutonium waste by basing the attenuation correction on the differential absorption of two different plutonium gamma rays (usually 129 keV and 414 keV). This procedure can also be combined with transmission measurements to provide information on possible lumps of emitting material. Due to the plutonium spectrum complexity, a high-resolution detector is required to use this technique; therefore it will not be described here. The reader should consult the references.[5.2,5.3]

In some cases, useful estimates of CF can be made by having some knowledge of the sample weight and composition. If the sample is full and if its weight and composition are known, the attenuation may often be calculated with sufficient accuracy so that no experimental measurement is required. Consider the example of a 55-gal drum of plutonium-contaminated combustible waste. The waste material must be well segregated (no lathe beds, ball mills, etc., mixed with the combustibles) and the plutonium concentration must be low so that it is a minor part of the total attenuation. Combustible waste will have attenuation properties similar to water.

TABLE 5.4

COMPARISON OF APPROXIMATE AND EXACT EXPRESSIONS FOR CF

T	$1/\sqrt{T}$	$\frac{-\ln T}{1-T}$	$1/\sqrt{T^{\pi/4}}$	$\frac{-\pi/4 \ln T}{1-T^{\pi/4}}$
1.0	1.0	1.0	1.0	1.0
0.8	1.118	1.116	1.092	1.090
0.6	1.291	1.277	1.222	1.214
0.4	1.581	1.527	1.433	1.402
0.2	2.236	2.012	1.881	1.761
0.1	3.162	2.558	2.469	2.162

Known:

net weight = 32-kg; size = 56-cm-diam by 89-cm-high; walls = 0.1-cm; volume = 0.22-m^3 .

Computations:

$$\text{density} = \frac{32\ \text{kg}}{0.22\ \text{m}^3} = 145\ \text{kg/m}^3$$

$$= 0.145\ \text{g/cm}^3 \ .$$

$$H_2O:\ \mu(414) = 0.104\ \text{cm}^2/\text{g}$$

$$\mu_\ell = (0.104)(0.145) = 0.015\ \text{cm}^{-1}$$

$$D = 56\ \text{cm}$$

$$\mu_\ell D = (0.015)(56) = 0.84 \ .$$

Using Eq. (5.7b),

$$CF = \frac{(0.785)(0.84)}{1 - e^{-(0.785)(0.84)}} = 1.37 \ .$$

Correcting for absorption in the wall of the drum,

$$\text{Fe}:\ \mu(414) = 0.09\ \text{cm}^2/\text{g}$$

$$\mu_\ell = (0.09)(7.9\ \text{g/cm}^3) = 0.71\ \text{cm}^{-1}$$

$$\mu_\ell L = (0.71)(0.1\ \text{cm}) = 0.071 \ .$$

Using Eq. (5.7c),

$$CF = e^{0.071} = 1.07 \ ,$$

so that the total correction factor is

$$CF = (1.07)(1.37) = 1.47 \ .$$

Consider the effect of 100 g of plutonium distributed uniformly in the drum.

$$\text{Pu density} = \frac{0.1\ \text{kg}}{0.22\ \text{m}^3} = 0.45\ \text{kg/m}^3$$

$$= 4.5 \times 10^{-4}\ \text{g/cm}^3 \ .$$

$$\text{Pu}:\ \mu(414) = 0.26\ \text{cm}^2/\text{g}$$

$$\mu_\ell = (0.26)(4.5 \times 10^{-4})$$

$$= 1.2 \times 10^{-4}\ \text{cm}^{-1}$$

$$\mu_\ell D = (1.2 \times 10^{-4})(56) = 6.7 \times 10^{-3} \ .$$

Using Eq. (5.7b),

$$CF = 1.003 \ .$$

This says that 100 g of plutonium will have a negligible effect on the attenuation in the drum if it is distributed so that there are no self-attenuating lumps.

The important factor in this attenuation correction is that the samples must be filled or the fill volume must be known. The attenuation correction is based on the density of the sample. Consider a group of samples filled to different heights with material of approximately constant density. Because the density is constant, the correction factor should be constant. However, if only the weight is known and the samples are assumed to be full, different correction factors will be applied to each sample.

The final procedure to be discussed involves the use of standards to cover the range of material to be measured. In this case, no explicit computation or measurement is made to correct for attenuation. The unknowns are assumed to have the same attenuation properties as do the standards. This procedure is acceptable where there is a class of samples very nearly identical in size, shape, and composition, varying only in concentration of uranium or plutonium. In such cases, the attenuation of the matrix will be nearly constant from one sample to another and the observed count rate will be uniquely related to the fissionable material concentration. This relationship can be determined by preparing a series of standards covering the expected concentration range and counting them in the same geometry as the unknowns. The resulting calibration curve may be somewhat nonlinear if the uranium or plutonium concentration is high enough so that it begins to contribute to the attenuation in the standard. This procedure is the simplest to use, and, where applicable, can yield acceptable results. At present, it is probably the most widely used gamma assay procedure.[5.4] For example, this would be used for product control or quality assurance where deviations from a mean (the standard) are to be measured. However, the standards procedure is susceptible to error and must be applied with caution. It should only be used on very well-controlled material because there is no check to prove that the unknowns actually do resemble the standards. The standards must have the same matrix attenuation as the unknowns, otherwise there will be a constant bias on all measurements. Some users have constructed standards by placing small amounts of uranium or plutonium in vials and distributing these vials throughout a standard matrix. This can be a particularly poor procedure because the probability of self-attenuation in lumps or uranium or plutonium is very high, as discussed earlier. Consider 0.5 g of uranium as UO_2 (bulk U density = 2 g/cm^3, ignore attenuation in O).

If contained in a cube, the dimension of that cube is

$$(0.5\ \mathrm{g}/2\ \mathrm{g/cm^3})^{\frac{1}{3}} = 0.63\ \mathrm{cm}$$

$$\mathrm{U}:\ \mu(186) = 1.5\ \mathrm{cm^2/g}\ .$$

Using Eq. (5.6),

$$\mu x = (1.5\ \mathrm{cm^2/g})(2\ \mathrm{g/cm^3})(0.63\ \mathrm{cm}) = 1.9$$

$$\mathrm{CF} = \frac{1.9}{1 - e^{-1.9}} = 2.2\ .$$

That is, less than half of the 186-keV gamma rays will get out of this volume unattenuated. For PuO_2, $\mu(414) = 0.26\ \mathrm{cm^2/g}$, so this becomes

$$\mu x = (0.26)(2)(0.63) = 0.33$$

$$\mathrm{CF} = 1.17\ .$$

Though the self-attenuation is smaller, it still represents a nonnegligible error that will show up as a bias (assay will be high) on all measurements. This problem must be considered when constructing standards for any gamma assay procedure; distributed vials of fissionable material are bad news. Other factors to consider include settlement and compaction in the standards (and the unknowns) and separation of the fissionable oxide from the matrix. The bulk density of most powders can be changed over a considerable range by agitation and vibration. These procedures can also cause the fissionable oxide to settle out of the matrix if there are grossly different particle size distributions. All of this indicates that care must be used when applying a gamma assay procedure that relies on standards only.

5.5. Example 1: Small Cans of Plutonium Incinerator Ash

This problem is the verification of the plutonium content of small cans of incinerator ash. The cans are 30-cm high by 15-cm o.d. and are doubly bagged. The contents have been blended, therefore it is safe to assume that the mixture of plutonium and matrix is uniform. Up to 100 g of plutonium will be encountered, all of constant isotopic , 85% ^{239}Pu. The equipment available is a 5- by 5-cm NaI detector with a portable electronics package containing two single-channel analyzers. There is also a simple rotator and a 400-μCi ^{22}Na source for transmission measurements. There is a single 50-g plutonium standard available in the same type of container. The slope of the Compton background around 400-600 keV can be assumed level so that k = 1 in Eq. (4.3a). One hundred grams of plutonium is less than 2% plutonium by weight, and the plutonium attenuation is small ($<10\%$). The matrix is assumed to attenuate like oxygen, $\mu(414)/\mu(511) \approx 1.1$. The assay procedure is outlined below for careful study.

A. Setup

1. Sample-to-detector distance = 45 cm (use 5.2, 1/2 height = 15 cm).
2. Detector to transmission source = 75 cm. Position the source to look through the center of the sample.
3. When the energy calibration is determined, set the windows as follows.

P: 375 - 450 keV	414-keV peak from ^{239}Pu.
B,T: 460 - 560 keV	414-keV background window and 511-keV peak window. The background window for the transmission gamma ray is omitted here to eliminate changing SCA threshold between measurements.

4. Put a cadmium absorber (0.08-cm to 0.15-cm) over the face of the detector to reduce the intensity of the 60-keV gamma ray from ^{241}Am.

B. Measurement Procedure

1. Using the high-energy window, measure the transmission source to determine the "straight-through" count rate, CR_0. Measure several times and take the average.
2. Calibrate the system by measuring the standard, then measure the unknowns. Recheck the instrument calibration occasionally by repeating the standard measurement.
3. Cover the transmission source with lead brick (or remove the source). Place the sample on the rotator and measure the activity in both windows, CR_p and CR_b.
4. Uncover the transmission source and measure the transmission through the sample (use the higher energy window) CR_t.

C. Results and Sample Computations

1. All counts are 60 s.
2. $CR_0 = 252\,000$.
3. Calibration, using the 50-g standard.

$$\left.\begin{aligned} CR_p &= 45\,000 \\ CR_b &= 6000 \\ CR_t &= 46\,300 \end{aligned}\right\} \text{measured counts in 60 s} .$$

Using Eq. (5.8),

$$T_t = \frac{CR_t - CR_b}{CR_o} = \frac{46\,300 - 6000}{252\,000} = 0.16 .$$

Using Eq. (5.10),

$$T_a = (0.16)^{1.1} = 0.133 .$$

Using Eq. (5.7b),

$$CF_s = \frac{-(0.785)\ln(0.133)}{1 - 0.133^{0.785}} = 1.99$$

$$CR_s = \frac{CR_p - CR_b}{60} = \frac{45\,000 - 6000}{60} = 650/s .$$

(It is not necessary to divide by the count time; this just keeps the numbers smaller.)

Using Eq. (5.2),

$$K = \frac{CR_s \cdot CF_s}{M_s} = \frac{650 \times 1.99}{50} = 25.9/g\text{-}s .$$

4. Uncertainty in calibration.

The standard is measured four more times yielding values of 25.5, 26.2, 25.8, and 26.1. The mean of these measurements is 25.9/g-s, and the standard deviation *in the mean* is 0.1/g-s.

5. Measurement of unknown.

$$\left.\begin{aligned} CR_p &= 21\,000 \\ CR_b &= 4000 \\ CR_t &= 36\,000 \end{aligned}\right\} \text{measured counts}$$

$$T_t = \frac{36\,000 - 4000}{252\,000} = 0.127$$

$$T_a = (0.127)^{1.1} = 0.103$$

$$CF = 2.14$$

$$CR = \frac{21.000 - 4000}{60} = 283 \ .$$

Using Eq. (5. 1),

$$M = \frac{CR \cdot CF}{K} = \frac{(283)(2.14)}{25.9} = 23.4 \text{ g Pu} \ .$$

6. Uncertainty in measuring the unknown.

A complete assay should include an estimate of the uncertainty in the measurement. This will be discussed more fully in Appendix B. For now, the formula below can be used to estimate the uncertainty in the measurement due to counting statistics. (This formula is approximate, and its derivation is not obvious.)

$$\frac{\sigma M}{M} \approx \sqrt{\frac{CR_p + CR_b}{(CR_p - CR_b)^2} + (0.25)\left(\frac{CR_t + CR_b}{(CR_t - CR_b)^2}\right) + \left(\frac{\sigma K}{K}\right)^2} \ . \tag{5.12}$$

Equation (5.12) gives $\sigma M/M \approx 0.01$. It should be emphasized that this is the uncertainty due to counting statistics only. The total uncertainty on a measurement such as this would be at least 10% (two sigma).

5.6. Example 2: Uranium-Contaminated Air Filters

This problem involves measuring HEPA air filters (60- by 60- by 30-cm) for uranium content. The uranium is of constant enrichment, 93% ^{235}U. The same detector and electronic equipment are available as in the previous example. There is no transmission source available, and the only standard is a small foil of uranium metal: 2.5- by 2.5- by 0.005-cm-thick, density = 19 g/cm^3, 0.59-g uranium (93% ^{235}U). The filter weighs about 9.1 kg excluding the wood frame. The filter medium should attenuate similar to water. Use k = 1.3 for Eq. (4.3a).

A. Setup

1. Sample-to-detector distance = 90 cm (use 5.2, 1/2 height = 30 cm).

2. Set the windows as follows.

P: 160 - 210 keV	186 keV peak from ^{235}U
B: 220 - 270 keV	Background from 186-keV peak

3. Put a 0.08-cm cadmium absorber over the detector to reduce the intensity of uranium x rays. Shield the detector with lead to reduce background radiation.

B. Measurement Procedure

1. Measure the foil standard for calibration. Be sure to consider possible attenuation in the foil. The foil must be measured close to the detector (30 cm or less) to get sufficient count rate. This necessitates applying a $1/r^2$ correction to the calibration.

2. Estimate the correction factor for the unknown filter.

3. Because of their shape, the filters should not be rotated, but should be counted on each side. Use the average of the two sides to compute the uranium assay. If these two counts differ greatly, the filter is not loaded uniformly. Another check on this last point would involve holding the detector close to the filter and looking for hot spots. If these considerations indicate gross nonuniformities, a large uncertainty should be assigned to the measurement.

4. Compute the uranium content of the filter and estimate the uranium attenuation assuming a uniform distribution. Air filters have been measured with 1 kg, or more, of enriched uranium in a nonuniform distribution. For such a case, the uranium self-attenuation is considerable and the simple computational procedure outlined here is not adequate. If less than about 100 g are found, this procedure is probably accurate.

C. Results and Sample Computations

1. Calibration foil attenuation.

$$\mu(186) = 1.5 \text{ cm}^2/\text{g} \ ,$$

$$\mu_\ell = (1.5 \text{ cm}^2/\text{g})(19 \text{ g/cm}^2)$$

$$= 28.5 \text{ cm}^{-1} \ , \text{ and}$$

$$\mu D = (28.5\ \text{cm}^{-1})(0.005\ \text{cm})$$

$$= 0.143\ .$$

Using Eq. (5.7a),

$$CF = \frac{0.143}{1 - e^{-0.143}} = 1.073\ .$$

2. Calibration. Measure foil at 30 cm. All count times = 60 s.

$$CR_p = 3370\ .$$

$$CR_b = 600\ ,\ \text{and}$$

$$CR_s = \frac{3370 - (1.3)(600)}{60} = 43.2/\text{s}\ .$$

Using Eq. (5.2),

$$K = \frac{(43.2)(1.073)}{(0.59)(9)} = 8.73/\text{g-s}\ .$$

(The $1/r^2$ correction for the different positions is 9, $(90/30)^2$.)

The standard is measured four more times yielding values of 8.47, 8.98, 8.76, and 8.87. The mean of these measurements is 8.76 and the standard deviation in the mean is 0.09. Considering the assumptions made and the computed correction factor, this should be rounded off to two significant figures.

$$K = 8.8 \pm 0.1.$$

3. Filter attenuation correction.

$$\text{volume} = (60 \times 60 \times 30)$$
$$= 1.08 \times 10^5\ \text{cm}^3\ ,$$

$$\text{density} = (9100\ \text{g})/(1.08 \times 10^5\ \text{cm}^3)$$
$$= 0.084\ \text{g/cm}^3\ ,\ \text{and}$$

$$\text{for water: } \mu(186) = 0.14\ \text{cm}^2/\text{g}\ .$$

Linear attenuation coefficient of filter medium:

$$\mu_\ell = (0.14)(0.084) = 0.012\ \text{cm}^{-1}$$

$$\mu_\ell D = (0.012\ \text{cm}^{-1})(30\ \text{cm}) = 0.36\ .$$

Using Eq. (5.7a).

$$CF = \frac{0.36}{1 - e^{-0.36}} = 1.19\ .$$

(This correction factor considers only the filter medium. There is no correction for self-absorption in the uranium.)

4. Measurement of unknown filter.

$$CR_p = 21\,600\ ,\ 21\,000\ ,$$

$$CR_b = 1200\ ,\ 1300\ ,$$

$$CR = 20\,040\ ,\ 19\,310\ ,$$

$$CR = \frac{20\,040 + 19\,310}{(2)(60)} = 328/\text{s}\ .$$

Using Eq. (5.1),

$$M = \frac{(328)(1.19)}{8.8} = 44\ \text{g uranium}\ .$$

There is a 4% difference between the count rates from the two sides. The relative precision of each count is about 0.7% $(1\sqrt{20\,000})$, therefore there is a slight difference in uranium activity between the two sides. This difference is small and should not affect the assay adversely.

5. Estimate of uranium attenuation.

$$\text{uranium density} = (44\ \text{g})/(1.08 \times 10^5\ \text{cm}^3)$$

$$= 4.1 \times 10^{-4}\ \text{g/cm}^3\ ,$$

$$\mu(186) = 1.5\ \mathrm{cm}^2/\mathrm{g}\ ,$$

$$\mu_\ell = (1.5)(4.1 \times 10^{-4})$$

$$= 6.1 \times 10^{-4}\ ,\ \text{and}$$

$$\mu D = (6.1 \times 10^{-4})(30\ \mathrm{cm})$$

$$= 0.018\ .$$

Using Eq. (5.7a),

$$CF = 1.01\ .$$

The uranium attenuation is indeed small, and the assumption to neglect it was justified. If the uranium content becomes much larger than this, its contribution to the attenuation must be considered. One kilogram of uranium uniformly distributed in the filter would require a correction factor of 1.22 (a total correction of 1.22 x 1.19 = 1.45). The assumption of a uniform distribution would probably not be justified for this case.

5.7. Example 3: Measurement of Equipment Holdup

The problem is to measure highly enriched (93% ^{235}U) uranium holdup in a low-velocity air duct used to carry machining residues away from various machines in a uranium fabrication shop. The shop has been shut down, but a small amount of uranium residue is left on the walls of the duct. The equipment includes a 5.1-cm-diam by 2.5-cm-thick NaI detector in a lead shield and collimator. The distance d from the detector face to the front of the cylindrical collimator is adjustable from 0 to 10 cm. A 0.08-cm-thick cadmium filter is taped to the detector face to attenuate low-energy x rays. The electronics is a portable unit containing a high-voltage supply, an amplifier, one SCA, a scaler, and a timer, all mounted on a small cart (Fig. 5.7). Figure 5.7 shows an actual measurement in progress. An enriched 19-g uranium foil (effective mass) is available for calibration.

The duct (41-cm-diam by 36-m-long) must be measured in sections. Physical obstructions limit the sample-to-detector distance to about 1.4 m or more. It is necessary to adjust the collimator for a convenient viewing angle. The geometry of the situation is illustrated in Fig. 5.8. The detection efficiency ε(R,r) is a function of R,r. At a given R it is maximum on the detector centerline and decreases off the centerline. The distance L defines the effective extent of the collimator's view. Figure 5.9 shows a typical efficiency curve obtained by counting the calibration source at a fixed R (1.4 m) and varying r. The collimator depth d is set at 6 cm. L/2 is defined as the width of a step function of height ε(R,0), which has the same area as the actual efficiency curve (Fig. 5.9). This definition is equivalent to assuming that the efficiency is

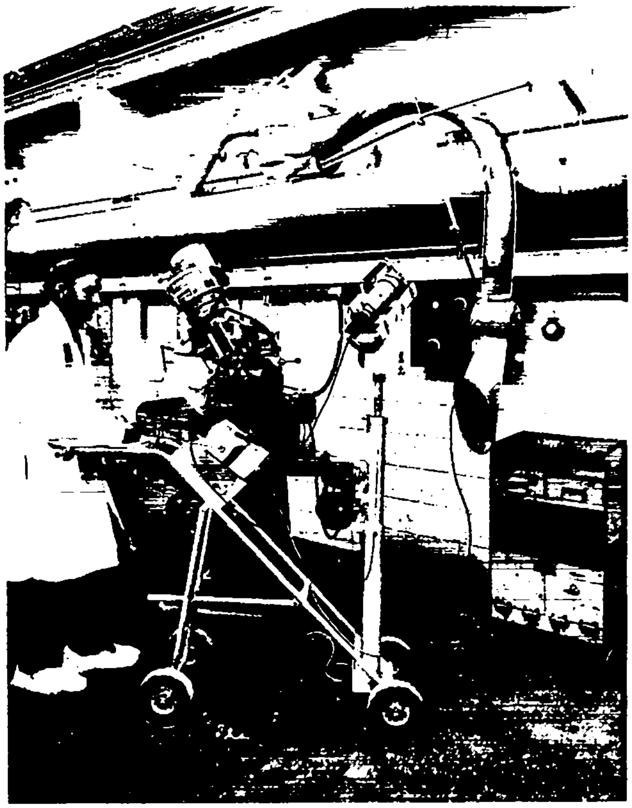

Fig. 5.7.
Measurement of uranium holdup in a duct using cart-mounted NaI and SAM-I.

$$\begin{aligned} \epsilon(R,r) &= \epsilon(R,0) \quad \text{if} \quad -L/2 \le r \le L/2 \\ &= 0 \quad \text{if} \quad |r| > L/2\ . \end{aligned} \tag{5.13}$$

This simplifies the calibration procedure because only a single measurement is required to determine ε(R,0). As shown in Fig. 5.9, the efficiency drops to

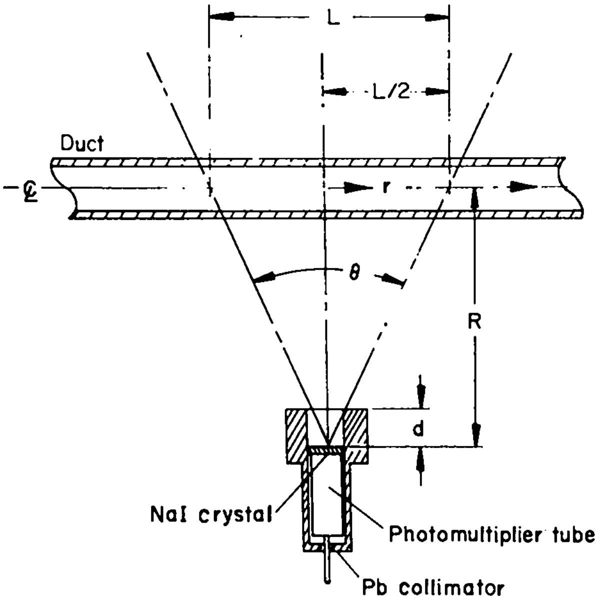

Fig. 5.8.
Diagram of duct measurement geometry.

$\sim 1/2\epsilon(R,0)$ at L/2. This is a good rule of thumb. L/2 is usually determined with sufficient accuracy by finding the point where the count rate from the calibration source drops to one-half the rate on the centerline.

The viewing angle, or collimation angle, θ can be defined as

$$\theta = 2 \tan^{-1}\left(\frac{L(R)}{2R}\right) . \qquad (5.14)$$

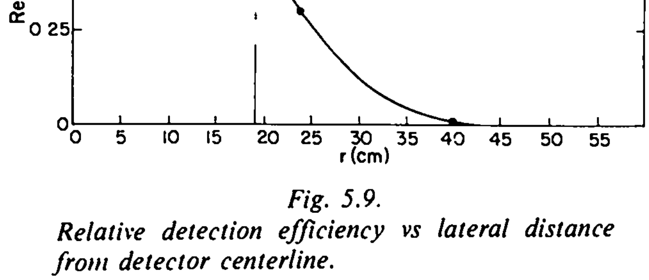

Fig. 5.9.
Relative detection efficiency vs lateral distance from detector centerline.

This is constant for $R \gg d$; θ is basically a function of d only. Having determined L for one distance R, it can be calculated for any other distance R_1 using

$$L(R_1) = \frac{R_1}{R} L(R) . \qquad (5.15)$$

At the different spacing the detection efficiency changes by the inverse square of the distance.

$$\epsilon(R_1, 0) = \left(\frac{R}{R_1}\right)^2 \epsilon(R, 0) . \qquad (5.16)$$

Physical obstructions may prohibit making all measurements at a fixed distance so that Eqs. (5.15) and (5.16) are used to make the appropriate corrections for different sample-to-detector distances. When setting up to make holdup measurements on any type of equipment, the first step is to select the proper collimation. For the situation described here ($R = 1.4$ m, $d = 6$ cm), $L \approx 1$m, which is convenient for the duct measurement.

The next step is to calibrate the system. The desired sample-to-detector distance is 1.4 m, as measured from the face of the detector to the center of the duct. Adjust the collimator to the desired depth, $d = 6$ cm. Tape the calibration source to a wall and aim the detector at the source. The separation must be 1.4 m. The SCA is set 130 to 210 keV. Because this is highly enriched uranium, the Compton background from the source is small, therefore the upper background window is not necessary. It is necessary to subtract the ambient background in the peak window. Take several 60-s counts with the detector aimed at the source; these average 3226. Now aim the detector away from the source (e.g., at the floor) and make several 60-s counts to measure the ambient background. Be sure that the detector is not pointing at any suspected uranium holdup area. The average of these measurements is 120. The calibration factor k is then

$$k = \frac{3226 - 120}{19} = 163 \text{ counts/g}$$

for a 60-s count.

The final step is to evaluate the attenuation. One method is to calculate the wall attenuation and assume that the uranium attenuation is small. The wall thickness is 0.08 cm of steel ($\mu \approx 1.2\ \mathrm{cm}^{-1}$). Using Eq. (5.7c), the appropriate correction factor is

$$CF = e^{(1.2)(0.08)} = 1.10 \ .$$

All measured counts are multiplied by CF. After the uranium is measured, it is possible to estimate the uranium attenuation by making reasonable assumptions about the distribution in the equipment. In some cases it may be reasonable to assume that the uranium is distributed in a uniform layer over the inner surface. This assumption allows computation of the layer thickness and the uranium attenuation correction. Suppose the measurement gives 200 g in a 1-m section. The thickness x of this layer is given by the mass divided by the surface area.

$$x = \frac{200}{\pi\,(41\ \mathrm{cm})(100\ \mathrm{cm})} = 0.015\ \mathrm{g/cm}^2 \ .$$

Using Eq. (5.7a), the appropriate correction factor would be ($\mu = 1.5\ \mathrm{cm}^2/\mathrm{g}$).

$$CF = \frac{(1.5)(0.015)}{1 - e^{-(1.5)(0.015)}} = 1.01 \ .$$

This is certainly small and can be neglected. It may seem more reasonable to assume the material is a layer spread more or less uniformly over the bottom of the duct (assume that 1/8 of the total surface area is covered). In this case, $x = 0.12\ \mathrm{g/cm}^2$, and CF = 1.09. This is a larger correction and illustrates the biggest problem with equipment holdup measurements. The material distribution will usually be uncertain or unknown and large errors can be introduced because of the uncertainty in the attenuation correction. If the 200 g is in one small lump in the bottom of the duct, an even larger error will result if the usual uniform distribution is assumed. In some cases careful transmission measurements may aid in evaluating the attenuation. However, a transmission measurement is only useful if the material approximates a uniform distribution. However, if the measurement shows less than 200 g in 1 m, there is a reasonable assurance from the above estimates that the answer is not off by more than 20%.

The actual measurements are then very straightforward. Make a 60-s count every 1 m of the duct (A) and the local background (B) (point detector away from duct).The uranium content of each section is computed from

$$gU = CF \cdot (A - B)/k = \frac{1.1}{163}(A - B)$$

$$= 6.7 \times 10^{-3}(A - B) \ .$$

Every so often the calibration foil should be counted to see that the instrument has not drifted. Some typical data are presented in Table 5.5, where the numbers give some confidence in the assumption of small uranium attenuation because they are all considerably below 200 g. Under favorable circumstances (i.e., small attenuation) as presented in this example, equipment holdup measurements can be accurate to ~20%. For equipment and uranium quantities where the attenuations are large, the associated measurement error will be large and probably will not be of a random nature. The gamma measurement of holdup usually will be biased low unless very conservative attenuation assumptions are made.

5.8. Instrument Dead Time

When a gamma ray interacts in a detector, there is a finite time before the counting system (detector and electronics) recovers and can accept another gamma-ray event. The time required for this recovery is called the "dead time," t_d. If the total count rate is high, the system may actually respond to only a fraction of the total gamma rays interacting in the detector, that is, the actual counting period is shorter than the "real time" indicated by a clock.

TABLE 5.5

URANIUM HOLDUP MEASUREMENT

Position (m)	A	B	gU
1	3480	110	23
2	7618	92	50
3	4906	77	32
4	9230	140	61
5	5121	123	33

The observed count must be corrected for the fraction of time the system is dead. If R is the total count rate, this correction is given approximately by the following expression.

$$CT = \frac{1}{1 - R \cdot t_d} \quad . \tag{5.17}$$

For the systems considered here, t_d is the order of 2-5 μs. If R is 10^4 counts/s, CT is 1.02 — 1.05. This correction is small and usually can be neglected if the total count rate is below 10^4 counts/s. It is advisable to operate portable instrumentation within this limit. It should be emphasized that the preceding discussion is a very simplified and incomplete treatment of instrument dead time; it is meant as a warning against high count rates.

REFERENCES

5.1. J. L. Parker, T. D. Reilly, J. E. Foley, R. B. Walton, and L. V. East, "Passive Assay-Innovations and Applications," Proceedings of the 12th Annual Meeting of the INMM, 1971, p. 514 ff. This paper discusses some of the scan techniques of gamma assay. There is a discussion of enrichment measurements and neutron counters which relates to other parts of this text.

5.2. J. E. Cline, "A Relatively Simple and Precise Technique for the Assay of Plutonium Waste," Aerojet Nuclear Company report ANCR-1055 (February 1972). This report describes the use of differential attenuation of different energy plutonium gamma rays to correct for sample attenuation. It also includes a good discussion of the operation of Ge(Li) detectors and their associated electronics. This report should be read in conjunction with the next report which describes some of the assumptions and limitations of the "contrast method" and reports some experimental results on plutonium waste standards.

5.3. T. D. Reilly and J. L. Parker, Los Alamos Scientific Laboratory A-1 Progress Report LA-5197-PR (1972), pp. 15-18. The title of this article is "The Contrast Method-Gamma Attenuation Correction Based on Differential Absorption."

5.4. "Proceedings of the Symposium on Passive Gamma Ray Assay," W. A. Higinbotham, Ed. This conference was held in Germantown, MD, November 19-20, 1970. This includes short reports from 12 nuclear facilities on their use of gamma assay equipment. Though somewhat outdated, it gives useful information on the gamma assay techniques in use at United States nuclear facilities.

6. ENRICHMENT MEASUREMENTS

6.1. Introduction

The previous chapter shows that the assay of ^{235}U is very difficult because of the high self-attenuation of uranium at 186 keV. The mass attenuation coefficient of uranium at 186 keV is about 1.5 cm^2/g, which is nearly 12 times greater than the average for all elements below atomic number $Z = 30$ (this is about 0.13 cm^2/g). This very circumstance makes the measurement of uranium enrichment relatively easy for many practical situations. The fundamental relationship is this: The intensity of 186-keV gamma rays emitted from a fixed area of a thick sample of uranium is proportional to the enrichment of the sample. "Thick" in this context means several mean free paths at 186 keV. This is usually thin physically; 2 mm of uranium metal is almost infinitely thick to these gamma rays. Numerous systems have successfully applied this concept with a variety of electronics and detectors to a wide range of problems. These include enrichment measurements of fuel pins, fuel plates, containers of UO_2, cylinders of UF_6, and in-line monitoring of liquid UF_6.

A detailed discussion of gamma-ray enrichment measurements is omitted here because the subject is well covered in the listed references.[6.1-6.4] The Kull report[6.1] should be read by anyone interested in enrichment measurements. This chapter will be confined to a simple derivation of the fundamental relationship and a description of how it may be applied to measuring uranium concentration and blending ratios as well as to enrichment measurements. A few comments will be made about determining plutonium isotopic distributions.

6.2. The Fundamental Relation

The detector illustrated in Fig. 6.1 views a fixed area of a uranium sample through an appropriate collimator. The sample is infinitely thick for 186-keV gamma rays (transmission ≤0.01) and consists of a *uniform* mixture of uranium and matrix (everything else). The density of uranium is ρ_u, and matrix ρ_m. The mass attenuation coefficients at this energy are μ_u and μ_m. The count rate can be expressed by the integral relation

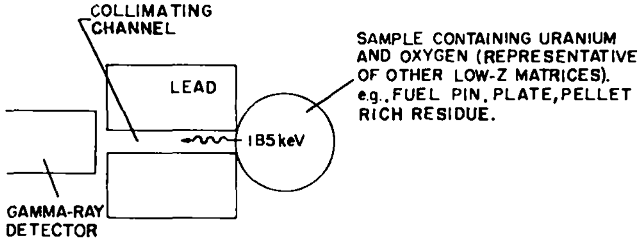

Fig. 6.1.
Schematic illustration of uranium enrichment measurement.

$$CR = I\Gamma\epsilon A\rho_u \int_0^\infty \exp[-(\rho_u\mu_u + \rho_m\mu_m)x]dx \ , \qquad (6.1)$$

where $I = {}^{235}U$ enrichment,

ϵ = total efficiency of counting system,

Γ = specific activity of ^{235}U (4.3×10^4/g-s),

A = area of sample viewed, and

x = distance (within sample) to front edge of sample.

This relationship assumes that the variation in sample-to-detector distance from different parts of the sample may be ignored (ϵ = constant, independent of x). It also ignores any attenuation by sample packaging. For many situations, this relationship gives an adequate description of the problem. The integral is easily evaluated and yields the expression

$$\boxed{CR = \frac{K \cdot I}{1 + \frac{\mu_m}{\mu_u}\frac{\rho_m}{\rho_u}}} \ , \qquad (6.2)$$

where $K = \Gamma\epsilon A/\mu_u$, a constant which is determined by calibration with a known standard.

A thorough understanding of Eq. (6.2) is essential to measure enrichment. There are other considerations of equipment, procedure, wall corrections, unusual geometries, etc., which are not represented in Eq. (6.2). Many of these are covered in Ref. 6.1. However, Eq. (6.2) is the fundamental relation that contains all the basic information for measuring enrichment. Three areas of application exist as defined by different values of the ratios μ_m/μ_u and ρ_m/ρ_u, which will be discussed separately.

6.3. Enrichment Region

The important parameter is the value of $\mu_m\rho_m/\mu_u\rho_u$. If $\mu_m\rho_m/\mu_u\rho_u \leq 0.1$, the observed count rate (CR) is proportional to the enrichment with an error of 10% or less. For matrix material with $Z \leq 30$, $\mu_m/\mu_u \sim 0.08$. Thus, $\mu_m\rho_m/\mu_u\rho_u \leq 0.1$ if $\rho_m/\rho_u \leq 1$. A half-and-half mixture of uranium and low-Z material would give less than 10% fewer counts than a slab of uranium metal having the same enrichment. A wide range of compounds and mixtures may be measured by comparison to a single standard with only small corrections for the variation in composition. If a standard and a series of unknown samples are known to be the same compound or mixture, the enrichments will be directly proportional to the observed rates. For example, if both standard and samples are pure UF_6, the term $(1 + \mu_m\rho_m/\mu_u\rho_u)$ can be neglected. If the standard were UO_2 and the unknowns UF_6, a small correction might be applied to the calibration to account for the denominator of Eq. (6.2). If the uranium concentration is known, the denominator can be evaluated directly and the range of the enrichment measurement can be extended to lower concentrations. In favorable circumstances, accurate enrichment measurements have been made on residues with less than 10% uranium by weight.

6.4. Concentration Region

Now consider the case where $\mu_m\rho_m/\mu_u\rho_u \geq 10$. With an error of 10% or less, Eq. (6.2) becomes

$$CR \approx K' I \rho_u/\rho_m \ . \tag{6.3}$$

Thus, *if the enrichment (I) is known*, the count rate is directly proportional to the relative concentration of uranium and matrix. Because $\mu_m/\mu_u \sim 0.08$ $(Z \leq 30)$, $\mu_m\rho_m/\mu_u\rho_u \geq 10$ if $\rho_m/\rho_u \gtrsim 100$. Consider a dilute uranium solution (less than 1% uranium by weight). If the enrichment is known, the uranium concentration can be computed directly from the 186-keV count rate. The total uranium can then be computed from the net weight of the solution. For dilute mixtures, Eq. (6.3) might be said to define a "concentration meter." It is important to remember that Eq. (6.2) is based on the assumption that the sample is infinitely attenuating to the gamma rays of interest (186 keV). The concentration limit occurs when the matrix is the dominant part of the attenuation. The mean free path of 186-keV gamma rays in low-Z material can be quite long (~7 cm in H_2O) so that more material is required to define a thick sample. Concentration measurements should be attempted with caution in cases where matrix density or sample size varies.

6.5. Mass Fraction for High-Z Mixtures

Sometimes the matrix material is another high-Z element, e.g., thorium or plutonium. For both of these cases, μ_m differs from μ_u by 5% or less. Thus, with a small error, $\mu_m/\mu_u \approx 1$, and Eq. (6.2) becomes

$$CR \approx \frac{K \cdot I}{1 + \rho_m/\rho_u} \cdot K \cdot I \cdot \frac{\rho_u}{\rho_u + \rho_m} \ . \tag{6.4}$$

If the enrichment is known, the count becomes a measure of the uranium mass fraction f. This can be rewritten as

$$CR \approx K \cdot I \cdot f \ , \tag{6.5}$$

where

$$f = \frac{\rho_u}{\rho_u + \rho_m}$$

to emphasize the fact that the measured count rate is proportional to the product of the uranium enrichment and the uranium mass fraction. If either quantity is known, the other can be measured. This relation applies equally well to the measurement of plutonium isotopic ratios and to plutonium blending ratios in mixed oxide fuel. Note, however, that most work with uranium-plutonium mixtures will require a high resolution detector. Reference 6.2 discusses this case in more detail and accounts for the fact that $\mu_m/\mu_u = 1$ is not strictly true.

6.6. Summary of Relations

($\approx$ implies an error less than 10%)

Fundamental Relation

$$CR = \frac{K \cdot I}{1 + \frac{\mu_m \rho_m}{\mu_u \rho_u}} \quad . \qquad (6.2)$$

Enrichment Region

$$CR \approx K \cdot I \quad \text{if} \; \frac{\mu_m \rho_m}{\mu_u \rho_u} \le 0.1$$

$$\text{for } Z \le 30 \; \frac{\mu_m}{\mu_u} \sim 0.1 \; ,$$

the condition is met

$$\text{if} \; \frac{\rho_m}{\rho_u} \le 1 \; .$$

Concentration Region

$$CR \approx K' \cdot I \cdot \rho_u/\rho_m$$

$$\text{if} \; \frac{\mu_m \rho_m}{\mu_u \rho_u} \ge 10 \qquad (6.3)$$

$$\text{for } Z \le 30, \text{ this holds if } \frac{\rho_m}{\rho_u} \gtrsim 100 \; .$$

Mass Fraction for High-Z Mixtures

$$CR \approx K \cdot I \cdot \frac{\rho_u}{\rho_u + \rho_m}$$

$$\text{if} \; \frac{|\mu_m - \mu_u|}{\mu_u} \le 0.1 \; . \qquad (6.4)$$

This condition is met for $88 \le Z \le 96$.

6.7. Example 1. Measurement of Highly Enriched UF$_6$ Cylinders

This problem is to verify the stated enrichment values of three UF$_6$ cylinders (Type 5A, 13-cm-diam by 90-cm-high). The available equipment includes a 5.1-cm-diam by 2.5 cm-thick NaI detector with a lead shield and collimator; a portable electronics package including a high-voltage supply, amplifier, two single-channel analyzers, and digital rate multipliers (DRM) for automatic background subtraction and a portable ultrasonic thickness gauge. This equipment is mounted on a small cart as shown in Fig. 6.2.

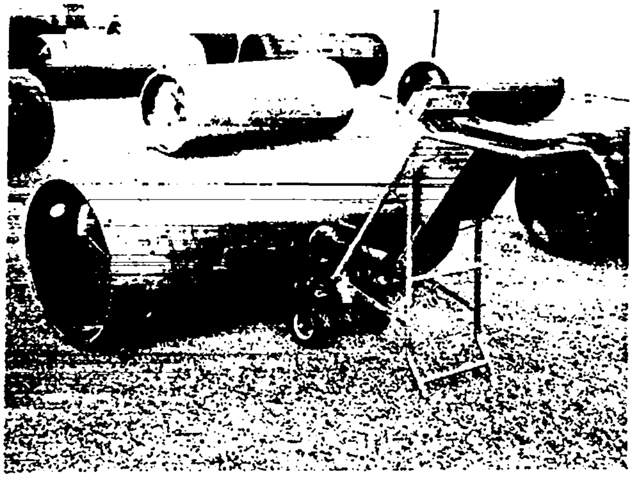

Fig. 6.2.
Gamma-ray enrichment measurement with Eberline SAM-II gamma unit and Branson ultrasonic thickness gauge.

The verification procedure is to use one of the cylinders as a standard and measure the others relative to this. The detector is positioned 7.6 cm back from the front of the lead collimator which is held against the side of the cylinder. A 0.08-cm cadmium foil is taped to the detector face to attenuate low-energy x rays. The two SCA's are set to count events in the 130- to 210-keV energy region (channel A) and the 230- to 310-keV energy region (channel B). The net count rate is computed as

$$R = A - 1.3\,B \ . \tag{6.6}$$

The DRM's are set at 1.0 and 1.3, so that R is displayed directly. Several 6-s counts are made on each cylinder. The cylinder wall thickness at the gamma measurement point is measured with an ultrasonic thickness gauge. The wall thickness of 5A cylinders is not uniform and errors of 5% or more can result if the variation is not taken into account. If a thickness gauge is not available, several gamma measurements should be made around the circumference of the cylinder and then averaged. The cylinder enrichment is computed from

$$I = K\,R\,e^{1.17\,x} \ , \tag{6.7}$$

where

I = cylinder enrichment (% ^{235}U),

K = calibration determined from standard,

R = observed net count [Eq. (6.5)], and

x = measured wall thickness (the effective absorption coefficient is 1.17 cm^{-1} for Monel and 0.95 cm^{-1} for steel).

The measured results are presented in Table 6.1, which gives actual data and shows the accuracy that can be obtained for such measurements. If the wall thickness correction had been omitted, the deviations would be +2.0% for Cylinder 2 and —3.2% for Cylinder 3. In some cases, this correction will be larger. Recent measurements using the procedure and equipment described in this example show that highly enriched UF$_6$ cylinders (type 5A) can be measured with a relative accuracy of better than 2%.[6.5] The calibration procedure described in the next example can also be used for this problem. The measurement of larger, thick-walled, low-enrichment cylinders would be by the same procedure but would be subject to larger error due to the increased absorbtion and poorer signal to background.

6.8. Example 2: Enrichment Calibration Procedure

This problem is to determine an independent calibration for ^{235}U enrichment measurements. The equipment is the same as for Example 1. Two uranium oxide standards of known enrichment (10.0 and 0.72 %^{235}U) are available for calibration. The material is contained in small cans, 10-cm-diam by 13-cm-high. The detector is positioned 7.6 cm from the front of the collimator, which is now supported in the vertical position. The can is positioned on top of the collimator so that the detector does not view the edge of the can. The SCA windows are set as before (A = 130-210 keV, B = 230-310 keV). Several 60-s counts are taken on each can. The average count is presented in Table 6.2.

The enrichment is assumed to obey the equation

$$I = a\,A - b\,B \ , \tag{6.8}$$

where a,b are constants determined by solving the following simultaneous equations.

$$I_1 = a\,A(I_1) - b\,B(I_1) \tag{6.9}$$

$$I_2 = a\,A(I_2) - b\,B(I_2) \ ,$$

and I_1, I_2 are the known enrichments 10.0, 0.72 %^{235}U. The solution of this is given as

$$a = \frac{I_1 \cdot B(I_2) - I_2 \cdot B(I_1)}{D} \tag{6.10}$$

$$b = \frac{I_1 \cdot A(I_2) - I_2 \cdot A(I_1)}{D}$$

$$D = A(I_1) \cdot B(I_2) - A(I_2) \cdot B(I_1) \ .$$

TABLE 6.1

MEASUREMENT OF UF_6 CYLINDERS

Cyl	$I_{tag}(\%)$	R(6s)	X(cm)	$I_m(\%)$	$[(I_m - I_{tag})] \times 100\%$
1^a	97.6	29030	0.645	97.6	0
2	46.8	14210	0.622	46.5	—0.6
3	19.9	5732	0.660	19.6	—1.5

---

[a] Taken as the standard $K = 97.6/[29030 \times \cdot e^{(1.17)(0.645)}]$
$= 1.58 \times 10^{-3}$

Substituting the values from Table 6.2,

$$D = (80\ 125)(10\ 902) - (18\ 146)(9790) = 6.96 \times 10^{8}$$

$$a = \frac{(10)(10\ 902) - (0.72)(9790)}{6.96 \times 10^{8}} = 1.47 \times 10^{-4}$$

$$b = \frac{(10)(18\ 146) - (0.72)(80\ 125)}{6.96 \times 10^{8}} = 1.78 \times 10^{-4} \ .$$

With the constants determined, other cans of uranium oxide can now be measured directly. An unknown can is measured and counts A = 45090, B = 10100. The measured enrichment of this can is given by Eq. (6.8).

$$I = (1.47 \times 10^{-4})(45\ 090) - (1.78 \times 10^{-4})(10\ 100)$$
$$= 4.8\% \ .$$

TABLE 6.2

MEASUREMENT OF URANIUM OXIDE ENRICHMENT STANDARDS

Enrichment ($\%^{235}U$)	A(counts)	B(counts)
10.0	80 125	9 790
0.72	18 146	10 902

For the specified equipment, the constants can be set on the DRM and the solution of Eq. (6.8) will be displayed directly in $\%^{235}U$.

This procedure can be adapted to calibrate the instrument for UF_6 cylinder measurements. The collimator restricts the detector view to a fixed area whether the sample is a small can or a large cylinder. It is advisable to perform the calibration with an iron or nickel plate of the approximate cylinder wall thickness under the can. This more closely approximates the cylinder measurement so that relatively small corrections are required for variations in wall thickness.

REFERENCES

6.1. L. A. Kull and R. O. Ginaven, "Guidelines for Gamma-Ray Spectroscopy Measurements of ^{235}U Enrichment," Brookhaven National Laboratory report BNL-50414 (1974). This was prepared for the USAEC Directorate of Regulatory Standards and was used as the basis for Regulatory Guide 5.21. It is a rather complete treatment of the subject of uranium enrichment measurements.

6.2. T. D. Reilly, R. B. Walton, and J. L. Parker, Los Alamos Scientific Laboratory A-1 Progress Report LA-4605-MS (1970), pp. 19-21. The title of this article is "The 'Enrichment Meter'—A Simple Method for Measuring Isotopic Enrichment." This is the original reference to the "enrichment meter" principle and the fundamental relation [Eq. (6.2)]. It includes a discussion of the measurement of Pu-U blending ratios. Other related progress report references on concentration measurements are Refs. 6.3 and 6.4.

6.3. M. M. Thorpe, R. B. Walton, and L. V. East, Los Alamos Scientific Laboratory A-1 Progress Report LA-4794-MS (1971), pp. 14-16. The title of this article is "Assay of Uranium Solution Storage Tanks."

6.4. J. L. Parker and T. D. Reilly, Los Alamos Scientific Laboratory A-1 Progress Report LA-5197-PR (1972), pp. 11-12. The title of this article is "The Enrichment Meter as a Concentration Meter."

6.5. R. B. Walton, T. D. Reilly, J. L. Parker, J. H. Menzel, E. D. Marshall, and L. W. Fields, "Measurements of UF_6 Cylinders with Portable Instruments," Nucl. Technol. **21**, 133-148 (1974). This reports measurements of high and low enriched UF_6 product cylinders using gamma enrichment measurements (NaI + ultrasonic measurement of cylinder wall thickness) and several neutron measurement techniques.

7. NEUTRON PRODUCTION AND APPLICABLE SIGNATURES

7.1 Introduction

There are some measurement problems for which the counting of passive neutrons is an attractive method of assay. These situations usually involve one or more of the following circumstances.

1. Well-characterized material, both isotopic and chemical composition, e.g., pure PuO_2 or enriched UF_6.
2. Large quantities of relatively dense material, e.g., plutonium buttons.
3. Material with high gamma backgrounds, e.g., slightly irradiated plutonium fuel.

Care must be exercised in using total neutron counting as an assay tool; but for appropriate cases, it provides a simple assay method.

Neutrons from fissionable material, other than those produced by induced fission, are emitted as a result of two processes: spontaneous fission and the interaction of alpha radiation with light elements. Under proper circumstances, neutrons from either process can be a useful assay signature.

7.2. Alpha-Induced Neutron Emission

Historically, the first free neutrons observed by man were produced by the interaction of alpha particles from the decay of polonium on beryllium. The nuclear reaction involved is

$$^{9}\mathrm{Be} + {}^{4}\mathrm{He} \longrightarrow {}^{12}\mathrm{C} + \mathrm{n} + 5.708\ \mathrm{MeV}\ .$$

The energy of the alpha particle (5.3 MeV for ^{210}Po) is added to the indicated energy released in the reaction. Most of this total energy is released as the kinetic energy of the neutron, resulting in neutrons with energies up to about 10 MeV. Neutrons of lesser energy are produced when the residual ^{12}C nucleus is left in an excited state of 4.43 or 7.65 MeV, which subsequently decays by gamma radiation. The emitted neutron energy is also reduced if the alpha particle is slowed down by atomic collisions before entering into the reaction with the beryllium nucleus. The result of all these processes is a fairly continuous spectrum of neutrons with a maximum intensity around 4.5 MeV, tailing off to zero intensity at maximum energy and at very low energies.[7.1] The maximum alpha energy of various fissionable nuclides is indicated in Table 7.2, column 4. Depending on the light element combined with the fissionable nuclide, the maximum neutron energy can vary from approximately 1 MeV (Li) up to 10 MeV (Be).[7.2]

Thus, the neutron signature does not consist of narrow, well-defined lines as do the gamma signatures. As a consequence, it is not possible to measure uniquely the amount of a given isotope in a sample without additional information.

Many light elements have isotopes that yield neutrons from the (α,n) reaction when bombarded by energetic alpha particles. A partial list of such elements, and the yield of neutrons emitted per 10^6 alpha particles, is given in Table 7.1, assuming polonium alpha particles strike a thick target of the element. The actual yield of neutrons is very dependent upon the energy of the alpha particles.[7.3] Table 7.2 lists known heavy isotopes of interest to the nuclear fuel cycle, their decay rates and alpha energies, and expected neutron yields from the $^{9}\mathrm{Be}(\alpha,n)^{12}\mathrm{C}$ reaction. Note that because fissionable fuel materials are often found in the manufacturing cycle as pure oxides or fluorides, the reactions with these two light elements are particularly interesting from an assay standpoint. Table 7.3 lists the data relevant to these compounds.

The maximum yield of neutrons to be expected from any combination of fissionable material and light elements can be obtained by taking the neutron yield for alphas on beryllium from the last column of Table 7.2 and multiplying it by the third (yield relative to beryllium) column of Table 7.1. In all cases the yield actually obtained will be less because of the slowing down effect of alpha particles between the time they leave their parent nuclei and the time that they react with light-element nuclei. The amount of this slowing down depends upon the ratio of the alpha-emitting isotope to the particular light element, the presence of nonproductive or lesser productive heavy isotopes, and the physical mixing of material in the sample.

The counting of (α,n) neutrons as a quantitative assay signature is restricted to those cases where the material to be assayed is homogeneous and of known

TABLE 7.1

(α,n) NEUTRON YIELDS FOR VARIOUS LIGHT ELEMENTS

Element X	Neutron Yield per 10^6 α's[a]	Yield Relative to Beryllium
Be	80	1.00
B	24	3.0×10^{-1}
F	12	1.5×10^{-1}
Li	2.6	3.6×10^{-2}
Na	1.5	1.9×10^{-2}
Mg	1.4	1.8×10^{-2}
Al	0.74	9.3×10^{-3}
As	0.38	4.8×10^{-3}
Si	0.16	2.0×10^{-3}
Cl	0.11	1.4×10^{-3}
C	0.11	1.4×10^{-3}
O	0.07	8.8×10^{-4}
N	0.01	1.25×10^{-4}

---

[a] J. H. Roberts, "Neutron Yields of Several Light Elements Bombarded with Polonium Alpha Particles," Los Alamos Scientific Laboratory internal document (1944).

chemical composition. Because numerous isotopic combinations could be made up to give the same neutron output, counting (α,n) neutrons must be considered as a verification or comparison check only and must not be relied upon for the quantitative assay of parcels with totally unknown contents.

7.3. Neutrons from Spontaneous Fission

Spontaneous fission is a form of breakdown of unstable heavy nuclides which competes with alpha, beta, and gamma radiation as a means for these nuclides to decay into more stable species. All fissionable isotopes undergo spontaneous fission to some degree, although in only a few cases is the rate of fission great enough to yield a quantity of neutrons adequate for assay purposes.

As is the case for the more familiar neutron-induced fission, when a nucleus undergoes spontaneous fission, it breaks up into two smaller nuclei plus a number of free neutrons. The breakup is a statistical process in which the two fission fragments can have a broad range of nuclear masses; therefore, the number of leftover free neutrons released is indeterminate for a single fission event. Averaged over many fissions of a single isotope, however, the number of neutrons $\bar{\nu}$ released by spontaneous fission of that isotope is well determined by the nature of the fission process. Because a spontaneously fissioning nucleus has one less neutron than a nucleus of the same isotope which is undergoing fission after absorption of a neutron, $\bar{\nu}$ for spontaneous fission of a given isotope is always somewhat lower than $\bar{\nu}$ for neutron-induced fission. Figure 7.1 shows a typical energy spectrum of fission neutrons, where the neutrons have a broad range of energies peaking below 1 MeV with an average energy between 1 and 2 MeV.

Table 7.4 lists spontaneous fission half-lives, prompt-neutron yields per fission, and spontaneous fission rates per gram of fissionable isotopes found in the fuel cycle. Note that the fertile species ^{238}U and ^{240}Pu have higher spontaneous fission rates than the fissile isotopes ^{235}U and ^{239}Pu.

$$\frac{\lambda_{SF}(^{238}U)}{\lambda_{SF}(^{235}U)} \approx 18 ,$$

and

TABLE 7.2

ALPHA AND (α,n) NEUTRON EMISSION FROM FISSIONABLE ISOTOPES

Isotope	α Half-Life[a] (yr)	α/s/g	Approximate α Energy[a]	Neutrons/s/ 10^6 α's on Be[b]	Neutrons/s/g on Be[c]
^{233}U	1.62×10^5	3.5×10^8	4.8	48	1.7×10^4
^{234}U	2.47×10^5	2.3×10^8	4.7	45	1.04×10^4
^{235}U	7.1×10^8	7.9×10^4	4.3 to 4.4	30	2.4
^{236}U	2.4×10^7	2.3×10^6	4.5	35	81
^{238}U	4.5×10^9	1.2×10^4	4.2	28	0.3
^{238}Pu	88	6.4×10^{11}	5.5	72	4.5×10^7
^{239}Pu	2.4×10^4	2.3×10^9	5.1 to 5.2	60	1.38×10^5
^{240}Pu	6.6×10^3	8.4×10^9	5.1 to 5.2	60	5.0×10^5
^{241}Pu	14.4[d]	9.4×10^7	4.9	50	4700
^{241}Am	432	1.3×10^{11}	5.5	72	9.4×10^6
^{242}Pu	3.79×10^5	1.4×10^8	4.9	50	7000

---

[a] C. M. Lederer, J. M. Hollander, and I. Perlman, *Table of Isotopes*, 6th Ed. (John Wiley & Sons, 1968); F. A. O'Hara et al., "Determination of Pu in Reactor Feed Materials," Monsanto Research Corp, Mound Laboratory report MLM-1798 (1972).

[b] Calculated from A. O. Hanson, Chapter 1A, in Fast Neutron Physics, J. B. Marion and J. L. Fowler, Eds. (Interscience, 1960), Vol. 1, p. 11, Fig. 7.

[c] [Column (5) x Column (3)] ÷ 10^6.

[d] 0.00246% α branching ratio: most of the time it beta decays to ^{241}Am.

TABLE 7.3

(α,n) YIELDS FROM OXIDES AND FLUORIDES

Material	Yield (neutrons/s/g)
$^{234}UO_2$	~14
$^{234}UF_6$	5.8×10^2
$^{235}UF_6$	12.2×10^{-2}
$^{238}UF_6$	12.9×10^{-3}
$^{238}PuO_2$	1.4×10^4
$^{238}PuF_4$	2.1×10^6
$^{239}PuO_2$	45
$^{239}PuF_4$	4300
$^{240}PuO_2$	170
$^{240}PuF_4$	1.6×10^4
$^{241}PuO_2$	~10
$^{241}AmO_2$	3754
$^{242}PuO_2$	~10

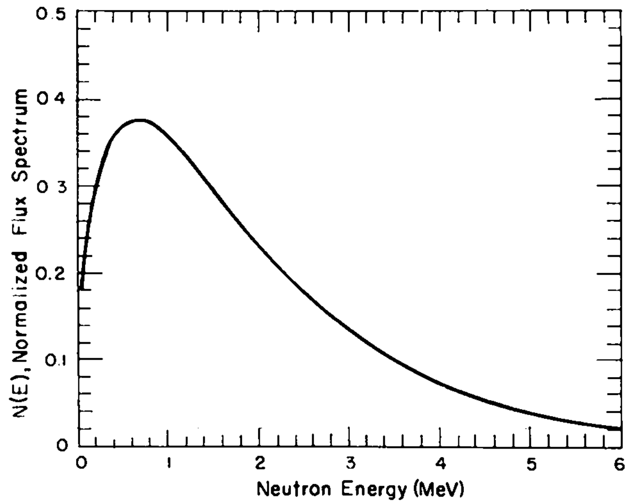

Fig. 7.1.
Typical energy spectrum of fission neutrons.

$$\frac{\lambda_{SF}(^{240}Pu)}{\lambda_{SF}(^{239}Pu)} = 4.7 \times 10^4 ,$$

where λ is the disintegration constant, that is, number of fissions per unit time.

Spontaneous fission is a process that occurs entirely within one nucleus. The (α,n) reaction, however, involves transport of the alpha particles through the material being investigated. Whereas the rate of emission of (α,n) neutrons is highly dependent upon the nature of the matrix containing the fissionable material being assayed, the rate of neutron emission from the spontaneous fission process depends only upon the nuclear properties and the quantities of the fissioning isotopes present. Although the number of neutrons detected from a sample will be influenced by neutron absorption and scattering within the sample, these effects are in general far less severe than the alpha-attenuation effects that influence the yield from (α,n) reactions. Therefore, for accurate assay by passive neutron counting, one usually selects the spontaneous-fission neutrons, discriminating against (α,n) neutrons by requiring that detected neutrons be in coincident pairs. Even then it is necessary to know the isotopic composition to arrive at a measure of the fissile components.

7.4. Interaction of Neutrons with Matter

The interaction probability of neutrons passing through a slab of material is expressed by an equation identical in form to Eq. (1.7), namely,

$$N = N_o e^{-\mu \rho \ell} .$$

However, the practice is to express μ_m in the following form.

$$\mu_m = \frac{A_o}{A} \sigma(E_n) \text{ cm}^2/\text{g} , \qquad (7.1)$$

where

A_o ≡ Avogadro's number ≅ 0.6023×10^{24},

A ≡ atomic weight, and

σ ≡ cross section with units of cm^2/atom.

TABLE 7.4

SPONTANEOUS FISSION OF FISSIONABLE ISOTOPES

Isotope	SF Half-Life (yr)[a]	$\bar{\nu}$ (SF)	SF/g-s
^{232}Th	1.4×10^{18}		4.1×10^{-5}
^{234}U	2.0×10^{16}	~2	2.8×10^{-3}
^{235}U	1.9×10^{17}	~2	2.96×10^{-4}
^{236}U	2×10^{16}	~2	2.8×10^{-3}
^{238}U	9.86×10^{15}[b]	1.95[d]	5.64×10^{-3}
^{238}Pu	4.9×10^{10}	2.26[d]	1.1×10^{3}
^{239}Pu	5.5×10^{15}	2.2[f]	1.0×10^{-2}
^{240}Pu	1.17×10^{11}[c]	2.17[c]	4.71×10^{2}
^{241}Pu	5.0×10^{15}[e]	2.2	1.1×10^{-2}
^{242}Pu	6.8×10^{10}[e]	2.16	8.0×10^{2}
^{241}Am	2×10^{14}[f]	2.3[g]	0.27
^{252}Cf	86[h]	3.8	6.14×10^{11}

---

[a] C. M. Lederer, J. M. Hollander, and I. Perlman, *Table of Isotopes*, 6th Ed., (John Wiley & Sons, 1968); see also A. Ghiorso, "Spontaneous Fission Correlations," Proceedings of the International Conference on the Peaceful Uses of Atomic Energy—Geneva, 1955, **7**, p. 15.

[b] J. H. Roberts, R. Gold, and R. J. Armani, "Spontaneous Fission Decay Constant of ^{238}U," Phys. Rev. **174**, 1482 (1968).

[c] P. Fieldhouse, D. S. Mather, and E. R. Culliford, "The Spontaneous Fission Half-Life of ^{240}Pu," J. Nucl. Energy **21**, 749 (1967).

[d] C. J. Orth, "The Average Number of Neutrons Emitted in the Spontaneous Fission of Some Even-Even Heavy Nuclides," Nucl. Sci. Eng. **43**, 54 (1971) and listed references.

[e] M. Taherzadeh, "Neutron Radiation Characteristics of PuO_2 Fuel," JPL Technical Report 32—1555 (1972).

[f] Private communication, R. C. Smith of Batelle Northwest to Eugene Weinstock of TSO, March 16, 1970.

[g] Quoted as "estimated" in reference f.

[h] A. Prince, "Nuclear and Physical Properties of ^{252}Cf," Brookhaven National Laboratory report BNL 50168 (T-530) (1969).

The concept of cross section refers to the effective target area a nucleus presents to the approaching neutron. Just as in archery, the larger the target the higher the probability of interaction. Cross sections are commonly given in units of barns, where 1 b equals 10^{-24} cm^2. Equation (7.1) then simplifies to

$$\mu_m = \frac{0.6023}{A}\,\sigma(E_n) \,, \qquad (7.2)$$

where σ is given in barns. The quantity $\mu_m\rho$ is given the name macroscopic cross section with the symbol Σ. At thermal energy the absorption cross section for plutonium is $\sim$1000 b. Therefore the transmission through 0.0254 cm (0.010 in.) of plutonium metal (ρ = 18 g/cm^3) is

$$\mu_m \rho l = \frac{(0.6)(1000)(18)(0.01)(2.54)}{239} = 1.15$$

$$\frac{N}{N_o} = e^{-1.15} = 0.32 = \text{number of neutrons that pass through the foil without interacting.}$$

Only 30% of incident thermal neutrons would be transmitted through a 10-mil foil. Cross-section values in general become smaller at higher neutron energies. For example, the absorption cross section for plutonium at 1 MeV is $\sim$500 times less than thermal value. This smaller cross section means greater penetrability through material. The total cross section is made up of partial cross sections corresponding to different reactions the neutron can have with the nucleus. (Neutrons interact with the nucleus and gamma rays interact with atomic electrons.) Values for cross sections are tabulated in a series of books, BNL 325,[7.4] known as the "barn books." Table 7.5 presents a comparison of attenuations for 400-keV gammas and 1-MeV neutrons, representative of signatures used in plutonium assay. The values in Table 7.5 show that neutron penetration at this energy is much higher than that of gamma rays through high-Z materials but is comparable for lower-Z materials. The values in Table 7.5 relate to the probability of any interaction occurring. Most of the neutron interactions do, in fact, still result in a neutron being detected. It is a situation analogous to the small-angle Compton scattering discussed in Sec. 1.2.f, only to a greater degree. This point will be discussed further at the end of Sec. 7.5.c.

TABLE 7.5

MEAN FREE PATH FOR 1-MeV NEUTRONS AND 400-keV GAMMA RAYS THROUGH VARIOUS MATERIALS

Material	ρ(g/cm^3)	$\frac{1}{\mu_\ell}$ (cm) 400-keV Gammas	$\frac{1}{\Sigma_{total}}$ (cm) 1-MeV Neutrons
H_2O	1	9.9	2.0
C	1.5	6.9	5.1
Al	2.70	4.1	5.6
Fe	7.86	1.4	4.8
Pb	11.35	0.43	6.1
U	18	0.20	3.0

7.5.a. Interaction Processes

It is possible to classify the kinds of neutron-matter interactions as follows.

1. Interactions in which the neutron is absorbed: (n,α) and (n,γ) reactions.
2. Scattering processes resulting in neutron energy loss: elastic and inelastic scattering.
3. Processes leading to additional neutrons being emitted: (n,2n) and fission processes.

A rough analogy exists between neutron interactions and photoelectric, Compton scattering, and pair production processes. However, the relative importance of each process and its Z and energy dependence will be significantly different for neutrons as compared to gammas. These differences make neutron counting preferable to gamma counting in some situations, and vice versa.[7.5]

7.5.b. Interactions in Which the Neutron Is Absorbed

The incoming neutron can be absorbed by the nucleus and subsequently emit another particle or gamma ray. One example would be the (n,α) reaction in which an alpha particle is emitted after the neutron is absorbed. This is the inverse of the (α,n) process discussed earlier. For most nuclides, this reaction is important only for neutron energies greater than approximately 5 MeV.

A second type of reacton is called "neutron capture" in which the nucleus absorbs a neutron followed by gamma-ray emission. This reaction is large at thermal or near-thermal neutron energies for some nuclides. Neutron capture is the mechanism which makes breeding of fissionable material possible. For example,

$$^{238}U + n \rightarrow {}^{239}U \xrightarrow{\beta^-} {}^{239}Np \xrightarrow{\beta^-} {}^{239}Pu \ .$$

Some materials, well known for their large capture cross sections, are used in reactor control rods or in shielding to remove neutrons. These materials, commonly called neutron poisons, include boron, cadmium, and gadolinium. The presence of poisons in combination with moderating material will significantly affect neutron assay results.

There are two absorption reactions of particular importance to neutron detection. These are

$$^3He(n,p)^3H$$

and

$$^{10}B(n,\alpha)^7Li \ .$$

Further discussion of these reactions is included in Sec. 8.2, Gas Proportional Counter Tubes.

7.5.c. Scattering Interactions

Neutron scattering by nuclei is a major interaction process for the energy range spanned by passive neutrons. (200 keV to several MeV). There are two kinds of possible scattering interactions that can occur: elastic or inelastic. The relative number of each type of scattering interaction occurring at a particular energy is given by the respective cross-section values at that energy.

Elastic scattering can be thought of as a collision between billiard balls of different weights. For a heavier nucleus, such as uranium, the neutron can scatter with a large change in direction but with very little energy loss. As the scattering nucleus becomes lighter, the maximum energy the neutron can lose becomes larger. In a collision with hydrogen, the neutron can lose up to all its energy in a single event. The amount of energy loss depends on the angle of scattering as it did for Compton scattering. The expression for the maximum energy loss, analogous to the Compton edge, is

$$\Delta E_{max} = E_n \frac{4mM}{(M+m)^2} \ ,$$

where

ΔE_{max} = maximum energy loss of the neutron ,

E_n = initial neutron energy ,

m = neutron mass , and

M = mass of scattering nucleus .

Table 7.6 shows the percent maximum energy loss for seven target nuclei.

Inelastic scattering involves internal excitation of the target nucleus by the incident neutron. This process is something like throwing a stone against a heavy bell. The bell does not recoil significantly, but vibrates to produce a ringing sound. The vibration is an internal excitation. Inelastic scattering is a mechanism whereby a neutron may lose a larger amount of energy in a collision with a heavy nucleus than would be possible through an elastic collision. For example, a 1-MeV neutron will lose a maximum of 17 keV in an elastic collision with ^{238}U. A 1-MeV neutron will lose 300 keV in every inelastic scattering with ^{238}U. In general, inelastic scattering cross sections are largest for heavier elements and for $E_n > 1$ MeV.

The process of slowing down neutrons by scattering interactions is called moderation. Table 7.6 shows that the lighter elements are the most efficient moderators, with hydrogen being the best. This is illustrated further in Table 7.7 where the average number of collisions required to thermalize 1 MeV neutrons is given for some common materials. It takes an order of magnitude fewer collisions to thermalize in H_2O than in heavier materials. Hydrogenous

TABLE 7.6

MAXIMUM ENERGY LOSS FOR TARGET NUCLEI (%)

Scattering Nucleus	$\Delta E_{max}/E_n \times 100$
H	100
^2H	89
^4He	64
^{16}O	22
^{56}Fe	7
^{208}Pb	2
^{238}U	1.7

compounds, e.g., H_2O and CH_2, in a sample will usually significantly influence the assay measurement. However, elastic scattering processes from heavier elements will have relatively little effect on the neutron count rate. This is due to two factors. First, the neutron detectors used for passive assay have relatively constant detection efficiency for neutron energies over a wide range, with no attempt made to distinguish one energy neutron from another. Thus, the energy loss due to a scattering event will usually not prevent the neutron from being counted. The second factor is the large-angle scattering that a neutron can undergo with only a small energy change. The values in Table 7.6 are for neutron scattering through 180°. Consequently, although some neutrons are scattered away from the detector, this may be compensated for by other neutrons being scattered into the detector. In fact, neutrons can be scattered into the detector or back into the sample by materials close to the counting setup, e.g., a concrete floor or wall.

Therefore we conclude that the calculation of sample attenuation is not straightforward. Using the total cross section will overpredict the sample attenuation.

7.5.d. Multiplication Processes

There are two kinds of neutron interactions that result in an increased number of free neutrons (multiplication). The first of these, the (n,2n) reaction, occurs only above approximately $E_n = 7$ MeV, with the exception of interactions with ^{9}Be and ^{2}D. For these two isotopes the thresholds are ~2.6 and ~3.2 MeV, respectively, with comparatively small cross sections. In most passive assay situations the (n,2n) will not contribute significantly.

The second type of multiplicative interaction is very important, namely, neutron-induced fission. Fissionable isotopes fall into two categories with respect to neutron-induced fission, fissile and fertile isotopes. The fissile isotopes are those which undergo fission for neutrons with energies down to thermal, whereas the fertile isotopes require the incoming neutron to have some minimum energy before fission will take place. The threshold energy varies from ~500 keV for ^{240}Pu to ~2 MeV for ^{232}Th. Figure 7.2 shows the fission cross section as a function of neutron energy for some of the isotopes.

As mentioned in Sec. 7.3, for a given atomic number Z, the fertile isotopes will have higher spontaneous fission rates than the fissile species. However, these emitted neutrons have a certain probability of interacting with the fissile material in the sample, causing additional fission neutrons to be emitted. Several factors influence the magnitude of the multiplication in a given sample.

1. Quantity and density of fissionable material—the more material localized in the sample, the better the chance for interaction.
2. Presence of moderator—because the fission cross section for the fissile species becomes as large as 800 b at very low neutron energies, the presence of moderating material, particularly hydrogen, will increase the magnitude of the fission multiplication significantly.
3. Reflecting material in the vicinity of the sample—reflecting neutrons into the sample will give

TABLE 7.7

NEUTRON MODERATION PARAMETERS FOR COMMON NDA MATERIAL

Material	Density (g/cm^3)	No. of Collisions for Thermalization[a]	Mean Free Path—Thermal (cm)[b]
H_2O	1.00	18	0.29
C	1.60	111	2.60
Al	2.70	242	10.2
Zr	6.40	803	2.89
Pb	11.35	1823	2.71
UO_2	10.0	486	1.85

---

[a] Parameter corresponds to number of elastic collisions required to lower energy from 1 MeV to 0.025 eV (thermal).

[b] Parameter corresponds to mean distance traveled between collisions by a thermal-energy neutron.

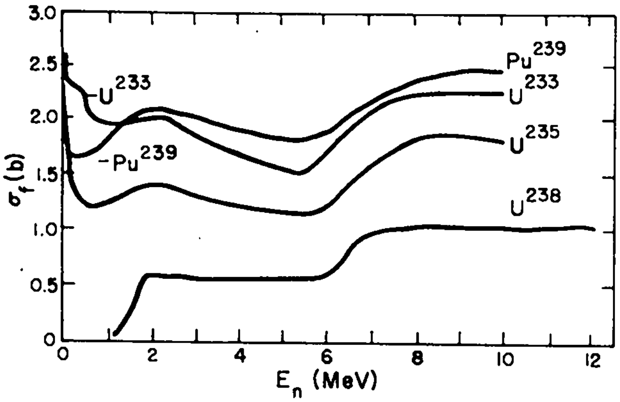

Fig. 7.2.
Neutron-induced fission cross section vs neutron energy.

the neutron another opportunity to cause a fission, particularly if it comes back at a lower energy.

4. Shape of sample, in particular the ratio of surface area to volume—in simplest terms the greater the surface area the more likely a neutron will leak out before interacting.

Multiplication and its effect on assay are discussed in more detail in Sec. 9.2.

REFERENCES

7.1. A. O. Hanson, in *Fast Neutron Physics*, J. B. Marion and J. L. Fowler, Eds. (Interscience Publishers, Inc., NY, 1960), Vol. 1, Chap. 1A.

7.2. H. Werle, "Spectrum Measurements of Radioactive Neutron Sources in the 10 keV - 10 MeV Energy Region with Proton-Recoil Counters," Karlsruhe Nuclear Research Center External Report INR-4170-25 (February 1970), Translation ORNL-tr-2415.

7.3. E. Amaldi, *Encyclopedia of Physics* (Springer-Verlag, Berlin 1959), Vol. 38, p. 119.

7.4. Brookhaven National Laboratory, "Neutron Cross Sections," Brookhaven National Laboratory Report BNL 325, Vol. I-III (May 1964 - Feb. 1965).

7.5. S. Glasstone and M. C. Edlund, *The Elements of Nuclear Reactor Theory* (Van Nostrand Company, NJ, 1952). This is an excellent reference book. Chapters 3 and 4 are of particular interest in that they deal with many of the subjects discussed in this manual.

8. NEUTRON DETECTORS

8.1. Introduction

There are two basic mechanisms by which a fast neutron can be detected. First, the neutron may collide with matter in a detecting medium and give up recoil energy to the medium, which is converted either into light or electrical charge, the magnitude of which is a measure of kinetic energy of the neutron. Secondly, if the medium contains isotopes with which the neutrons can enter into an exoergic nuclear reaction, the energy of this reaction can be converted into ionization, the presence of which indicates the interaction of a neutron with the detecting medium. For a comprehensive discussion of all kinds of neutron detectors, the reader is referred to Chaps. II and III of Marion and Fowler[8.1] and Chap. 10 of Price.[8.2]

When no information is desired about the energy of detected neutrons, and sensitivity is needed over a broad neutron energy range, the simplest, most stable type of fast-neutron detector system is one in which the neutrons are first thermalized by moderation in a hydrogen-containing medium such as polyethylene, paraffin, or water; and the thermal neutrons are detected using either the $^{10}B(n,\alpha)^7Li$ reaction or the $^3He(n,p)^3H$ reaction. The large thermal-neutron cross sections for these two reactions (3837 b for the former, 5327 b for the latter) make possible the construction of very efficient detectors. Normally, the thermal-neutron detectors are gas proportional counter tubes in which the energetic charged particles, which result from the reactions, dissipate their energy by ionizing the gas in the counter tube. The liberated electric charge is collected and amplified to generate a signal.

8.2. Gas Proportional Counter Tubes

One of the oldest devices employed for nuclear radiation detection is a gas-filled chamber with electrodes arranged to collect the electric charge produced by the interaction of nuclear radiation with the chamber gas. The chamber is usually a metal cylinder with a thin, insulated wire mounted on its axis (Fig. 8.1). The center wire, or anode, is maintained at a positive potential of from several hundred to several thousand volts with respect to the outer cylinder, or cathode, which also serves as the container for the counter gas.

Nuclear radiation interacts with the counter gas in a number of ways. Gamma radiation produces energetic free electrons by Compton scattering, photoelectric effect, or pair production. The free electrons so produced are slowed down by ionizing collisions with counter gas molecules, and a free charge $Q = Ee/\varphi$ is produced where E is the initial photon energy, e is the electronic charge, and φ is the average energy necessary to produce an ion pair. A beta particle energetic enough to penetrate the chamber wall (or originating from a source placed within the counter) will interact directly with the counter gas to produce a track of ion pairs. Heavier charged particles, such as alphas, likewise lose energy by ionizing gas molecules in their path. However neutrons having no charge will not produce ionization along their paths through matter. A neutron loses energy by colliding with an atomic nucleus, to which it gives up part of its energy by momentum transfer. This is the scattering reaction discussed in Sec. 7.5.c. The recoiling atom then ionizes and gives up the energy it has gained by ionizing other molecules. For the momentum-transfer process to be most effective, the atom against which the neutron recoils should be hydrogen, in which case the neutron can transfer up to all of its energy to the recoiling proton (see Table 7.6).

Another way of detecting a neutron is to have it cause an exoergic (energy-releasing) nuclear reaction, the products of which are charged particles. Such a reaction can occur when a neutron reacts with ^{10}B.

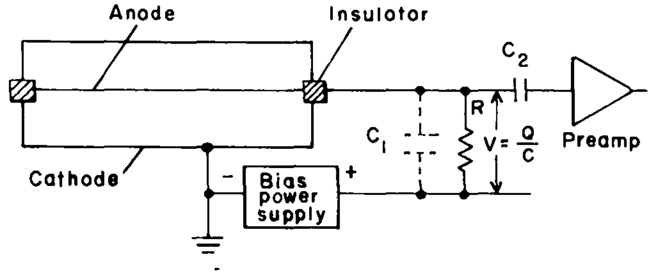

Fig. 8.1.
Typical proportional counter setup.

$$^{10}\text{B} + n \rightarrow {}^{7}\text{Li} + {}^{4}\text{He} + 2.78\ \text{MeV},$$

in which case the 2.78 MeV is shared by the product ^{7}Li and ^{4}He, or

$$^{10}\text{B} + n \rightarrow {}^{7}\text{Li}^{*} + {}^{4}\text{He} + 2.30\ \text{MeV}$$

$$^{7}\text{Li}^{*} \rightarrow {}^{7}\text{Li} + 0.48\ \text{MeV}\ ,$$

in which latter case the gamma-ray energy is usually lost from the detector.

An alternate nuclear reaction that can be used for detecting neutrons in a gas counter uses ^{3}He.

$$^{3}\text{He} + n \rightarrow {}^{3}\text{H} + {}^{1}\text{H} + 765\ \text{keV},$$

which is then converted to energy of ionization as before.

What happens to the ion pairs generated within the detector volume depends upon the voltage applied between the cathode and anode. At low voltages the primary ions and electrons have a chance to recombine before they are collected at the walls or center wire of the detector. As voltage is increased (Fig. 8.2), a point is reached where all of the ion pairs are collected, and at this point a plateau is reached where further voltage increase produces no more ion pairs. In this state, the tube is said to be an ionization chamber. The charge collected at the anode is proportional to the energy deposited within the detector and is independent of the anode voltage.

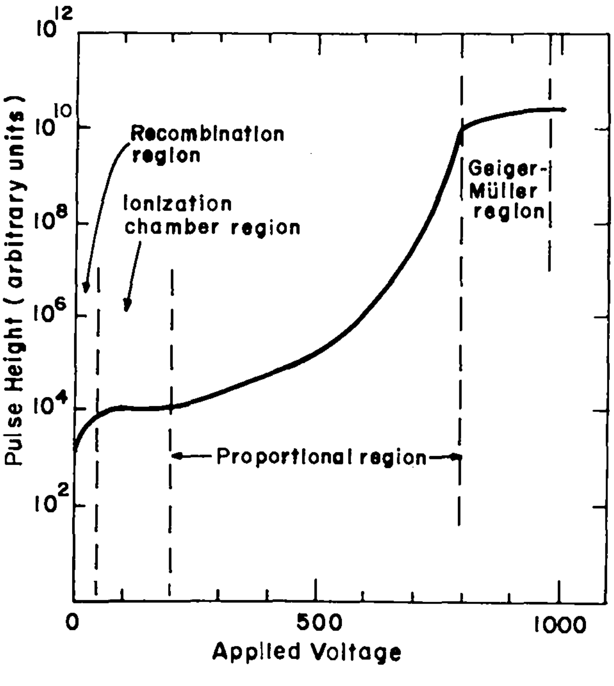

Fig. 8.2.
Pulse-height vs applied-voltage curves to illustrate ionization, proportional, and Geiger-Muller regions of operation.

As voltage is increased further, however, a point is reached where primary ions in the chamber can be accelerated between intermolecular collisions enough so that they can ionize other molecules. The result is a multiplication process in which the total charge collected on the anode is still dependent directly upon the initial energy deposited in the detector, but also increases rapidly with applied voltage. This is the so-called proportional-counter mode of detector operation. Charge multiplication of 10^{6} or more is possible before the counter loses its ability to distinguish between events of different energies.

As the voltage is increased even more, a point is reached where the charge collected is independent of the quantity of ionization initiating the event. The size of the pulse from the tube is characteristic only of the tube geometry and filling and of the external electronic circuitry. The detector is then a Geiger-Muller tube. Geiger tubes are used in most low-level survey instruments and in applications where it is not necessary to determine the type or energy spectrum of the radiation being counted. The amplification available in the tube and the uniform pulse heights for detected radiation make the Geiger-Muller tube one of the easiest nuclear radiation detectors to use.

Neutrons are almost always accompanied by gamma radiation. Therefore, it is usually desirable that a neutron detector be capable of distinguishing between a neutron and a gamma ray. For this reason, gaseous neutron detectors are usually operated in the proportional region (in rare cases, in the ionization-chamber region).

If it is not necessary to know the energy of the neutron, it is expedient to slow down or moderate the neutron before detecting it to take advantage of the large thermal cross section of either the $^{10}\text{B}(n,\alpha)^{7}\text{Li}$ reaction or the $^{3}\text{He}(n,p)^{3}\text{H}$ reaction. Normally, the boron is in the form of BF_3 gas; it can also be introduced as a thin layer on the inside wall of the detector. If ^{3}He gas is used, it is usually mixed with a heavy gas such as argon or krypton to assure that the protons released in the $^{3}\text{He}(n,p)$ reaction are stopped before they reach the counter wall.

A pulse-height distribution from thermal neutrons incident upon typical ^{3}He proportional counters is shown in Fig. 8.3. The full-energy peak corresponds to events where the reaction products are stopped completely in the active region of the counter gas. The spread of the full-energy peak is due to the statistical nature of the ionization process and to the unevenness of the accelerating field over the volume of the tube. There is a low-energy tail of pulses due to neutrons that react near the walls or field-free "dead spaces" at the ends of the tubes. For these events, some of the reaction product energy has been dissipated in the tube wall or end spaces and has therefore not been converted into ion pairs. Finally, at low pulse heights the response to gamma radiation is seen. Because the electrons released by photon interactions have much greater track lengths than the ions created by neutron reactions, there is an upper limit (around 300 to 500 keV) to the energy which can be deposited in this type of counter by a Compton or photoelectron. However, if the gamma field is intense, it is possible for pulses due to gamma radiation to overlap and to give "pileup" pulses, which will overlap part of the neutron pulse distribution.

It is possible to discriminate between neutron and gamma pulses in these detectors. Because the track lengths of Compton electrons are longer than those of neutron reaction products, the collection of ion pairs in an electron track will usually spread over a greater time interval than will the collection of ion pairs produced in a proton, alpha, or triton track with the same total energy. Therefore, the risetimes of counter pulses arising from gamma radiation are generally longer than those from neutrons. Circuitry exists which uses this principle to reduce the gamma pileup effect in neutron proportional counters. Where gamma fields are high, this technique is sometimes helpful.

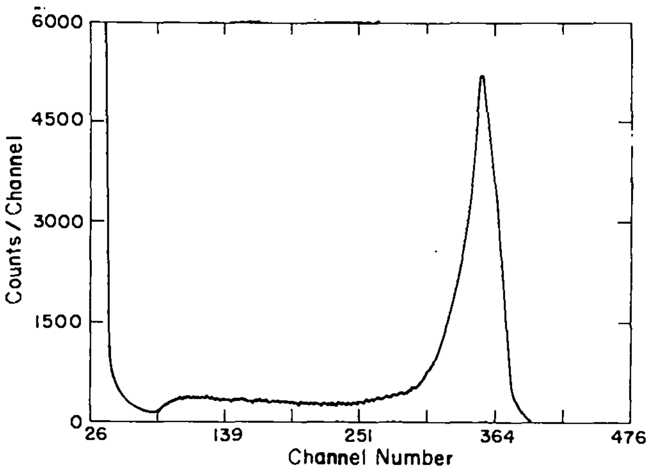

Fig. 8.3.

Differential pulse-height distribution from thermal neutrons in a ^{3}He-filled proportional counter tube.

8.3. Moderator Assemblies

Thermalization of fast neutrons before detection serves two purposes: it increases detection efficiency and reduces energy dependence of the overall detection system efficiency. As discussed in Chap. 7, a detection efficiency independent of energy tends to make the assay independent of matrix effects due to scattering in the sample. One of the oldest applications of this principle is the "Long Counter" of Hanson and McKibben.[8.3] This counter, consisting of a BF_3 tube imbedded axially in a paraffin cylinder, 20-cm-diam by 30-cm-long, has a response to neutrons which is energy independent from 25 keV to 5 MeV to within 15%. Improved versions of this counter have been made employing shielding to achieve directional sensitivity, with some holes drilled in the front detector wall to improve the flatness of response at low energies. Allen[8.4] discusses the design of these counters in detail.

Two more efficient and flatter response counters were developed by East and Walton[8.5] to implement neutron-counting techniques being developed for nondestructive assay of fissionable materials. One of these, similar in size and shape to the long counter, employs five ^{3}He proportional counter tubes and is 11.5% efficient (intrinsic) over the 23-cm-diam sensitive region and is flat to within ±3% from 25 keV to 5 MeV. The other is a 50- by 61- by 15-cm polyethylene slab containing 13 ^{3}He counters with an intrinsic efficiency of 18%. This "slab detector" is shown in Fig. 8.4.

8.4. Portable Neutron Probe, "SNAP"

A shielded neutron assay probe (SNAP)[8.6] has been designed to use with commercially available portable electronic units, e.g., Eberline SAM I and Ludlum Model 22. The SNAP detector consists of two (or one) 2-cm-diam by 14-cm-long (active), 4-atm ^{3}He counters contained in a 7.6-cm-diam, 23-cm-long polyethylene cylinder surrounded by a cadmium sheet. This probe may be used without shielding, or be placed inside a directional shield, as shown in Fig. 8.5. The weight of SNAP, including shield, is approximately 9 kg (20 lb), which is adequately portable. Figure 8.6 shows a SNAP system complete with a portable electronic unit.

The total detection efficiency of SNAP (with its shield) for a point neutron source 1 m from the detector is given in Table 8.1 and Fig. 8.7. Corresponding efficiency values for the slab detector shown in Fig. 8.4 are included for comparison. However, the weight of the slab detector with shield is greater than 90 kg (200 lb), hardly portable. Because the SNAP is

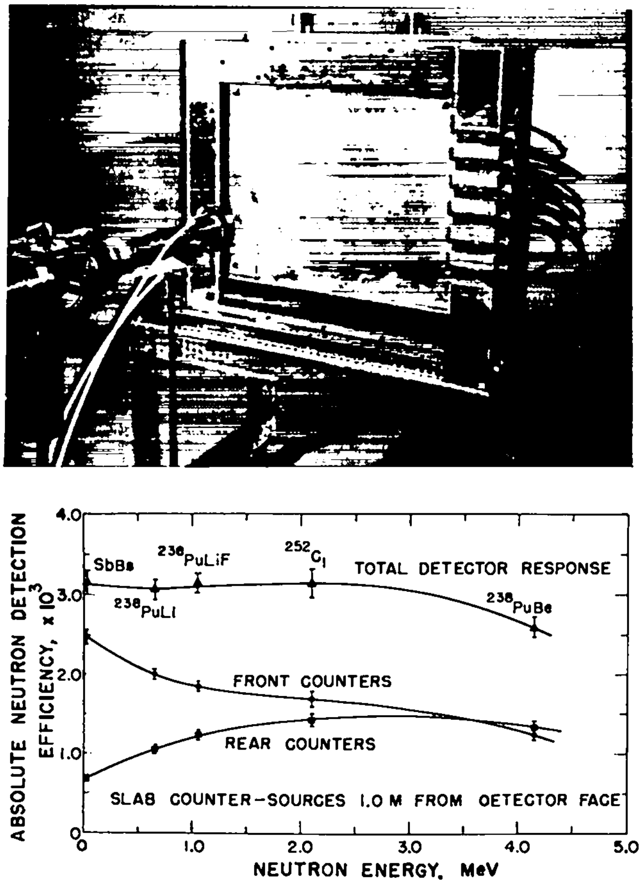

Fig. 8.4.
High efficiency slab neutron detector.

not flat in energy response, it will have a slightly enhanced sensitivity to sample moderation.

As a function of radial distance r from the axis of the detector, the efficiency has been found to vary as $(r + 2.54)^{-2}$, where r is measured in centimeters and $r \geq 13$ cm. When performing measurements in close proximity to surfaces that are highly reflective to fast neutrons (such as concrete), the efficiency will decrease less strongly than $(r + 2.54)^{-2}$. The directional sensitivity of SNAP, measured with a ^{238}PuLi source as a function of angle around the detector, is presented in Fig. 8.8. SNAP provides approximately 120° of sensitivity in the forward direction and exhibits a shielding factor of greater than 4.2 for background neutrons impinging at angles between 80 and 280°. For source neutrons of higher mean energy than 650 keV, the shielding factor is somewhat less; for example, it is about 2.25 for ^{252}Cf source neutrons.

Current applications involving SNAP include verification of UF_6 cylinder contents, UF_4 "green" salt, and metallic plutonium buttons.

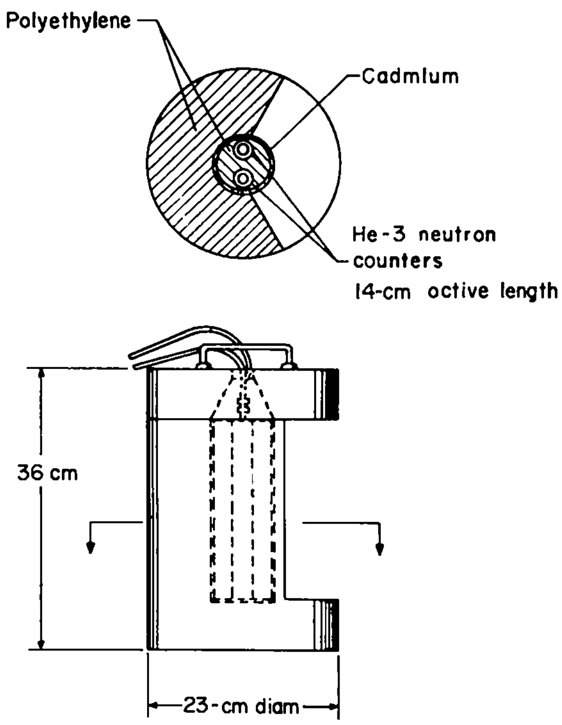

Fig. 8.5.
Assembly drawing of the portable shielded neutron assay probe (SNAP).

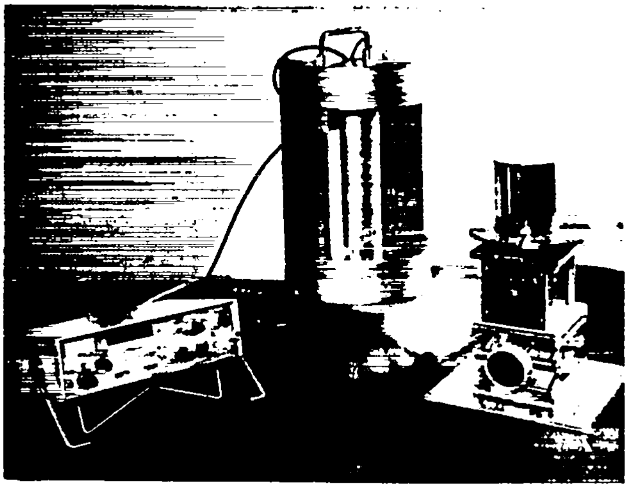

Fig. 8.6.
A portable shielded neutron assay probe (SNAP), complete with electronics.

8.5. Other Neutron Detectors

1. Plastic and Liquid Scintillators. Plastic and liquid scintillators are sometimes used for the detection and energy measurement of fast neutrons. The

TABLE 8.1

TOTAL EFFICIENCY FOR POINT SOURCE AT ONE METER

Source	$\bar{E}_n$ (MeV)	SNAP[a]	Slab Detector[a]
^{238}PuLi	0.65	9.7×10^{-5}	3.1×10^{-3}
^{238}PuLiF	1.1	8.3×10^{-5}	3.1×10^{-3}
^{252}Cf	2.2	6.6×10^{-5}	3.1×10^{-3}

---

[a] Total Efficiency $\left(\frac{\text{Neutrons Detected}}{\text{Neutrons Emitted}}\right)$

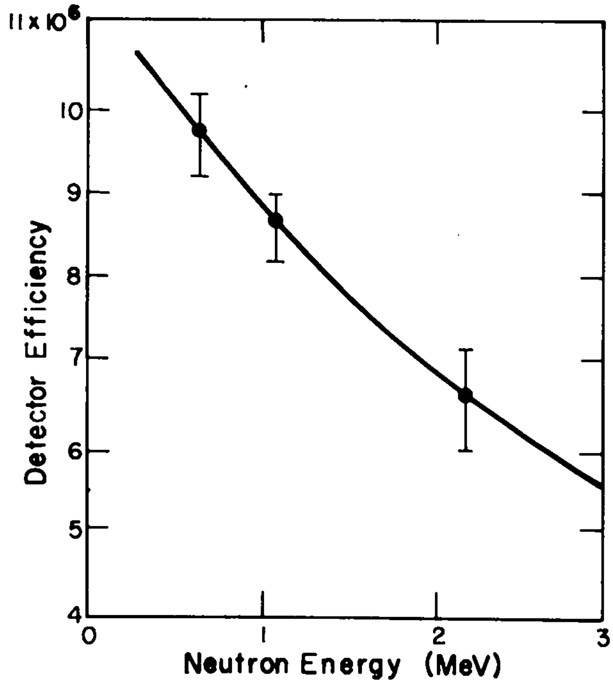

Fig. 8.7.
Efficiency vs neutron energy for SNAP detector.

detection mechanism is the recoil of hydrogen atoms in the scintillator and subsequent conversion of the recoil energy into pulses of light, which are detected by a photomultiplier tube. Plastic and liquid scintillators have the advantage that, although the risetime of proportional counter signals is of the order of a few microseconds, the scintillators have risetimes in the nanosecond range. Thus, scintillator systems can be operated at much greater counting rates without pileup or deadtime problems.

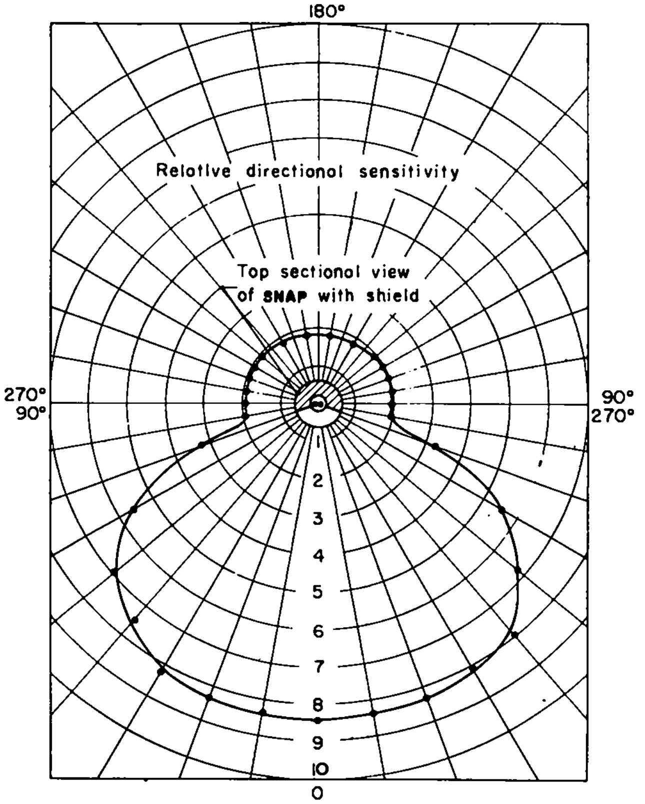

Fig. 8.8.
Directional sensitivity of SNAP as a function of angle, as measured in the midplane of the detector with a PuLi point source ($E_n \simeq 0.65$ MeV).

A further advantage accrues when contrasting plastic-scintillator neutron coincidence counting systems with the more frequently used (for safeguards) thermalizing coincidence systems with proportional counters. Because the average neutron lifetime in detectors of the latter type is between 15 and 100 μs, very long coincidence gates must be used if the systems are to be efficient.

The weakness of plastic or liquid recoil scintillators is their sensitivity to gamma radiation. Pulses from gamma rays and from neutrons are approximately the same size in these detectors. Differences do exist, however, between the shapes of neutron- and gamma-ray-induced pulses from some liquid scintillators. These differences have been used to make such detectors less gamma sensitive.[8.7]

2. *Hornyak Buttons.*[8.8] A Lucite block impregnated with silver-activated zinc sulphide will scintillate when irradiated with fast neutrons. The principal means for detection is recoil of the hydrogen in the Lucite; however, the ^{32}S(n,p)^{32}P and ^{32}S(n,α)^{29}Si reactions also contribute. These detectors have a

maximum efficiency for 5-MeV neutrons.[8.9] Gamma-ray discrimination is available on the basis of pulse-height differences.

3. ^{4}He and Proton-Recoil Proportional Counters. For fast-neutron detection without previous thermalization, recoil of neutrons from light nuclei in proportional counters is used as a means of detection and energy measurement. Techniques for neutron spectroscopy with proton-recoil counting have been developed and used by Bennett et al.[8.10] The ^{4}He counter is used in numerous safeguards active assay systems. This latter type of counter is relatively insensitive to gamma radiation and low-energy neutrons and is used for detection of fast neutrons from fission in the presence of thermal neutrons inducing fission.

REFERENCES

8.1. J. B. Marion and J. L. Fowler, "Fast Neutron Physics, Part I," (Interscience Publishers, NY, 1960).

8.2. W. J. Price, "Nuclear Radiation Detection," (McGraw-Hill Inc., NY, 1958).

8.3. A. O. Hanson and J. L. McKibbon, "A Neutron Detector Having Uniform Sensitivity from 10 keV to 3 MeV," Phys. Rev. **72**, 673 (1947).

8.4. W. D. Allen, Chap. III.A of Ref. 8.1.

8.5 L. V. East and R. B. Walton, "Polyethylene Moderated ^{3}He Neutron Detectors," Nucl. Instrum. Methods **72**, 161 (1969).

8.6. R. B. Walton and T. L. Atwell, Los Alamos Scientific Laboratory A-1 Progress Report LA-5291-PR (1973), p. 14. The title of this article is "Portable Neutron Probe, 'SNAP'."

8.7. R. A. Winyard, J. E. Lutkin, and G. W. McBeth, "Pulse Shape Discrimination in Inorganic and Organic Scintillators.I," Nucl. Instrum. Methods **95**, 141 (1971).

8.8. W. F. Hornyak, "A Fast Neutron Detector," Rev. Sci. Instrum. **23**, 264 (1952).

8.9. C. O. Muilhause, pp. 405-407 of Ref. 8.1.

8.10. E. F. Bennett and T. J. Yale, "Techniques and Analyses of Fast Reactor Neutron Spectroscopy with Proton-Recoil Proportional Counters," Argonne National Laboratory report ANL-7763 (1973).

9. PASSIVE NEUTRON VERIFICATION MEASUREMENTS

9.1. Considerations in Applying Passive Neutron Counting

In approaching an assay problem for which passive neutron counting will be used as the signature, the first step is to calculate the contribution of the various isotopes and neutron processes to the total count rate. To do this, information on the chemical form and isotopic composition is needed. Consider the following three chemical forms of recycle plutonium: metal, PuO_2, and PuF_4. Table 9.1 lists the individual neutron emission rates for each isotope and process. The rates were computed from the values given in Tables 7.2, 7.3, and 7.4. The spontaneous fission rate, being independent of chemical form, is the same in each case whereas the (α,n) rate changes dramatically. General conclusions that can be reached for this particular plutonium isotopic composition are

1. For metal having no (α,n) component, the quantity being measured is ^{240}Pu (with contributions from ^{238}Pu and ^{242}Pu). This will be true for almost any ^{240}Pu isotopic percentage found in the nuclear fuel cycle. It will not be true for material rich in ^{238}Pu such as is used in the heart pacer program.

2. The neutron output from PuO_2 has comparable contributions from both processes, 107 n/g-s from (α,n) and 210 n/g-s from spontaneous fission. The small amount of ^{238}Pu (0.3%) contributes 14% of the total output.

3. For PuF_4, the neutron rate is dominated by the (α,n) processes and therefore is more sensitive to the amount of the minor ^{238}Pu isotope. It is interesting to note that, in this situation, neutron counting gives the same information as calorimetry, namely, the α emission rate.

The above examples do not include the contribution from ^{241}Am that will increase as ^{241}Pu decays. Three to four years after chemical separation, the ^{241}Am (α,n) rate will be comparable to that of ^{239}Pu and ^{240}Pu for this recycle material.

Light element impurities, particularly beryllium, can affect the total neutron rate. Consult Table 7.1 for the specific elements of possible concern.

Once the emission rates have been calculated, an estimate of the counting rate in the detector can be made. The counting rate is the emission rate times the total detection efficiency (Sec. 2.4.b). Consider counting the plutonium samples described above using the SNAP probe at a sample-to-detector distance of 30 cm. The overall efficiency is

TABLE 9.1

NEUTRON EMISSION RATES FOR Pu METAL, PuO_2 AND PuF_4

		Neutron Rate for 100 g of Pu (n/s)		
Isotope	Wt%	Metal (Spontaneous Fission)	PuO_2 (α,n)	PuF_4 (α,n)
^{238}Pu	0.3	746	4 200	630 000
^{239}Pu	75.6	2	3 400	325 080
^{240}Pu	18.0	18 400	3 060	288 000
^{241}Pu	5.0	~0	50	5 000
^{242}Pu	1.1	1 900	10	1 000
	Total	21 048	10 720	1 249 080

$$\epsilon = (6.6 \times 10^{-5})\left(\frac{102.54}{32.54}\right)^2$$

$$= 6.6 \times 10^{-4} \text{ counts/neutron emitted} .$$

This efficiency was obtained by correcting the value given in Sec. 8.4 for a closer sample-detector separation $[(r + 2.54)^{-2}$ dependence$]$. Counting rates for the three 100-g plutonium samples are plutonium metal, 13.9 counts/s; PuO_2, 21.0 counts/s; and PuF_4, 838 counts/s.

These rates must now be compared to the background rates expected at the counting location. Knowledge of backgrounds can only be obtained by experience and direct measurement. The SNAP detector is designed to preferentially detect neutrons striking its front face. Backgrounds will be reduced if the detector is oriented with the front face away from the major sources of background, such as storage vaults.

With the exception of hydrogen (e.g., H_2O and CH_2), matrix materials commonly found in assay samples do not greatly affect fast-neutron flux. To illustrate the effect that matrix material has on neutron counting, the following experiment was performed using the SNAP detector (Sec. 8.4). A 4-liter can was placed 30 cm from the front face of the SNAP unit with provision for positioning a neutron source in the center of the can. The counting rate of the source was measured for the empty can. Matrix material was added to the can and the rate was remeasured. Table 9.2 presents the results of these measurements normalized to the empty can case. An examination of column 5 indicates that most of the outgoing source neutrons do, in these examples, interact with the matrix material before emerging from the can. The dominant interaction is by elastic scattering with varying amounts of energy loss depending on the particular scattering material. Because the scattering material is located symmetrically around the neutron source, the number of neutrons scattered away from the detector is balanced by neutrons scattered into the SNAP, that is, inscattering equals outscattering. The counting rate is greater with the material present because the detector efficiency is higher at lower neutron energies (Fig. 8.7).

For the hydrogenous material, the count rate increases at the lowest density, but as more hydrogen is added the rate decreases. With the higher density sample, a greater number of the neutrons are moderated to the point where they are absorbed before they reach the detector tubes. They can be absorbed by the cadmium cover of the SNAP unit or by the hydrogen, either in the sample or in the detector. The SNAP detector is said to be undermoderated.

The SNAP detector was designed for a specific situation in which the matrix material did not vary. It is possible to modify the SNAP detector design to make its efficiency less energy dependent with a small increase in weight. But even as presently

TABLE 9.2

MATRIX EFFECTS ON NEUTRON COUNTING

(~4-liter container 16.5-cm-diam by 19-cm-high)

Material	Weight		Density	Interaction[a] Probability	Normalized Counting
	kg	lb	(g/cm^3)	(%)	Rate
Empty	0	0	0	0	1.00[b]
Pb	26	58	6.9	57	1.06
Fe	17	37	4.4	63	1.10
SiO_2	6	13	1.6	80	1.12
CH_2	0.7	1.6	0.2	60	1.21
CH_2	2.5	5.6	0.7	95	1.06
H_2O	3.6	8	1.0	98	0.73

---

[a] Interaction probability $\equiv (1 - e^{\Sigma \cdot \ell}) \times 100$.

[b] Normalization point.

TABLE 9.3

MULTIPLICATION OF Pu FOR VARIOUS SHAPES
(Pu Weight—2 kg; 10% ^{240}Pu)

Shape	Dimensions (cm)	Total Neutrons Emitted from Sample / No. of Spontaneous Fission Neutrons
Sphere	$r = 2.98$	1.80
Cube	$\ell = 4.81$	1.73
Cylinder	$d = 5.21, h = 5.21$	1.74
Cylinder	$d = 7.07, h = 2.83$	1.63
"Pancake"	$d = 8.91, h = 1.78$	1.47

designed, the sensitivity to matrix material is relatively small. Twenty-six kilograms of lead changed the counting rate by only 6%.

The discussion in Sec. 5.2 of count rate sensitivity to the location of nuclear material within the sample container is also applicable to neutron counting. The recommendations for sample-to-detector distances combined with sample rotation should be followed.

The type of calculations presented above provides guidance for planning the assay measurement. However, as was recommended earlier, the use of standard samples matching the unknown samples will lead to more accurate assay values.

9.2. Multiplication

Many situations for which passive neutron counting is applicable involve large quantities of dense fissionable material, such as plutonium buttons. In these cases, the observed neutron emission rate from a sample can be increased when the initial (α,n) and spontaneous fission neutrons induce additional fission reactions before passing out of the sample. In addition, the neutrons that have escaped from the sample can reflect back into the sample, usually after thermalization, and induce additional fission reactions. Because the neutron fission reaction releases more neutrons than it uses, there is a net gain or multiplication in the neutron emission rate. The magnitude of this multiplication is very dependent on the mass, density, and spatial distribution of fissionable material in the sample. For example, Table 9.3 lists the multiplication for 2 kg of plutonium metal in different shapes: sphere, cylinder, "pancake," and cube. It can be seen that the multiplication effect is large and is sensitive to the shape of the sample. Where possible, standards spanning the mass range of the unknowns should be used to correct for multiplication as well as for other matrix effects.

An article by Atwell et al.[9.2] is recommended as a detailed example of neutron counting applications, including corrections for multiplication, to the verification of plutonium metal buttons.

9.3. Neutron Counting of Uranium Samples

Total neutron counting of uranium samples is also feasible although usually larger quantities are required. The primary neutron source for some uranium common materials are given here.

1. Low enrichment UO_2—neutron yield dominated by spontaneous fission in ^{238}U; therefore gross counts nominally proportional to ^{238}U weight.

2. High enrichment UO_2—neutron yield dominated by ^{234}U alpha decay reacting with the ^{18}O (0.20% abundant in normal oxygen).

3. UF_6—all enrichments—neutron yield dominated by ^{234}U alpha decay reacting with fluorine.

Passive neutron counting can be used for the ^{235}U assay of UF_6 cylinders if the $^{235}U/^{234}U$ ratio is known. Because ^{234}U is the dominant alpha emitter in enriched uranium, it is the principal source of neutrons from $^{19}F(\alpha,n)$ neutrons in UF_6. The $^{235}U/^{234}U$ ratio may vary by as much as a factor of two over the complete range of enrichment; but for low enriched uranium (<5%), it is more nearly constant and verification measurements of limited accuracy may be possible without specific ^{234}U isotopic data.[9.3]

Table 9.4 lists alpha activities and neutron yields of the uranium isotopes. These data were used to

TABLE 9.4

ALPHA-DECAY AND UF_6 NEUTRON YIELDS FOR U ISOTOPES

Isotope	$T_{1/2}$ (yr)	Alpha Activity (α/g)	f_{α}^{a}	Neutrons/g-s
^{234}U	2.48×10^{5}	2.27×10^{8}	1.00	5.8×10^{2}
^{235}U	7.13×10^{8}	7.90×10^{4}	0.56	12.2×10^{-2}
^{236}U	2.39×10^{7}	2.35×10^{6}	0.75	3.95×10^{0}
^{238}U	4.51×10^{9}	1.23×10^{4}	0.38	12.9×10^{-3}

---

[a] f_α is the F(α,n) yield correction factor (relative to ^{234}U) which accounts for effect of different alpha particle energies.

calculate the neutron yields of the isotopes of normal uranium (0.71% $^{235}U/^{234}U = 125$) shown in Table 9.5. An approximate expression for the neutron yield of UF_6 is

$$S(\text{neutrons/s}) = M_U(0.0285 + 5.76\ I_{234}) \ , \qquad (9.1)$$

where

M_U = mass of uranium in grams, and

I_{234} = ^{234}U isotopic abundance in percent.

Estimates of the neutron source strengths of 2268 kg (5000 lb) of normal UF_6 and 3% enriched UF_6 are 9.4×10^4 and 2.6×10^5 n/s, respectively.

TABLE 9.5

UF_6 NEUTRON YIELDS OF NORMAL URANIUM

Isotope	Neutrons per s-g U	Relative Yield (%)
^{234}U	3.3×10^{-2}	53.5
^{235}U	8.7×10^{-4}	1.4
^{238}U	12.8×10^{-3}	21.0
^{238}U s. f.[a]	1.5×10^{-2}	24.1
Total:	6.2×10^{-2}	

---

[a] Spontaneous fission.

Passive neutron counting of UF_6 cylinders is one of the fastest, simplest, and least expensive methods for verification (±6%, 1 σ) of low enriched UF_6. If either the specific neutron yield of the UF_6 or the ^{234}U isotopic abundance were included in the cylinder specifications from the originating station, passive neutron counting would provide an accurate verification procedure.

9.4. Spontaneous Fission Coincidence Counting

To avoid the ambiguities caused by variable (α,n) yields from assay samples, neutron coincidence counting[9.5,9.6] of spontaneous fission neutrons provides a useful assay technique if the isotopic composition is known. During a spontaneous fission reaction, two to three neutrons are emitted at essentially the same time. Neutron coincidence detectors are designed to separate the multiple neutron emission events from the (α,n) background neutrons.

Because the spontaneous fission rates are rather low (Table 7.4), high-efficiency detection systems are essential for rapid, quantitative assay. Thermal-neutron detectors having ^3He or BF_3 proportional counters and polyethylene moderators with efficiencies as large as 60% for total neutron detection have been developed for this purpose. These detectors completely surround the sample. The sensitivity of the units with high efficiency is ~1 mg ^{240}Pu and 50 g ^{238}U, and the variable neutron die-away time (the average time for fission spectrum neutrons to thermalize) makes it possible to assay a wide range of plutonium loading (~1- to 1000-g plutonium). The long slowing-down times (10- to 150-μs) require correspondingly large coincidence gate times, and this results in sizable accidental neutron background rates—especially in samples with high-neutron emission rates.

In addition to the thermal-neutron detectors, organic scintillation detectors have been used for coincidence detection of spontaneous fission.[9.7,9.8] Usually these scintillators detect both fast neutrons and gamma rays emitted during the fission process, therefore the effective multiplicity of detectable emissions is greatly increased because there are about three times more prompt gamma rays than prompt neutrons. There is no slowing down process required in the detector, therefore the coincidence gate times are $\sim 10^3$ times shorter than for thermal-neutron detectors. These short coincidence gate times (~50 ns) result in a small accidental background rate even for high count rate samples. However, the assay results are more dependent on sample geometry and matrix materials. Many of the problem areas encountered in using neutron coincidence counters are summarized elsewhere.[9.9] An additional problem area, namely criticality, is discussed in Appendix C.

REFERENCES

9.1 J. E. Foley, Los Alamos Scientific Laboratory A-1 Progress Report, LA-4605-MS (1970), p. 25. The title of this article is "4π-Neutron Counter for 55-Gallon Barrels."

9.2. T. L. Atwell, D. B. Smith, and A. C. Walker, Los Alamos Scientific Laboratory A-1 Progress Report, LA-5431-PR (1973), p. 20. The title of this article is "Assay of Plutonium Metal Buttons with a Portable Neutron Counter."

9.3. R. B. Walton, T. D. Reilly, J. L. Parker, J. H. Menzel, E. D. Marshall, and L. W. Fields, "Measurements of UF_6 Cylinders with Portable Instruments," Nucl. Tech. **21**, No. 2, 133, (1974).

9.4. Thomas E. Sampson, "Neutron Yields from Uranium Isotopes in Uranium Hexafluoride," Nucl. Engr. Sci. **54**, No. 4, 470 (1974).

9.5. G. R. Keepin, "LASL Safeguards Research and Development Program," Proc. AEC Symposium on Safeguards Research and Development, Los Alamos, NM (1969), WASH-1147, p. 114.

9.6. R. Sher, "Operating Characteristics of Neutron Well Coincidence Counters," Brookhaven National Laboratory report BNL 50332, TSO, BNL (1972).

9.7. T. Gozani and D. G. Costello, "Isotopic Source Assay System for Nuclear Materials," Trans. Amer. Nucl. Soc. 13, 2, 746 (1970).

9.8. R. B. Walton and A. C. Berick, Los Alamos Scientific Laboratory A-1 Progress Report, LA-4070-MS (1969), p. 20. The title of this article is "Gamma Ray 'SLAB' Scintillation Detector."

9.9. H. O. Menlove, "Do's and Dont's of Nondestructive Assay Measurements," LASL Internal Document.

APPENDIX A

GAMMA-RAY SIGNATURES

This is a listing of the gamma rays from the fissionable nuclides.[A.1] The branching intensity is given in gammas/disintegration and the error is given in percent. These measurements are being repeated and an updated listing should be available by 1975.

REFERENCE

A.1. R. Gunnink and J. F. Tinney, "Analysis of Fuel Rods by Gamma-Ray Spectroscopy," Lawrence Livermore Laboratory report UCRL-51086 (1971).

	NUCLIDE	HALF-LIFE (DAYS)	ENERGY (KEV)	BRANCHING INTENSITY	ERROR
1	90 TH 228	6.976E+02	115.24	5.500E-03	5
			215.92	2.300E-03	10
			238.62	4.400E-01	1
			241.00	4.000E-02	2
			252.50	2.750E-03	7
			277.34	2.330E-02	2
			288.16	3.300E-03	7
			300.14	3.300E-02	1
			452.90	3.900E-03	10
			510.73	9.500E-02	3
			583.15	3.100E-01	1
			727.26	6.800E-02	2
			763.30	6.600E-03	5
			785.46	1.150E-02	5
			860.49	4.650E-02	2
			893.33	3.700E-03	10
			1078.70	5.500E-03	5
			1592.69	PAIR PEAK	
			1620.63	1.540E-02	5
			2103.70	PAIR PEAK	
			2614.71	3.600E-01	1
2	90 TH 231	1.067E+00	42.81	5.400E-04	3
			58.55	4.200E-03	1
			72.76	2.200E-03	2
			81.21	7.440E-03	2
			82.06	3.410E-03	2
			84.20	5.600E-02	1
			89.93	8.400E-03	2
			92.27	3.800E-03	1
			92.94	6.600E-04	2
			95.85	5.600E-03	1
			99.27	1.180E-03	2
			102.29	3.800E-03	1
			107.60	6.800E-04	2
			108.44	1.310E-02	1
			111.54	5.450E-04	3
			112.48	1.940E-04	10
			116.83	2.000E-04	4
			124.95	5.340E-04	3
			134.03	2.180E-04	5
			135.69	7.170E-04	2
			136.80	3.000E-05	35
			145.13	5.600E-05	20
			145.96	2.800E-04	2
			163.16	1.390E-03	1
3	92 U X-RAYS		94.67	6.240E-01	
			98.44	1.000E+00	
			110.41	1.280E-01	

	NUCLIDE		HALF-LIFE (DAYS)	ENERGY (KEV)	BRANCHING INTENSITY	ERROR
3	92	U X-RAYS		111.29	2.320E-01	
				114.50	9.300E-02	
				115.40	3.000E-02	
4	92	U 235	2.604E+11	89.96	2.450E-02	3
				93.35	4.000E-02	2
				104.82	4.560E-03	2
				105.61	9.100E-03	2
				140.75	2.080E-03	5
				143.77	1.070E-01	1
				163.37	4.850E-02	1
				182.57	3.600E-03	3
				185.72	5.610E-01	1
				194.94	6.150E-03	1
				202.10	1.070E-02	1
				205.33	4.870E-02	1
				215.35	2.750E-04	3
				233.54	2.750E-04	2
				240.93	6.400E-04	4
				246.88	5.200E-04	4
				275.34	2.690E-04	3
				291.63	2.000E-04	10
				345.89	3.000E-04	5
				387.81	1.200E-04	6
5	92	U 237	6.750E+00	26.75	2.390E-02	2
				33.51	1.240E-03	6
				51.09	5.150E-03	4
				59.54	3.620E-01	1
				64.82	1.370E-02	2
				97.08	1.475E-01	1
				101.07	2.355E-01	1
				113.27	2.880E-02	1
				114.20	5.400E-02	1
				114.84	3.700E-03	40
				117.47	2.260E-02	3
				118.40	7.800E-03	10
				164.59	1.830E-02	2
				207.97	2.080E-01	2
				221.80	2.200E-04	20
				267.45	7.200E-03	2
				332.29	1.140E-02	2
				335.33	1.100E-03	5
				368.70	4.300E-04	2
				370.80	1.050E-03	10
6	92	U 238	1.647E+12	258.23	7.300E-04	3
				294.90	4.800E-05	8
				369.50	4.800E-05	8
				371.90	2.300E-05	15

	NUCLIDE	HALF-LIFE (DAYS)	ENERGY (KEV)	BRANCHING INTENSITY	ERROR
6	92 U 238	1.647E+12	451.00	3.500E-05	10
			453.90	2.100E-05	10
			458.20	2.200E-05	1
			468.30	1.960E-05	20
			475.80	1.730E-05	20
			544.00	3.500E-05	20
			569.29	2.020E-04	4
			654.30	2.160E-05	15
			691.30	9.000E-05	5
			699.00	6.000E-05	10
			702.10	7.000E-05	10
			706.00	7.000E-05	10
			733.39	1.060E-04	5
			739.70	1.100E-04	10
			742.79	9.500E-04	2
			766.39	3.130E-03	1
			781.50	7.000E-05	10
			786.30	5.500E-04	2
			796.40	6.650E-05	10
			805.80	7.600E-05	5
			808.40	2.870E-05	12
			819.10	2.300E-05	15
			825.00	6.000E-05	5
			831.30	7.400E-05	5
			851.66	7.400E-05	5
			866.50	1.200E-05	20
			876.10	4.000E-05	10
			880.50	1.960E-04	2
			883.24	1.970E-04	3
			887.39	6.300E-05	5
			898.67	4.500E-05	5
			921.77	1.250E-04	5
			925.07	1.360E-04	7
			926.68	1.910E-04	5
			936.70	7.500E-06	25
			941.50	2.400E-05	10
			946.07	3.550E-04	2
			965.70	5.650E-06	30
			980.50	4.200E-05	4
			984.10	2.700E-05	6
			994.90	7.480E-05	5
			1001.10	8.280E-03	1
			1028.70	5.540E-06	24
			1041.70	9.580E-06	20
			1044.30	7.460E-06	25
			1061.86	2.400E-05	10
			1083.70	1.600E-05	15
			1122.00	6.530E-06	30
			1125.10	4.700E-05	5
			1151.10	3.900E-06	35

	NUCLIDE	HALF-LIFE (DAYS)	ENERGY (KEV)	BRANCHING INTENSITY	ERROR
6	92 U 238	1.647E+12	1193.76	1.340E-05	2
			1220.10	8.750E-06	22
			1237.26	4.900E-05	4
			1292.70	8.600E-06	20
			1320.50	2.900E-06	60
			1352.90	2.240E-05	10
			1393.50	3.700E-05	12
			1413.90	2.310E-05	6
			1434.27	9.000E-05	5
			1445.80	4.000E-06	26
			1452.60	9.500E-06	12
			1510.32	1.300E-04	2
			1527.25	2.180E-05	6
			1548.24	1.400E-05	8
			1553.80	8.200E-05	2
			1558.90	7.000E-06	15
			1570.80	1.050E-05	15
			1593.20	2.650E-05	10
			1593.20	3.400E-06	32
			1638.10	3.800E-06	30
			1654.10	3.300E-06	40
			1668.40	1.200E-05	10
			1685.80	2.970E-06	25
			1694.30	1.280E-05	8
			1716.50	1.940E-06	40
			1737.91	2.120E-04	1
			1750.20	1.610E-06	40
			1760.05	1.440E-05	4
			1765.80	7.600E-05	2
			1796.70	5.700E-06	15
			1809.25	3.700E-05	3
			1819.80	8.550E-06	7
			1831.48	1.750E-04	1
			1863.00	1.150E-04	8
			1867.48	9.150E-05	1
			1874.77	7.800E-05	2
			1877.00	1.930E-05	10
			1890.50	2.000E-06	30
			1893.65	2.130E-05	4
			1911.21	6.100E-05	2
			1925.78	5.700E-06	8
			1937.06	2.870E-05	2
			1969.04	4.000E-06	8
			2022.50	1.870E-06	16
			2041.00	8.970E-07	25
			2065.50	8.000E-07	25
			2136.40	8.250E-07	25
7	94 PU X-RAYS		99.54	6.310E-01	
			103.75	1.000E+00	

	NUCLIDE	HALF-LIFE (DAYS)	ENERGY (KEV)	BRANCHING INTENSITY	ERROR
7	94 PU X-RAYS		116.22	1.280E-01	
			117.20	2.320E-01	
			120.60	9.300E-02	
			121.60	3.000E-02	
8	94 PU 238	3.200E+04	43.49	3.900E-04	1
			94.67	9.000E-07	3
			98.44	1.480E-06	2
			99.87	7.400E-05	1
			110.41	1.990E-07	2
			111.29	3.070E-07	2
			114.45	1.160E-07	2
			152.77	1.010E-05	2
			200.98	4.280E-08	2
			252.41	3.530E-09	7
			258.23	6.770E-10	20
			299.10	4.700E-10	30
			705.60	5.400E-10	40
			708.40	5.380E-09	10
			742.82	5.550E-08	1
			766.41	2.400E-07	1
			786.30	3.530E-08	1
			805.42	1.390E-09	15
			808.23	8.580E-09	3
			851.73	1.390E-08	2
			883.21	6.530E-09	10
			904.34	6.210E-10	30
			926.73	6.150E-09	4
			942.02	5.260E-09	4
			946.12	1.030E-09	20
			1001.20	1.300E-08	6
			1041.90	2.290E-09	10
			1085.40	8.850E-10	20
9	94 PU 239	8.908E+06	30.09	1.050E-06	10
			32.24	1.370E-05	3
			36.39	4.230E-06	2
			37.28	1.030E-06	8
			38.69	5.860E-05	1
			40.57	2.560E-07	25
			46.23	5.110E-06	3
			47.56	2.870E-07	25
			51.63	2.080E-04	1
			54.05	1.690E-06	4
			56.83	9.300E-06	1
			65.69	3.350E-07	15
			67.66	1.420E-06	5
			68.73	5.990E-06	5
			74.96	3.800E-07	15
			77.60	4.270E-06	2

	NUCLIDE	HALF-LIFE (DAYS)	ENERGY (KEV)	BRANCHING INTENSITY	ERROR
9	94 PU 239	8.908E+06	78.38	1.690E-06	5
			89.59	1.340E-07	40
			94.67	3.670E-05	1
			98.44	5.900E-05	1
			98.81	1.300E-05	10
			103.03	1.790E-06	5
			110.41	7.760E-06	1
			111.29	1.470E-05	1
			114.32	5.590E-06	1
			115.35	6.760E-06	1
			116.24	5.960E-06	1
			119.72	3.030E-07	7
			123.67	1.680E-07	10
			124.52	6.230E-07	4
			125.17	5.790E-07	4
			129.28	6.200E-05	1
			141.64	3.110E-07	5
			144.19	2.840E-06	3
			146.05	1.130E-06	3
			158.30	8.000E-08	30
			161.45	1.300E-06	3
			168.10	3.800E-08	25
			171.34	1.090E-06	2
			173.60	4.900E-08	25
			179.17	6.390E-07	2
			184.30	1.630E-08	35
			188.27	9.600E-08	10
			189.34	7.760E-07	2
			195.65	1.070E-06	2
			197.98	5.000E-08	15
			203.52	5.630E-06	2
			225.43	1.630E-07	4
			237.77	1.500E-07	10
			242.09	8.320E-08	15
			243.33	2.320E-07	5
			244.80	5.230E-08	15
			248.95	7.500E-08	7
			255.33	8.030E-07	2
			263.93	2.550E-07	5
			265.54	2.850E-08	25
			281.20	2.140E-08	30
			285.30	1.500E-08	40
			297.43	5.000E-07	1
			302.87	5.700E-08	10
			307.81	6.200E-08	10
			311.69	2.740E-07	2
			313.50	2.000E-08	40
			316.35	1.410E-07	4
			320.81	5.690E-07	1
			323.76	5.390E-07	2

	NUCLIDE	HALF-LIFE (DAYS)	ENERGY (KEV)	BRANCHING INTENSITY	ERROR
9	94 PU 239	8.908E+06	332.80	5.050E-06	1
			336.06	1.130E-06	1
			341.48	6.630E-07	1
			344.96	5.610E-06	1
			354.10	8.000E-09	40
			361.90	1.170E-07	3
			367.02	8.720E-07	1
			368.53	8.960E-07	1
			375.02	1.585E-05	1
			380.16	3.075E-06	1
			382.70	2.600E-06	1
			392.37	1.160E-06	10
			393.04	4.440E-06	3
			399.44	6.130E-08	5
			410.77	8.000E-08	50
			413.69	1.506E-05	1
			422.57	1.190E-06	1
			426.67	2.290E-07	3
			430.00	4.910E-08	6
			445.78	9.100E-08	4
			451.45	1.920E-06	1
			457.57	1.540E-08	7
			461.29	2.020E-08	10
			463.80	1.570E-09	30
			474.40	9.420E-10	30
			481.55	4.770E-08	2
			487.00	2.500E-09	15
			493.10	8.800E-09	6
			538.90	3.000E-09	20
			550.60	4.000E-09	10
			557.70	6.000E-10	40
			586.40	1.420E-09	15
			598.10	1.900E-08	3
			607.30	1.450E-09	15
			612.90	8.100E-09	4
			617.40	2.040E-08	4
			618.90	2.440E-08	4
			624.80	4.000E-09	6
			633.19	2.320E-08	3
			637.97	2.500E-08	5
			640.15	7.950E-08	3
			646.02	1.450E-07	2
			649.50	8.100E-09	20
			652.19	6.400E-08	3
			654.86	2.150E-08	8
			658.99	9.500E-08	2
			664.67	1.540E-08	4
			674.20	5.200E-09	4
			686.16	8.900E-09	4
			690.85	5.500E-09	6

	NUCLIDE	HALF-LIFE (DAYS)	ENERGY (KEV)	BRANCHING INTENSITY	ERROR
9	94 PU 239	8.908E+06	701.00	5.400E-09	6
			703.79	3.880E-08	2
			717.76	2.670E-08	3
			727.81	1.090E-09	8
			756.40	3.370E-08	2
			769.38	1.100E-07	1
			779.50	1.330E-09	5
			787.21	8.400E-10	7
			793.00	2.500E-10	20
			796.50	3.200E-10	16
			803.28	4.450E-10	15
			808.14	1.470E-09	5
			813.89	6.200E-10	15
			821.02	5.110E-10	10
			828.61	1.380E-09	5
			832.06	2.540E-10	20
			840.00	2.800E-10	30
			843.75	1.500E-09	10
			878.96	5.110E-10	15
			891.00	7.760E-10	15
			940.00	4.200E-10	15
			956.40	5.600E-10	15
			979.50	2.260E-10	20
			986.70	1.200E-10	40
			992.40	2.260E-10	20
			1005.50	1.200E-10	35
			1057.30	4.500E-10	15
10	94 PU 240	2.410E+06	45.24	4.500E-04	1
			94.67	6.150E-07	10
			98.44	1.000E-06	5
			104.23	7.000E-05	1
			111.29	3.600E-07	10
			114.50	1.230E-07	
			160.35	4.200E-06	1
			642.30	1.450E-07	3
			687.63	3.700E-08	4
11	94 PU 241	2.070E+08*	44.19	1.820E-03	3
			44.83	4.500E-04	10
			56.30	1.500E-03	5
			71.60	1.100E-03	5
			76.96	9.800E-03	
			94.67	1.210E-01	1
			98.44	1.910E-01	1
			103.67	4.210E-02	1
			110.42	2.390E-02	1
			111.30	4.410E-02	1
			111.96	1.720E-03	
			114.50	1.820E-02	2

*α-branch half-life.

	NUCLIDE	HALF-LIFE (DAYS)	ENERGY (KEV)	BRANCHING INTENSITY	ERROR
11	94 PU 241	2.070E+08	115.41	5.400E-03	2
			148.60	7.740E-02	1
			160.00	2.620E-03	2
12	95 AM 241	1.582E+05	43.40	9.100E-04	20
			59.54	3.590E-01	1
			69.90	2.010E-05	6
			97.10	1.130E-05	7
			99.00	2.020E-04	2
			101.09	1.880E-05	5
			103.00	1.950E-04	2
			113.27	2.400E-06	
			114.20	4.780E-06	
			118.00	2.210E-06	
			123.01	1.020E-05	3
			125.30	3.950E-05	3
			146.55	4.580E-06	3
			150.12	7.200E-07	4
			158.80	1.140E-08	50
			161.60	2.300E-08	20
			164.60	6.200E-07	4
			165.95	2.430E-07	5
			169.57	1.680E-06	3
			175.16	1.840E-07	6
			191.90	2.200E-07	4
			194.70	1.700E-08	25
			204.00	3.200E-08	25
			207.98	7.600E-06	2
			221.49	4.000E-07	4
			233.02	4.800E-08	10
			234.40	6.000E-09	40
			246.72	2.000E-08	25
			260.98	8.600E-09	30
			264.92	8.270E-08	5
			267.50	2.450E-07	3
			275.72	6.220E-08	6
			291.15	3.150E-08	15
			292.72	1.310E-07	5
			300.09	5.740E-08	8
			304.16	8.000E-09	35
			311.94	3.900E-07	3
			322.48	1.440E-06	2
			332.33	1.450E-06	2
			335.38	4.700E-06	2
			337.69	3.050E-08	15
			340.40	2.500E-08	25
			350.40	1.400E-08	30
			358.20	1.510E-08	20
			368.60	2.080E-06	2
			370.91	4.910E-07	2

	NUCLIDE	HALF-LIFE (DAYS)	ENERGY (KEV)	BRANCHING INTENSITY	ERROR
12	95 AM 241	1.582E+05	376.57	1.330E-06	1
			383.74	2.900E-07	1
			390.53	6.100E-08	5
			398.50	1.500E-08	30
			406.46	1.200E-08	35
			415.90	1.610E-08	25
			419.19	2.760E-07	3
			426.34	2.400E-07	4
			429.60	5.000E-09	50
			442.75	3.400E-08	20
			452.23	1.700E-08	25
			454.58	9.300E-08	6
			459.40	3.200E-08	15
			467.90	2.500E-08	25
			486.30	1.200E-08	40
			514.10	2.700E-08	30
			521.90	7.000E-09	50
			574.00	1.450E-08	20
			586.52	1.430E-08	20
			590.30	1.520E-08	20
			597.39	6.500E-08	5
			618.96	5.550E-07	2
			626.90	3.600E-09	50
			632.80	1.100E-08	25
			641.37	6.450E-08	4
			652.88	3.540E-07	2
			662.37	3.460E-06	1
			675.70	6.800E-09	30
			679.99	2.600E-08	10
			688.70	2.920E-07	2
			693.41	3.160E-08	5
			696.34	4.900E-08	4
			709.30	5.800E-08	4
			721.92	1.850E-06	1
			729.46	1.300E-08	15
			737.22	7.500E-08	3
			755.87	7.100E-08	3
			759.37	1.650E-08	8
			766.87	5.100E-08	4
			770.93	6.470E-08	4
			780.42	2.700E-09	50
			811.80	5.200E-09	2
			851.90	2.800E-09	45
			862.90	5.100E-09	30

	NUCLIDE	ENERGY (KEV)	BRANCHING INTENSITY	ASSOCIATIVE GAMMA RAYS	
1	92 U 237	26.75	2.390E-02	59.54	207.97
2	94 PU 239	30.09	1.050E-06	51.63	98.44
3	94 PU 239	32.24	1.370E-05	51.63	98.44
4	92 U 237	33.51	1.240E-03	59.54	207.97
5	94 PU 239	36.39	4.230E-06	51.63	98.44
6	94 PU 239	37.28	1.030E-06	51.63	98.44
7	94 PU 239	38.69	5.860E-05	51.63	98.44
8	94 PU 239	40.57	2.560E-07	51.63	98.44
9	90 TH 231	42.81	5.400E-04	84.20	185.72
10	95 AM 241	43.40	9.100E-04	59.54	0.
11	94 PU 238	43.49	3.900E-04	99.87	152.77
12	94 PU 241	44.19	1.820E-03	59.54	148.60
13	94 PU 241	44.83	4.500E-04	59.54	148.60
14	94 PU 240	45.24	4.500E-04	104.23	160.35
15	94 PU 239	46.23	5.110E-06	51.63	98.44
16	94 PU 239	47.56	2.870E-07	51.63	98.44
17	92 U 237	51.09	5.150E-03	59.54	207.97
18	94 PU 239	51.63	2.080E-04	94.67	98.44
19	94 PU 239	54.05	1.690E-06	51.63	98.44
20	94 PU 241	56.30	1.500E-03	59.54	148.60
21	94 PU 239	56.83	9.300E-06	51.63	98.44
22	90 TH 231	58.55	4.200E-03	84.20	185.72
23	95 AM 241	59.54	3.590E-01	99.00	103.00
24	92 U 237	59.54	3.620E-01	164.59	207.97
25	92 U 237	64.82	1.370E-02	164.59	207.97
26	94 PU 239	65.69	3.350E-07	51.63	98.44
27	94 PU 239	67.66	1.420E-06	51.63	98.44

	NUCLIDE	ENERGY (KEV)	BRANCHING INTENSITY	ASSCCIATIVE GAMMA RAYS	
28	94 PU 239	68.73	5.990E-06	51.63	98.44
29	95 AM 241	69.90	2.010E-05	59.54	99.00
30	94 PU 241	71.60	1.100E-03	59.54	148.60
31	90 TH 231	72.76	2.200E-03	84.20	185.72
32	94 PU 239	74.96	3.800E-07	94.67	129.28
33	94 PU 241	76.96	9.800E-03	59.54	148.60
34	94 PU 239	77.60	4.270E-06	94.67	98.44
35	94 PU 239	78.38	1.690E-06	94.67	98.44
36	90 TH 231	81.21	7.440E-03	84.20	185.72
37	90 TH 231	82.06	3.410E-03	84.20	185.72
38	90 TH 231	84.20	5.600E-02	89.93	185.72
39	94 PU 239	89.59	1.340E-07	94.67	98.44
40	90 TH 231	89.93	8.400E-03	84.20	185.72
41	92 U 235	89.96	2.450E-02	84.20	185.72
42	90 TH 231	92.27	3.800E-03	84.20	185.72
43	90 TH 231	92.94	6.600E-04	84.20	185.72
44	92 U 235	93.35	4.000E-02	84.20	185.72
45	94 PU 241	94.67	1.210E-01	59.54	148.60
46	94 PU 240	94.67	6.150E-07	45.24	104.23
47	94 PU 239	94.67	3.670E-05	98.44	129.28
48	94 PU 238	94.67	9.000E-07	43.49	99.87
49	92 U X-RAY	94.67	6.240E-01	98.44	111.29
50	90 TH 231	95.85	5.600E-03	84.20	185.72
51	92 U 237	97.08	1.475E-01	164.59	207.97
52	95 AM 241	97.10	1.130E-05	59.54	99.00
53	94 PU 241	98.44	1.910E-01	59.54	148.60
54	94 PU 240	98.44	1.000E-06	45.24	104.23

	NUCLIDE	ENERGY (KEV)	BRANCHING INTENSITY	ASSOCIATIVE GAMMA RAYS	
55	94 PU 239	98.44	5.900E-05	94.67	129.28
56	94 PU 238	98.44	1.480E-06	43.49	99.87
57	92 U X-RAY	98.44	1.000E+00	94.67	111.29
58	94 PU 239	98.81	1.300E-05	94.67	129.28
59	95 AM 241	99.00	2.020E-04	59.54	103.00
60	90 TH 231	99.27	1.180E-03	84.20	185.72
61	94 PU X-RAY	99.54	6.310E-01	103.75	117.20
62	94 PU 238	99.87	7.400E-05	43.49	152.77
63	92 U 237	101.07	2.355E-01	164.59	207.97
64	95 AM 241	101.09	1.880E-05	59.54	103.00
65	90 TH 231	102.29	3.800E-03	84.20	185.72
66	95 AM 241	103.00	1.950E-04	59.54	99.00
67	94 PU 239	103.03	1.790E-06	94.67	129.28
68	94 PU 241	103.67	4.210E-02	59.54	148.60
69	94 PU X-RAY	103.75	1.000E+00	99.54	117.20
70	94 PU 240	104.23	7.000E-05	45.24	160.35
71	92 U 235	104.82	4.560E-03	84.20	185.72
72	92 U 235	105.61	9.100E-03	84.20	185.72
73	90 TH 231	107.60	6.800E-04	84.20	185.72
74	90 TH 231	108.44	1.310E-02	84.20	185.72
75	94 PU 239	110.41	7.760E-06	98.44	129.28
76	94 PU 238	110.41	1.990E-07	99.87	152.77
77	92 U X-RAY	110.41	1.280E-01	94.67	98.44
78	94 PU 241	110.42	2.390E-02	59.54	148.60
79	94 PU 240	111.29	3.600E-07	104.23	160.35
80	94 PU 239	111.29	1.470E-05	98.44	129.28
81	94 PU 238	111.29	3.070E-07	99.87	152.77

	NUCLIDE	ENERGY (KEV)	BRANCHING INTENSITY	ASSOCIATIVE GAMMA RAYS	
82	92 U X-RAY	111.29	2.320E-01	94.67	98.44
83	94 PU 241	111.30	4.410E-02	59.54	148.60
84	90 TH 231	111.54	5.450E-04	84.20	185.72
85	94 PU 241	111.96	1.720E-03	59.54	148.60
86	90 TH 231	112.48	1.940E-04	84.20	185.72
87	95 AM 241	113.27	2.400E-06	59.54	103.00
88	92 U 237	113.27	2.880E-02	164.59	207.97
89	95 AM 241	114.20	4.780E-06	59.54	103.00
90	92 U 237	114.20	5.400E-02	164.59	207.97
91	94 PU 239	114.32	5.590E-06	98.44	129.28
92	94 PU 238	114.45	1.160E-07	99.87	152.77
93	94 PU 241	114.50	1.820E-02	59.54	148.60
94	94 PU 240	114.50	1.230E-07	104.23	160.35
95	92 U X-RAY	114.50	9.300E-02	94.67	98.44
96	92 U 237	114.84	3.700E-03	164.59	207.97
97	90 TH 228	115.24	5.500E-03	238.62	583.15
98	94 PU 239	115.35	6.760E-06	98.44	129.28
99	92 U X-RAY	115.40	3.000E-02	94.67	98.44
100	94 PU 241	115.41	5.400E-03	59.54	148.60
101	94 PU X-RAY	116.22	1.280E-01	99.54	103.75
102	94 PU 239	116.24	5.960E-06	98.44	129.28
103	90 TH 231	116.83	2.000E-04	84.20	185.72
104	94 PU X-RAY	117.20	2.320E-01	99.54	103.75
105	92 U 237	117.47	2.260E-02	164.59	207.97
106	95 AM 241	118.00	2.210E-06	59.54	103.00
107	92 U 237	118.40	7.800E-03	164.59	207.97
108	94 PU 239	119.72	3.030E-07	98.44	129.28

	NUCLIDE	ENERGY (KEV)	BRANCHING INTENSITY	ASSOCIATIVE GAMMA RAYS	
109	94 PU X-RAY	120.60	9.300E-02	99.54	103.75
110	94 PU X-RAY	121.60	3.000E-02	99.54	103.75
111	95 AM 241	123.01	1.020E-05	59.54	103.00
112	94 PU 239	123.67	1.680E-07	98.44	129.28
113	94 PU 239	124.52	6.230E-07	98.44	129.28
114	90 TH 231	124.95	5.340E-04	84.20	185.72
115	94 PU 239	125.17	5.790E-07	98.44	129.28
116	95 AM 241	125.30	3.950E-05	59.54	103.00
117	94 PU 239	129.28	6.200E-05	98.44	375.02
118	90 TH 231	134.03	2.180E-04	84.20	185.72
119	90 TH 231	135.69	7.170E-04	84.20	185.72
120	90 TH 231	136.80	3.000E-05	84.20	185.72
121	92 U 235	140.75	2.080E-03	185.72	163.37
122	94 PU 239	141.64	3.110E-07	129.28	375.02
123	92 U 235	143.77	1.070E-01	185.72	163.37
124	94 PU 239	144.19	2.840E-06	129.28	375.02
125	90 TH 231	145.13	5.600E-05	84.20	185.72
126	90 TH 231	145.96	2.800E-04	84.20	185.72
127	94 PU 239	146.05	1.130E-06	129.28	375.02
128	95 AM 241	146.55	4.580E-06	59.54	103.00
129	94 PU 241	148.60	7.740E-02	164.59	207.97
130	95 AM 241	150.12	7.200E-07	59.54	103.00
131	94 PU 238	152.77	1.010E-05	99.87	766.41
132	94 PU 239	158.30	8.000E-08	129.28	375.02
133	95 AM 241	158.80	1.140E-08	59.54	103.00
134	94 PU 241	160.00	2.620E-03	164.59	207.97
135	94 PU 240	160.35	4.200E-06	45.24	104.23

	NUCLIDE	ENERGY (KEV)	BRANCHING INTENSITY	ASSOCIATIVE GAMMA RAYS	
136	94 PU 239	161.45	1.300E-06	129.28	375.02
137	95 AM 241	161.60	2.300E-08	59.54	103.00
138	90 TH 231	163.16	1.390E-03	84.20	185.72
139	92 U 235	163.37	4.850E-02	185.72	143.77
140	92 U 237	164.59	1.830E-02	148.60	207.97
141	95 AM 241	164.60	6.200E-07	59.54	103.00
142	95 AM 241	165.95	2.430E-07	59.54	103.00
143	94 PU 239	168.10	3.800E-08	129.28	375.02
144	95 AM 241	169.57	1.680E-06	59.54	103.00
145	94 PU 239	171.34	1.090E-06	129.28	375.02
146	94 PU 239	173.60	4.900E-08	129.28	375.02
147	95 AM 241	175.16	1.840E-07	59.54	103.00
148	94 PU 239	179.17	6.390E-07	129.28	375.02
149	92 U 235	182.57	3.600E-03	185.72	163.37
150	94 PU 239	184.30	1.630E-08	129.28	375.02
151	92 U 235	185.72	5.610E-01	143.77	163.37
152	94 PU 239	188.27	9.600E-08	129.28	375.02
153	94 PU 239	189.34	7.760E-07	129.28	375.02
154	95 AM 241	191.90	2.200E-07	59.54	103.00
155	95 AM 241	194.70	1.700E-08	59.54	103.00
156	92 U 235	194.94	6.150E-03	185.72	163.37
157	94 PU 239	195.65	1.070E-06	129.28	375.02
158	94 PU 239	197.98	5.000E-08	129.28	375.02
159	94 PU 238	200.98	4.280E-08	152.77	766.41
160	92 U 235	202.10	1.070E-02	185.72	163.37
161	94 PU 239	203.52	5.630E-06	129.28	375.02
162	95 AM 241	204.00	3.200E-08	59.54	103.00

	NUCLIDE	ENERGY (KEV)	BRANCHING INTENSITY	ASSOCIATIVE GAMMA RAYS	
163	92 U 235	205.33	4.870E-02	185.72	163.37
164	92 U 237	207.97	2.080E-01	164.59	148.60
165	95 AM 241	207.98	7.600E-06	59.54	103.00
166	92 U 235	215.35	2.750E-04	185.72	163.37
167	90 TH 228	215.92	2.300E-03	238.62	583.15
168	95 AM 241	221.49	4.000E-07	59.54	103.00
169	92 U 237	221.80	2.200E-04	164.59	207.97
170	94 PU 239	225.43	1.630E-07	129.28	375.02
171	95 AM 241	233.02	4.800E-08	59.54	103.00
172	92 U 235	233.54	2.750E-04	185.72	163.37
173	95 AM 241	234.40	6.000E-09	59.54	103.00
174	94 PU 239	237.77	1.500E-07	129.28	375.02
175	90 TH 228	238.62	4.400E-01	2614.71	583.15
176	92 U 235	240.93	6.400E-04	185.72	163.37
177	90 TH 228	241.00	4.000E-02	2614.71	583.15
178	94 PU 239	242.09	8.320E-08	129.28	375.02
179	94 PU 239	243.33	2.320E-07	129.28	375.02
180	94 PU 239	244.80	5.230E-08	129.28	375.02
181	95 AM 241	246.72	2.000E-08	59.54	103.00
182	92 U 235	246.88	5.200E-04	185.72	163.37
183	94 PU 239	248.95	7.500E-08	129.28	375.02
184	94 PU 238	252.41	3.530E-09	152.77	766.41
185	90 TH 228	252.50	2.750E-03	238.62	583.15
186	94 PU 239	255.33	8.030E-07	129.28	375.02
187	94 PU 238	258.23	6.770E-10	152.77	766.41
188	92 U 238	258.23	7.300E-04	766.39	1001.10
189	95 AM 241	260.98	8.600E-09	59.54	103.00

	NUCLIDE	ENERGY (KEV)	BRANCHING INTENSITY	ASSCCIATIVE GAMMA RAYS	
190	94 PU 239	263.93	2.550E-07	129.28	375.02
191	95 AM 241	264.92	8.270E-08	59.54	103.00
192	94 PU 239	265.54	2.850E-08	129.28	375.02
193	92 U 237	267.45	7.200E-03	164.59	207.97
194	95 AM 241	267.50	2.450E-07	59.54	103.00
195	92 U 235	275.34	2.690E-04	185.72	163.37
196	95 AM 241	275.72	6.220E-08	59.54	103.00
197	90 TH 228	277.34	2.330E-02	238.62	583.15
198	94 PU 239	281.20	2.140E-08	129.28	375.02
199	94 PU 239	285.30	1.500E-08	129.28	375.02
200	90 TH 228	288.16	3.300E-03	238.62	583.15
201	95 AM 241	291.15	3.150E-08	59.54	103.00
202	92 U 235	291.63	2.000E-04	185.72	163.37
203	95 AM 241	292.72	1.310E-07	59.54	103.00
204	92 U 238	294.90	4.800E-05	766.39	1001.10
205	94 PU 239	297.43	5.000E-07	129.28	375.02
206	94 PU 238	299.10	4.700E-10	152.77	766.41
207	95 AM 241	300.09	5.740E-08	59.54	103.00
208	90 TH 228	300.14	3.300E-02	238.62	583.15
209	94 PU 239	302.87	5.700E-08	129.28	375.02
210	95 AM 241	304.16	8.000E-09	59.54	103.00
211	94 PU 239	307.81	6.200E-08	129.28	375.02
212	94 PU 239	311.69	2.740E-07	129.28	375.02
213	95 AM 241	311.94	3.900E-07	59.54	103.00
214	94 PU 239	313.50	2.000E-08	129.28	375.02
215	94 PU 239	316.35	1.410E-07	375.02	413.69
216	94 PU 239	320.81	5.690E-07	129.28	375.02

	NUCLIDE	ENERGY (KEV)	BRANCHING INTENSITY	ASSCCIATIVE GAMMA RAYS	
217	95 AM 241	322.48	1.440E-06	59.54	103.00
218	94 PU 239	323.76	5.390E-07	129.28	375.02
219	92 U 237	332.29	1.140E-02	164.59	207.97
220	95 AM 241	332.33	1.450E-06	59.54	103.00
221	94 PU 239	332.80	5.050E-06	375.02	413.69
222	92 U 237	335.33	1.100E-03	164.59	207.97
223	95 AM 241	335.38	4.700E-06	59.54	103.00
224	94 PU 239	336.06	1.130E-06	375.02	413.69
225	95 AM 241	337.69	3.050E-08	59.54	103.00
226	95 AM 241	340.40	2.500E-08	59.54	103.00
227	94 PU 239	341.48	6.630E-07	375.02	413.69
228	94 PU 239	344.96	5.610E-06	375.02	413.69
229	92 U 235	345.89	3.000E-04	185.72	163.37
230	95 AM 241	350.40	1.400E-08	59.54	103.00
231	94 PU 239	354.10	8.000E-09	375.02	413.69
232	95 AM 241	358.20	1.510E-08	59.54	103.00
233	94 PU 239	361.90	1.170E-07	129.28	375.02
234	94 PU 239	367.02	8.720E-07	375.02	413.69
235	94 PU 239	368.53	8.960E-07	375.02	413.69
236	95 AM 241	368.60	2.080E-06	59.54	103.00
237	92 U 237	368.70	4.300E-04	164.59	207.97
238	92 U 238	369.50	4.800E-05	766.39	1001.10
239	92 U 237	370.80	1.050E-03	164.59	207.97
240	95 AM 241	370.91	4.910E-07	59.54	103.00
241	92 U 238	371.90	2.300E-05	766.39	1001.10
242	94 PU 239	375.02	1.585E-05	344.96	413.69
243	95 AM 241	376.57	1.330E-06	59.54	103.00

	NUCLIDE	ENERGY (KEV)	BRANCHING INTENSITY	ASSCCIATIVE GAMMA RAYS	
244	94 PU 239	380.16	3.075E-06	375.02	413.69
245	94 PU 239	382.70	2.600E-06	375.02	413.69
246	95 AM 241	383.74	2.900E-07	59.54	125.30
247	92 U 235	387.81	1.200E-04	185.72	163.37
248	95 AM 241	390.53	6.100E-08	59.54	125.30
249	94 PU 239	392.37	1.160E-06	375.02	413.69
250	94 PU 239	393.04	4.440E-06	375.02	413.69
251	95 AM 241	398.50	1.500E-08	59.54	125.30
252	94 PU 239	399.44	6.130E-08	375.02	413.69
253	95 AM 241	406.46	1.200E-08	59.54	125.30
254	94 PU 239	410.77	8.000E-08	375.02	413.69
255	94 PU 239	413.69	1.506E-05	375.02	393.04
256	95 AM 241	415.90	1.610E-08	59.54	125.30
257	95 AM 241	419.19	2.760E-07	59.54	125.30
258	94 PU 239	422.57	1.190E-06	375.02	413.69
259	95 AM 241	426.34	2.400E-07	59.54	125.30
260	94 PU 239	426.67	2.290E-07	129.28	375.02
261	95 AM 241	429.60	5.000E-09	59.54	125.30
262	94 PU 239	430.00	4.910E-08	375.02	413.69
263	95 AM 241	442.75	3.400E-08	59.54	125.30
264	94 PU 239	445.78	9.100E-08	375.02	413.69
265	92 U 238	451.00	3.500E-05	766.39	1001.10
266	94 PU 239	451.45	1.920E-06	375.02	413.69
267	95 AM 241	452.23	1.700E-08	59.54	125.30
268	90 TH 228	452.90	3.900E-03	238.62	583.15
269	92 U 238	453.90	2.100E-05	766.39	1001.10
270	95 AM 241	454.58	9.300E-08	59.54	125.30

	NUCLIDE	ENERGY (KEV)	BRANCHING INTENSITY	ASSOCIATIVE GAMMA RAYS	
271	94 PU 239	457.57	1.540E-08	375.02	413.69
272	92 U 238	458.20	2.200E-05	766.39	1001.10
273	95 AM 241	459.40	3.200E-08	59.54	125.30
274	94 PU 239	461.29	2.020E-08	375.02	413.69
275	94 PU 239	463.80	1.570E-09	375.02	413.69
276	95 AM 241	467.90	2.500E-08	59.54	125.30
277	92 U 238	468.30	1.960E-05	766.39	1001.10
278	94 PU 239	474.40	9.420E-10	375.02	413.69
279	92 U 238	475.80	1.730E-05	766.39	1001.10
280	94 PU 239	481.55	4.770E-08	375.02	413.69
281	95 AM 241	486.30	1.200E-08	59.54	125.30
282	94 PU 239	487.00	2.500E-09	375.02	413.69
283	94 PU 239	493.10	8.800E-09	375.02	413.69
284	90 TH 228	510.73	9.500E-02	238.62	583.15
285	95 AM 241	514.10	2.700E-08	59.54	125.30
286	95 AM 241	521.90	7.000E-09	59.54	125.30
287	94 PU 239	538.90	3.000E-09	375.02	413.69
288	92 U 238	544.00	3.500E-05	766.39	1001.10
289	94 PU 239	550.60	4.000E-09	375.02	413.69
290	94 PU 239	557.70	6.000E-10	375.02	413.69
291	92 U 238	569.29	2.020E-04	766.39	1001.10
292	95 AM 241	574.00	1.450E-08	59.54	125.30
293	90 TH 228	583.15	3.100E-01	238.62	2614.71
294	94 PU 239	586.40	1.420E-09	375.02	413.69
295	95 AM 241	586.52	1.430E-08	59.54	125.30
296	95 AM 241	590.30	1.520E-08	59.54	125.30
297	95 AM 241	597.39	6.500E-08	59.54	125.30

	NUCLIDE	ENERGY (KEV)	BRANCHING INTENSITY	ASSOCIATIVE GAMMA RAYS	
298	94 PU 239	598.10	1.900E-08	375.02	413.69
299	94 PU 239	607.30	1.450E-09	375.02	413.69
300	94 PU 239	612.90	8.100E-09	375.02	413.69
301	94 PU 239	617.40	2.040E-08	375.02	413.69
302	94 PU 239	618.90	2.440E-08	375.02	413.69
303	95 AM 241	618.96	5.550E-07	662.37	721.92
304	94 PU 239	624.80	4.000E-09	375.02	413.69
305	95 AM 241	626.90	3.600E-09	662.37	721.92
306	95 AM 241	632.80	1.100E-08	662.37	721.92
307	94 PU 239	633.19	2.320E-08	375.02	413.69
308	94 PU 239	637.97	2.500E-08	375.02	413.69
309	94 PU 239	640.15	7.950E-08	375.02	413.69
310	95 AM 241	641.37	6.450E-08	662.37	721.92
311	94 PU 240	642.30	1.450E-07	160.35	687.63
312	94 PU 239	646.02	1.450E-07	375.02	413.69
313	94 PU 239	649.50	8.100E-09	375.02	413.69
314	94 PU 239	652.19	6.400E-08	375.02	413.69
315	95 AM 241	652.88	3.540E-07	662.37	721.92
316	92 U 238	654.30	2.160E-05	766.39	1001.10
317	94 PU 239	654.86	2.150E-08	375.02	413.69
318	94 PU 239	658.99	9.500E-08	375.02	413.69
319	95 AM 241	662.37	3.460E-06	207.98	721.92
320	94 PU 239	664.67	1.540E-08	375.02	413.69
321	94 PU 239	674.20	5.200E-09	375.02	413.69
322	95 AM 241	675.70	6.800E-09	662.37	721.92
323	95 AM 241	679.99	2.600E-08	662.37	721.92
324	94 PU 239	686.16	8.900E-09	375.02	413.69

	NUCLIDE	ENERGY (KEV)	BRANCHING INTENSITY	ASSOCIATIVE GAMMA RAYS	
325	94 PU 240	687.63	3.700E-08	160.35	642.30
326	95 AM 241	688.70	2.920E-07	662.37	721.92
327	94 PU 239	690.85	5.500E-09	375.02	413.69
328	92 U 238	691.30	9.000E-05	766.39	1001.10
329	95 AM 241	693.41	3.160E-08	662.37	721.92
330	95 AM 241	696.34	4.900E-08	662.37	721.92
331	92 U 238	699.00	6.000E-05	766.39	1001.10
332	94 PU 239	701.00	5.400E-09	375.02	413.69
333	92 U 238	702.10	7.000E-05	766.39	1001.10
334	94 PU 239	703.79	3.880E-08	375.02	413.69
335	94 PU 238	705.60	5.400E-10	152.77	766.41
336	92 U 238	706.00	7.000E-05	766.39	1001.10
337	94 PU 238	708.40	5.380E-09	152.77	766.41
338	95 AM 241	709.30	5.800E-08	662.37	721.92
339	94 PU 239	717.76	2.670E-08	375.02	413.69
340	95 AM 241	721.92	1.850E-06	662.37	207.98
341	90 TH 228	727.26	6.800E-02	238.62	583.15
342	94 PU 239	727.81	1.090E-09	375.02	413.69
343	95 AM 241	729.46	1.300E-08	662.37	721.92
344	92 U 238	733.39	1.060E-04	766.39	1001.10
345	95 AM 241	737.22	7.500E-08	662.37	721.92
346	92 U 238	739.70	1.100E-04	766.39	1001.10
347	92 U 238	742.79	9.500E-04	766.39	1001.10
348	94 PU 238	742.82	5.550E-08	152.77	766.41
349	95 AM 241	755.87	7.100E-08	662.37	721.92
350	94 PU 239	756.40	3.370E-08	375.02	413.69
351	95 AM 241	759.37	1.650E-08	662.37	721.92

	NUCLIDE			ENERGY (KEV)	BRANCHING INTENSITY	ASSCCIATIVE GAMMA RAYS	
352	90	TH	228	763.30	6.600E-03	238.62	583.15
353	92	U	238	766.39	3.130E-03	742.79	1001.10
354	94	PU	238	766.41	2.400E-07	152.77	742.82
355	95	AM	241	766.87	5.100E-08	662.37	721.92
356	94	PU	239	769.38	1.100E-07	375.02	413.69
357	95	AM	241	770.93	6.470E-08	662.37	721.92
358	94	PU	239	779.50	1.330E-09	375.02	413.69
359	95	AM	241	780.42	2.700E-09	662.37	721.92
360	92	U	238	781.50	7.000E-05	766.39	1001.10
361	90	TH	228	785.46	1.150E-02	238.62	583.15
362	94	PU	238	786.30	3.530E-08	152.77	766.41
363	92	U	238	786.30	5.500E-04	766.39	1001.10
364	94	PU	239	787.21	8.400E-10	375.02	413.69
365	94	PU	239	793.00	2.500E-10	375.02	413.69
366	92	U	238	796.40	6.650E-05	766.39	1001.10
367	94	PU	239	796.50	3.200E-10	375.02	413.69
368	94	PU	239	803.28	4.450E-10	375.02	413.69
369	94	PU	238	805.42	1.390E-09	152.77	766.41
370	92	U	238	805.80	7.600E-05	766.39	1001.10
371	94	PU	239	808.14	1.470E-09	375.02	413.69
372	94	PU	238	808.23	8.580E-09	152.77	766.41
373	92	U	238	808.40	2.870E-05	766.39	1001.10
374	95	AM	241	811.80	5.200E-09	662.37	721.92
375	94	PU	239	813.89	6.200E-10	375.02	413.69
376	92	U	238	819.10	2.300E-05	766.39	1001.10
377	94	PU	239	821.02	5.110E-10	375.02	413.69
378	92	U	238	825.00	6.000E-05	766.39	1001.10

	NUCLIDE	ENERGY (KEV)	BRANCHING INTENSITY	ASSOCIATIVE GAMMA RAYS	
379	94 PU 239	828.61	1.380E-09	375.02	413.69
380	92 U 238	831.30	7.400E-05	766.39	1001.10
381	94 PU 239	832.06	2.540E-10	375.02	413.69
382	94 PU 239	840.00	2.800E-10	375.02	413.69
383	94 PU 239	843.75	1.500E-09	375.02	413.69
384	92 U 238	851.66	7.400E-05	766.39	1001.10
385	94 PU 238	851.73	1.390E-08	152.77	766.41
386	95 AM 241	851.90	2.800E-09	662.37	721.92
387	90 TH 228	860.49	4.650E-02	238.62	583.15
388	95 AM 241	862.90	5.100E-09	662.37	721.92
389	92 U 238	866.50	1.200E-05	766.39	1001.10
390	92 U 238	876.10	4.000E-05	766.39	1001.10
391	94 PU 239	878.96	5.110E-10	375.02	413.69
392	92 U 238	880.50	1.960E-04	766.39	1001.10
393	94 PU 238	883.21	6.530E-09	152.77	766.41
394	92 U 238	883.24	1.970E-04	766.39	1001.10
395	92 U 238	887.39	6.300E-05	766.39	1001.10
396	94 PU 239	891.00	7.760E-10	375.02	413.69
397	90 TH 228	893.33	3.700E-03	238.62	583.15
398	92 U 238	898.67	4.500E-05	766.39	1001.10
399	94 PU 238	904.34	6.210E-10	152.77	766.41
400	92 U 238	921.77	1.250E-04	766.39	1001.10
401	92 U 238	925.07	1.360E-04	766.39	1001.10
402	92 U 238	926.68	1.910E-04	766.39	1001.10
403	94 PU 238	926.73	6.150E-09	152.77	766.41
404	92 U 238	936.70	7.500E-06	766.39	1001.10
405	94 PU 239	940.00	4.200E-10	375.02	413.69

	NUCLIDE	ENERGY (KEV)	BRANCHING INTENSITY	ASSOCIATIVE GAMMA RAYS	
406	92 U 238	941.50	2.400E-05	766.39	1001.10
407	94 PU 238	942.02	5.260E-09	152.77	766.41
408	92 U 238	946.07	3.550E-04	766.39	1001.10
409	94 PU 238	946.12	1.030E-09	152.77	766.41
410	94 PU 239	956.40	5.600E-10	375.02	413.69
411	92 U 238	965.70	5.650E-06	766.39	1001.10
412	94 PU 239	979.50	2.260E-10	375.02	413.69
413	92 U 238	980.50	4.200E-05	766.39	1001.10
414	92 U 238	984.10	2.700E-05	766.39	1001.10
415	94 PU 239	986.70	1.200E-10	375.02	413.69
416	94 PU 239	992.40	2.260E-10	375.02	413.69
417	92 U 238	994.90	7.480E-05	766.39	1001.10
418	92 U 238	1001.10	8.280E-03	766.39	742.79
419	94 PU 238	1001.20	1.300E-08	152.77	766.41
420	94 PU 239	1005.50	1.200E-10	375.02	413.69
421	92 U 238	1028.70	5.540E-06	766.39	1001.10
422	92 U 238	1041.70	9.580E-06	766.39	1001.10
423	94 PU 238	1041.90	2.290E-09	152.77	766.41
424	92 U 238	1044.30	7.460E-06	766.39	1001.10
425	94 PU 239	1057.30	4.500E-10	375.02	413.69
426	92 U 238	1061.86	2.400E-05	766.39	1001.10
427	90 TH 228	1078.70	5.500E-03	238.62	583.15
428	92 U 238	1083.70	1.600E-05	766.39	1001.10
429	94 PU 238	1085.40	8.850E-10	152.77	766.41
430	92 U 238	1122.00	6.530E-06	766.39	1001.10
431	92 U 238	1125.10	4.700E-05	766.39	1001.10
432	92 U 238	1151.10	3.900E-06	766.39	1001.10

	NUCLIDE			ENERGY (KEV)	BRANCHING INTENSITY	ASSOCIATIVE GAMMA RAYS	
433	92	U	238	1193.76	1.340E-05	766.39	1001.10
434	92	U	238	1220.10	8.750E-06	766.39	1001.10
435	92	U	238	1237.26	4.900E-05	766.39	1001.10
436	92	U	238	1292.70	8.600E-06	766.39	1001.10
437	92	U	238	1320.50	2.900E-06	766.39	1001.10
438	92	U	238	1352.90	2.240E-05	766.39	1001.10
439	92	U	238	1393.50	3.700E-05	766.39	1001.10
440	92	U	238	1413.90	2.310E-05	766.39	1001.10
441	92	U	238	1434.27	9.000E-05	766.39	1001.10
442	92	U	238	1445.80	4.000E-06	766.39	1001.10
443	92	U	238	1452.60	9.500E-06	766.39	1001.10
444	92	U	238	1510.32	1.300E-04	766.39	1001.10
445	92	U	238	1527.25	2.180E-05	766.39	1001.10
446	92	U	238	1548.24	1.400E-05	766.39	1001.10
447	92	U	238	1553.80	8.200E-05	766.39	1001.10
448	92	U	238	1558.90	7.000E-06	766.39	1001.10
449	92	U	238	1570.80	1.050E-05	766.39	1001.10
450	90	TH	228	1592.69	PAIR PEAK	238.62	583.15
451	92	U	238	1593.20	3.400E-06	766.39	1001.10
452	92	U	238	1593.20	2.650E-05	766.39	1001.10
453	90	TH	228	1620.63	1.540E-02	238.62	583.15
454	92	U	238	1638.10	3.800E-06	766.39	1001.10
455	92	U	238	1654.10	3.300E-06	766.39	1001.10
456	92	U	238	1668.40	1.200E-05	766.39	1001.10
457	92	U	238	1685.80	2.970E-06	766.39	1001.10
458	92	U	238	1694.30	1.280E-05	766.39	1001.10
459	92	U	238	1716.50	1.940E-06	766.39	1001.10

APPENDIX B

STATISTICS

The following is a brief, nonrigorous discussion of the statistical treatment of nondestructive assay data. It is primarily a compilation of useful statistical formulas employed in reporting nuclear assay results. The discussion considers random errors only. There is no consideration of the often serious problem of systematic errors (biases). The notation, which often does not conform with modern statistical practice, has been chosen deliberately to convey a few basic ideas without providing the statistical fundamentals. The material in this appendix is not intended as a substitute for sound professional statistical consultation.

I. General

1. Consider a group of N measurements of some physical quantity X; e.g., X = grams plutonium as measured on a neutron counter.

2. The best estimate of X is the average, or mean, $\bar{X}$.

$$\bar{X} = \sum_{i=1}^{N} X_i / N \; . \qquad \text{(B-1)}$$

3. In general, each measurement, X_i, deviates from this average. A common indicator of the magnitude of this deviation is the standard deviation σ_{x_i}, which is estimated by

$$\sigma_{x_i} \simeq \sqrt{\frac{\sum_{i=1}^{N} (X_i - \bar{X})^2}{N - 1}} \; , \quad N > 1 \; . \qquad \text{(B-2)}$$

This may be quoted as the estimated relative standard deviation.

$$\sigma_r \cong \sigma_{x_i} / \bar{X} \cdot 100 \text{ percent} \; . \qquad \text{(B-3)}$$

4. It is usually assumed that the measurements are distributed about the mean according to a Gaussian (or normal) distribution. Assuming this, one can estimate the percentage of the measurements which should lie outside a specified interval about the mean.

Width of Region, $\bar{X} \pm f\sigma_{x_i}$	Estimated Percentage of Measurements Outside Region
f = 0.67	50
1.0	32
2.0	5
3.0	0.3

5. The estimated standard deviation of the mean $\bar{X}$ is given by

$$\sigma_{\bar{X}} = \sigma_{x_i} / \sqrt{N} \; . \qquad \text{(B-4)}$$

This indicates an increase in precision from repeated measurements.

There is ~68% probability that the correct answer lies within the range

$$\bar{X} - \sigma_{x_i} / \sqrt{N} < X < \bar{X} + \sigma_{x_i} / \sqrt{N} \quad \text{(one sigma).}$$

There is ~95% probability that the correct answer lies within the range

$$\bar{X} - 2\sigma_{x_i} / \sqrt{N} < X < \bar{X} + 2\sigma_{x_i} / \sqrt{N} \quad \text{(two sigma).}$$

6. The above expression for $\bar{X}$, σ_{x_i}, and $\sigma_{\bar{X}}$ should be used to analyze the results from a series of repeated measurements on a single sample.

II. Propagation of Errors

1. Often the final answer (grams plutonium) involves several measurements with different uncertainties,

for example, g Pu = C(P — k • B),

where

C = calibration (grams/count),
P = counts in peak window,
B = counts in background window, and
k = constant.

2. There are general formulas to handle most cases, several of the most commonly used expressions are presented here.

Let x have standard deviation σ_x,
let y have standard deviation σ_y, and
let k be a constant,
where x and y are independent.

a. If $z = x + y$ or $z = x - y$,

$$\sigma_z = \sqrt{\sigma_x^2 + \sigma_y^2} \quad . \tag{B-5}$$

b. If $z = x/y$ or $z = xy$,

$$\frac{\sigma_z}{z} \simeq \sqrt{\left(\frac{\sigma_x}{x}\right)^2 + \left(\frac{\sigma_y}{y}\right)^2} \quad . \tag{B-6}$$

c. If $z = kx$.

$$\sigma_z = k\sigma_x \quad . \tag{B-7}$$

3. For the example given in 1 above,

$$z = g\ Pu = C(P - k \cdot B) \ ,$$

$$\frac{\sigma_z}{z} \simeq \sqrt{\left(\frac{\sigma_C}{C}\right)^2 + \frac{\sigma_P^2 + k^2\sigma_B^2}{(P - k \cdot B)^2}} \quad .$$

III. Nuclear Counting Statistics

1. All of the description of parts I and II applies to measurements involving nuclear particle counting.

2. Let X be the actual number of counts from a nuclear counting measurement. It is possible to estimate the standard deviation

$$\sigma_X \simeq \sqrt{X} \quad . \tag{B-8}$$

Therefore, based on a single measurement of X, there is ~68% probability that the actual rate is included in the interval

$$(X \pm \sqrt{X})/t \ ,$$

where t is the count time.

3. Consider Example II.3. Assume that $k = 1$ and $\sigma_C = 0$.

$$z = C(P - B) \ ,$$

$$\sigma_P \simeq \sqrt{P} \ ,$$

$$\sigma_B \simeq \sqrt{B} \ , \text{ and}$$

$$\sigma_z \simeq C\sqrt{P + B} \quad .$$

The fractional standard deviation is given as

$$\frac{\sigma_z}{z} \simeq \frac{\sqrt{P + B}}{P - B} \quad .$$

4. If N measurements are made on the same sample, the relative standard deviation of the mean z (grams plutonium) can be computed from

$$\frac{\sigma_z}{z} \simeq \frac{\sqrt{\bar{P} + \bar{B}}}{\bar{P} - \bar{B}} \Big/ \sqrt{N} \quad . \tag{B-9}$$

For a large number of repeated measurements or when Eq. (B-8) is not a good approximation (see the following section) it is better to compute the standard deviation from Eqs. (B-2) and (B-4) with X_i replaced by z_i.

5. If the counting equipment is functioning properly, the estimated standard deviation of the distribution of repeated measurements [Eq. (B-2)] should agree reasonably well with that predicted from the square root of the number of counts [Eq. (B-8)]. If the former is very much larger, one should suspect a possible malfunction in the equipment or change in the sample-instrument configuration.

6. In general, unknowns will be counted only once so that error estimates are based on Eq. (B-8). A standard should be counted several times, therefore Eqs. (B-2) and (B-4) are used here.

7. Note that all of the preceding discussion pertains to the precision or repeatability of measurements. This analysis gives no information regarding the accuracy of a measurement (Is it related to the correct amount of material?).

IV. Example

1. Consider the following count data obtained from a plutonium sample.

	P	B	P-B
	104256	102374	1882
	103643	102044	1599
	104211	101487	2724
	104638	102225	2413
	104534	102025	2509
	104044	102039	2005
mean [Eq(B-1)] =	104221	102032	2189
sigma [Eq.(B-2)] =	357	300	428

2. Suppose P is directly proportional to grams plutonium (i.e., B = 0). The values of P indicate a very precise measurement. Using Eq. (B-8) the standard deviation of P is estimated as

$$\sigma_P \simeq \sqrt{104221} = 323 \ ,$$

which agrees with the value computed from Eq. (B-2). It should be emphasized that the sigma discussed here is the standard deviation of the distribution of individual measurements of P, not the standard deviation of the mean $\bar{P}$ (this is $\sigma_P/\sqrt{6} = 146$).

3. Suppose (P — B) is proportional to grams plutonium. The values indicate a rather imprecise measurement of (P — B). Equations (B-5) and (B-8) allow us to estimate the standard deviation of the distribution of P — B.

$$\sigma_{(P - B)} \simeq \sqrt{\bar{P} + \bar{B}} = 454 \ .$$

This is in good agreement with the value computed from Eq. (B-2). Note that both P and B are measured individually to better than 1/2% in a single measurement. However, the difference is measured to only 20%. This illustrates a very poor counting situation.

APPENDIX C

CRITICALITY SAFETY

Criticality is a result of the neutron fission process, and is characterized by the attainment of a self-sustaining fission chain reaction. A system is said to be just critical if a neutron population, once established, will maintain itself constant. This requires a delicate balance between fission and neutron capture plus leakage. If the introduction rate of neutrons into the system by fission exceeds the loss of neutrons by capture or by leakage from the system, the system is supercritical. The results can be devastating.

All parameters that influence neutron behavior in a system will also affect criticality. Therefore criticality depends not only on the quantity of fissile material present (e.g., ^{235}U or ^{239}Pu), but also on the size and shape of the container, on the nature of any additional material (moderator) present in the container, and on the presence of any adjacent material (including human bodies) which might reflect neutrons back into the container. To illustrate the effect of such parameters on criticality, consider a critical sphere of uranium metal at normal density and enriched to 93% of ^{235}U. Such a sphere has a diameter of ~17.5 cm and a mass of ~52 kg. If this sphere is immersed in water (or placed near any other material), some of the neutrons that would have leaked from the sphere and escaped the system are reflected back into the sphere, and it becomes supercritical. The critical diameter of the water-reflected uranium sphere drops to ~13.5 cm, and the corresponding uranium mass is ~24.5 kg. If sufficient water is also mixed homogeneously with the uranium, the critical diameter (of the water-reflected sphere) increases to ~31 cm, but the critical mass of ^{235}U is only ~0.8 kg. These last conditions are of special interest in that they represent the minimum critical mass of ^{235}U encountered in usual processes.

The nondestructive assay of fissile material by either active or passive techniques often involves placing the container into a highly reflecting counting geometry. In particular, neutron counters are often embedded in a relatively thick polyethylene moderator. Although this combination is usually not sufficiently well coupled to the sample to constitute a full reflector,* neither is it a minimum reflector. Although an individual container is expected to contain only a relatively small amount of fissile material, the assayist must be certain that it cannot inadvertently contain sufficient material to present a criticality safety hazard when placed into the counter. This is particularly a problem for the assay of unsegregated scrap or waste for which there is little or no reliable information on the amount or enrichment of the fissionable material or on the nature of the matrix material present. Past experience has shown that the tag information on a container of scrap is not always reliable. We have found enrichments nearly double those stated, "dry" scrap that sloshes when handled, and amounts of fissile material an order of magnitude greater than expected. Often, the only information available is the volume and gross weight of the container. This may be sufficient. The conservative assumption is that the assay system constitutes a fully reflected configuration, and a weight limit is established* sufficiently low so that the given volume could not contain a critical combination of fissile material and optimum moderator. If this is not possible—that is, if the containers to be assayed are too heavy—there are several possible ways to arrive at critically safe operating limits. Multiplication measurements may be made in place[C-1] in the assay system or detailed neutronics calculations may be made using properly validated computational methods.[C.2] If necessary, one or more parameters may be controlled either by additional measurements or screening, or perhaps by administrative procedures** to increase the critically safe operational limits. If all else fails, it may

---

*A full reflector is usually considered to be an unlimited quantity of water surrounding the system.

*Critical parameter data for metal-water mixtures, both reflected and unreflected, appear in the literature. Specific references are listed in the bibliography for this appendix. The fictitious homogeneous metal-water mixture is usually given as a reference composition because its critical mass is minimum at a given $H/^{235}U$ or $H/^{239}Pu$ ratio.

**Administrative control (e.g., on moisture content) is perhaps the most questionable or at least uncomfortable technique because people *do* make mistakes.

be necessary to repackage material into smaller containers for which critically safe limits can be established.

Regardless of how the critically safe limits and operating procedures are established for a given assay system, they *must* be determined with the close cooperation of the Criticality Safety Officer at the plant where the equipment is being used. This person is an expert because of his experience and training, and ultimately, the criticality safety of operations involving handling, storage, and measurement of fissionable material is his responsibility. Do not bypass him.

There is considerable literature available concerning criticality safety and critical limits. Some of this literature is described here. An excellent and very readable report entitled "Criticality Control in Operations with Fissile Material"[C.3] discusses in detail the factors influencing critical parameters, critical limit data, computational techniques, and general criticality-control practices. Several guides specify safety limits for a variety of conditions: two of these are "The Nuclear Safety Guide"[C.4] and "Nuclear Criticality Safety in Operations with Fissionable Materials Outside Reactors."[C.5] Two of the several available compilations of experimental and/or calculated critical data are "Critical Dimensions of Systems Containing ^{235}U, ^{239}Pu, and ^{233}U"[C.6] and "Criticality Data and Factors Affecting Criticality of Single Homogeneous Units."[C.7]

REFERENCES

C.1. American National Standard, "Safety in Conducting Subcritical Neutron-Multiplication Measurements *In Situ*." Report No. ANSI N16.3-1969.

C.2. Hugh K. Clark, "Establishing Subcritical Limits," Savannah River Laboratory report DP-MS-73-27 (1973). This paper was presented at the Nuclear Criticality Safety Short Course at Taos, NM, May 6-11 (1973). It presents and discusses the draft of a proposed standard prepared by Work Group ANS 8.11 of the ANS Standards Committee for validating calculational methods of establishing subcritical limits for operations with fissionable materials.

C.3. H. C. Paxton, "Criticality Control in Operations with Fissile Material," Los Alamos Scientific Laboratory report LA-3377 (Rev.) (1972).

C.4. *Nuclear Safety Guide*, Subcommittee 8 of the ASA Sectional Committee N6, and Project 8 of the ANS Standards Committee, USAEC report TID-7016, Rev. 1 (1961).

C.5. American National Standard, "Nuclear Criticality Safety in Operations with Fissionable Materials Outside Reactors." Report No. ANSI N16.1-1969 (Revision of N6.1-1964).

C.6. H. C. Paxton, J. T. Thomas, D. Callihan, and E. B. Johnson, "Critical Dimensions of Systems Containing ^{235}U, ^{239}Pu, and ^{233}U," USAEC report TID-7028 (1964).

C.7. W. R. Stratton, "Criticality Data and Factors Affecting Criticality of Single Homogeneous Units," Los Alamos Scientific Laboratory report LA-3612 (1967).

RECEIVED
SEP 26 '74
LASL LIBRARIES